博士論文

植物の機械的ストレスへの応答の分子機構に関する研究

尹 赫晟

Contents

Chapter 1

General introduction

Plants are exposed to mechanical stress from various sources such as rain, wind, animals, pathogens, and plants themselves (Benikhlef et al., 2013). Mechanical stress severely limits plant development and yield (Zhang et al., 2013). Plants execute various adaptive strategies at the physiological and molecular levels to cope with mechanical stress. For example, when roots of *Arabidopsis thaliana* touch an object, they bend to avoid the object (Grabov et al., 2012). When Arabidopsis leaves are gently touched, resistance to pathogens is increased (Benikhlef et al., 2013). When barley shoots are stamped, their subsequent growth is improved ("Mugifumi" effects) (Ohtani, 1950). Understanding these plant responses to mechanical stress is important because it can provide insights into how plant growth and yield can be improved under stressed conditions.

Mechanical stress changes tensions in cell membranes, activates mechanosensitive ion channels such as MID1-COMPLEMENTING ACTIVITY 1 (MCA1), MCA2 and MscS-like (MSL) proteins (MSL1-10), and thereby increases a cytosolic Ca^{2+} level, which acts as a second messenger for downstream signaling (Nakagawa et al., 2007; Haswell et al., 2008; Yamanaka et al., 2010). The increase in the cytosolic Ca^{2+} level is also caused by the receptor-like kinase FERONIA, which is localized to the plasma membrane and which can be activated when it touches the cell wall (Shih et al., 2014). Effects of knockouts of *MCA1*, *MCA2*, *MSL* genes and *FERONIA* on plant phenotypes are different from each other. This suggests that, although all of these proteins should regulate the Ca^{2+} level, their downstream effectors and physiological roles are different.

VirE2-INTERACTING PROTEIN1 (VIP1) is a basic leucine zipper (bZIP) protein in *Arabidopsis thaliana* (Tzfira et al., 2001). VIP1 has pleiotropic roles in plant growth and

responses to diverse stimuli such as sulfur deficiency (Wu et al., 2010), pathogens (Pitzschke et al., 2009; Lapham et al., 2018), hypo-osmotic stress, and touch stress (Tsugama et al., 2012a, 2016). Hypo-osmotic stress increases plasma membrane tension and turgor pressure, and thus at least partially mimics mechanical stress (Shih et al., 2014). VIP1 is phosphorylated by CALCIUM-DEPENDENT PROTEIN KINASE 21 (CPK21), bound by 14-3-3 proteins and retained in the cytoplasm under stable conditions (Takeo and Ito, 2017; Tsugama et al., 2018, 2019). However, VIP1 is transiently dephosphorylated, dissociated from 14-3-3 proteins and localized to the nucleus when Arabidopsis cells are exposed to either hypo-osmotic or touch stress (Takeo and Ito, 2017). VIP1 dephosphorylation is thought to be mediated by protein phosphatase 2A (PP2A) because VIP1 interacts with PP2A B”-family B subunits, which act as the substrate-binding B subunit of PP2A, in a Ca^{2+}-dependent manner, and because VIP1 nuclear localization is inhibited by Ca^{2+} signaling inhibitors (i.e., Ca^{2+} chelators and calmodulin (CaM) inhibitors) and by PP2A inhibitors (cantharidin and okadaic acid) (Tsugama et al., 2018, 2019). The VIP1 nuclear localization is induced by hypo-osmotic stress even in the *MCA1 MCA2* double-knockout background, suggesting that VIP1 is not a downstream effector of MCA1 and MCA2. VIP1 interacts with CaMs but the physiological relevance of this interaction is unclear (Tsugama et al., 2018). Further studies are needed to better understand how subcellular localization and other functions of VIP1 are regulated.

VIP1 has 11 close homologs in Arabidopsis (Jakoby et al., 2002). Of these genes, at least six (*bZIP29*, *bZIP30*, *PosF21*, *bZIP69*, *bZIP52* and *bZIP18*) as well as *VIP1* are strongly expressed in seedlings, roots, shoots and flowers (Tsugama et al., 2014). At least bZIP29, bZIP30, PosF21, bZIP69 and bZIP52 are transiently localized to the nucleus as is VIP1 when cells are exposed to hypo-osmotic stress, and all of them can bind promoter fragments of putative VIP1 target genes, *CYP707A1* and *CYP707A3* (Tsugama et al., 2014, 2016). A *VIP1*

bZIP29 PosF21 triple-knockout line (*vip1-1 bzip29 posf21*) exhibits phenotypes similar to phenotypes of the wild type under a normal growth condition (Lapham et al., 2018). These findings support the idea that these *VIP1* homologs have functional redundancy. VIP1-SRDX is a variant of VIP1 that has the transcriptional repression domain SRDX at the C-terminal end. VIP1-SRDX is expected to repress gene expression mediated by VIP1 and its close homologs if overexpressed in plants. In fact, in VIP1-SRDX-overexpressing plants, some of the putative VIP1 target genes are repressed, and touch-dependent root bending is enhanced. This effect of VIP1-SRDX is suppressed by overexpression of GFP-fused VIP1 (VIP1-GFPox) or VIP1 variants that is constitutively localized to the nucleus (Tsugama et al., 2016, 2019). Expression of SRDX-fused bZIP29 also enhances the touch-induced root bending (Van Leene et al., 2016). These findings support the idea that nuclear-localized VIP1 and its close homologs suppress the touch-induced root bending. However, roles for VIP1 and its close homologs need to be evaluated further.

Here, I show further characterization of the VIP1-mediated mechanical stress responses in Arabidopsis. Main findings are (1) that NDR/LATS-family protein kinases also phosphorylate VIP1, (2) that the PP2A B”-family subunits are indispensable for dephosphorylation of VIP1 *in vitro*, and (3) that VIP1 and its close homologs confer the mechanical stress tolerance in Arabidopsis leaves. The previous findings and those new findings are summarized in Figure 1.

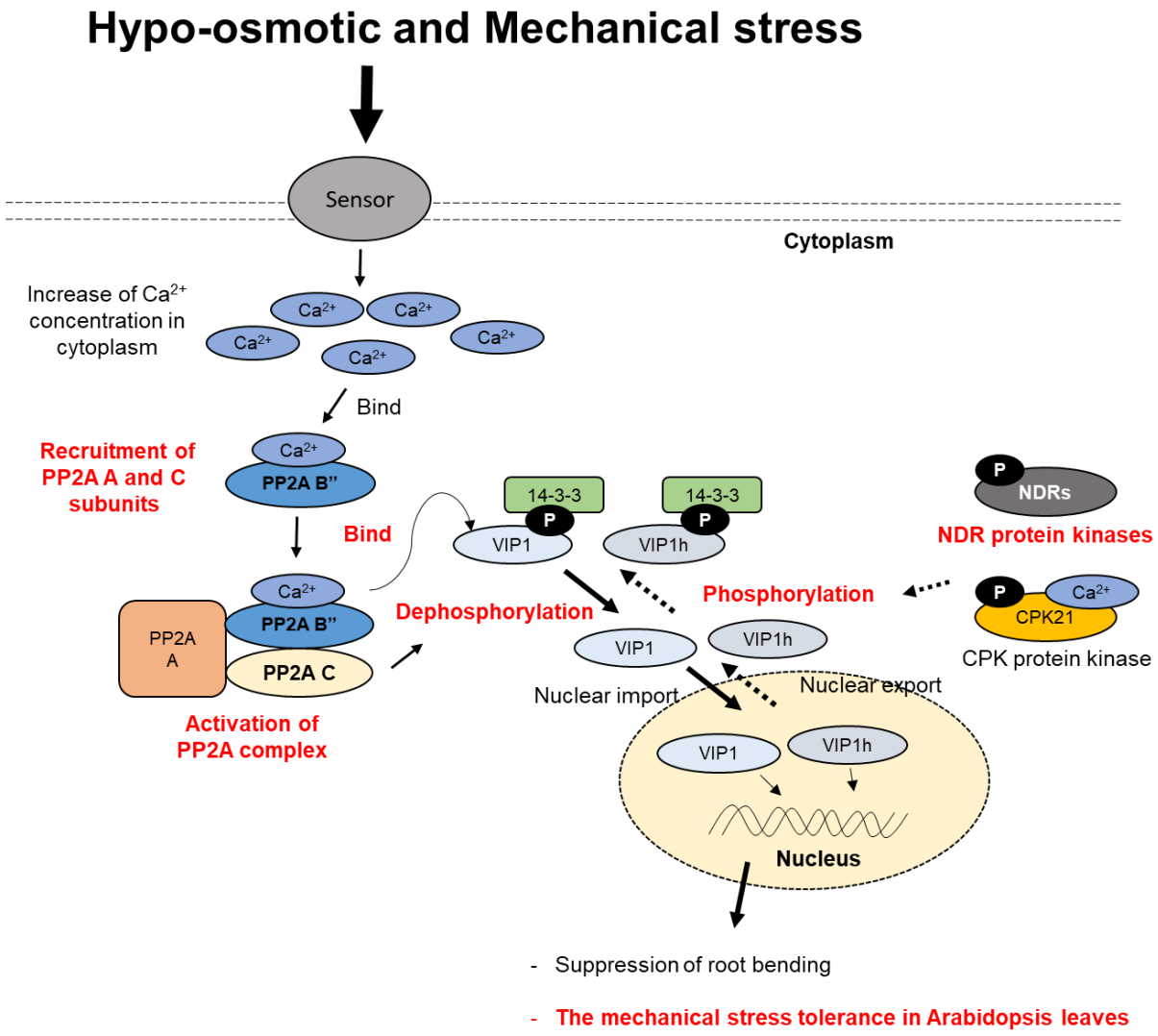

Figure 1. Mechanism of nuclear-cytoplasmic shuttling of VIP1 and its close homologs in response to hypo-osmotic and/or mechanical stress. Arabidopsis cells perceive either hypo-osmotic stress or mechanical stimuli through mechanosensors that induce Ca^{2+} influx into the cytoplasm. This Ca^{2+} influx can cause activation of PP2A B"-family subunits. VIP1 and its close homologs ("VIP1h") can be dephosphorylated by PP2A and localized to the nucleus. VIP1 and its close homologs can be phosphorylated by protein kinases such as CPK21 and localized to the cytoplasm. Findings presented in this dissertation are shown in red.

Chapter 2

NDR/LATS-family protein kinases phosphorylate VIP1 and are essential for embryogenesis

2.1. Introduction

The 35th, 115th, and 151st serine residues (S35, S115, and S151, respectively) of VIP1 are its putative phosphorylation sites and a part of canonical 14-3-3 interaction motifs (Takeo and Ito, 2017; Tsugama et al., 2019). By a motif scanning program, ELM (Kumar et al., 2020), all of these motifs were found to be a part of Hx[RK]xx[ST] (where x is any amino acid, [RK] is either R or K, and [ST] is either S or T), which is the consensus motif for phosphorylation by NDR (nuclear Dbf2-related)/LATS (large tumor suppressor)-family serine/threonine protein kinases (Figure 2.1A). This tempted us to characterize NDR/LATS-family protein kinases in Arabidopsis.

NDR/LATS-family protein kinases belong to the AGC (PK A, G, and C) superfamily and are conserved in eukaryotes including yeast, animals, and plants. Among protein kinases in the AGC superfamily, only NDR/LATS protein kinases require histidine at the beginning of consensus sequences for phosphorylation (Kumar et al., 2020). NDR/LATS-family protein kinases are involved in regulating the cell cycle in the budding yeast *Saccharomyces cerevisiae* (Johnston et al., 1990), the fruit fly *Drosophila melanogaster* (Justice et al., 1995; Xu et al., 1995) and *Homo sapiens* (Nishiyama et al., 1999; Tao et al., 1999). NDR/LATS-family protein kinases in these species can interact with Msp1-one binder (MOB) proteins and can be thereby activated (Millward et al., 1998; Colman-Lerner et al., 2001; Weiss et al., 2002; Bichsel et al., 2004; He et al., 2005; Lai et al., 2005). In *H. sapiens*, two homologous transcriptional coactivators, YAP (Yes-associated protein) and TAZ (transcriptional coactivator with PDZ binding motif), are phosphorylated by an NDR/LATS-family protein kinase, LATS2 (Zhao et al.,

2007; Lei et al., 2008). ASPP1 (apoptosis-stimulating protein of p53-1), a regulator of YAP and TAZ, is also phosphorylated by LATS2 (Aylon et al., 2010; Vigneron et al., 2010). Phosphorylation in those sites in YAP and TAZ promotes interactions between these proteins and 14-3-3 proteins, and thereby retains YAP and TAZ in the cytoplasm to inhibit their functions (Zhao et al., 2007; Lei et al., 2008). This phosphorylation- and 14-3-3 protein-dependent regulation of subcellular localization of YAP and TAZ appears to be comparable to that for VIP1. In contrast, in *S. cerevisiae*, a transcription factor, Ace2, is phosphorylated by an NDR/LATS-family protein kinase, Cbk1, and is retained in the nucleus because the Cbk1-dependent phosphorylation inactivates the Ace2 nuclear export signal (Weiss et al., 2002; Mazanka et al., 2008).

Arabidopsis has eight NDR/LATS-family protein kinase genes, *NDR1-8* (Bögre, et al., 2003). Of these genes, *NDR2*, *NDR4* and *NDR5* are more strongly expressed in pollen grains than in seedlings, leaves, roots and siliques, and an *NDR2 NDR4 NDR5* triple knockout causes male sterility. NDR2, NDR4 and NDR5 interact with two Arabidopsis MOB proteins, MOB1A and MOB1B (Zhou et al., 2021). An *MOB1A* knockout causes a semi-sterile phenotype (Pinosa et al., 2013). An *MOB1A MOB1B* double knockout impairs pollen development (Zhou et al., 2021). These findings suggest that the interactions between those NDR/LATS-family protein kinases and MOB proteins are important for pollen development and/or gametophyte viability in Arabidopsis. However, no other interacting partner of the Arabidopsis NDR/LATS-family protein kinases has been identified. Here, we show that at least NDR2, NDR3, and NDR8 phosphorylate S35 and S115 of VIP1 *in vitro*, and that *NDR4*, *NDR6*, *NDR7*, and *NDR8* are essential for embryogenesis.

2.2. Materials and methods

2.2.1. Plant material and culture conditions

Arabidopsis thaliana ecotype Col-0 was used as the wild-type control for all experiments. Seeds of the lines that have transfer DNA (T-DNA) in *NDR4*, *NDR6*, *NDR7*, and *NDR8* were obtained from the Arabidopsis Biological Resource Center (ABRC, https://abrc.osu.edu/). Stock numbers of them were SALK_035906C, SALK_130076C, SALK_037043C, and SALK_075540C, respectively. These lines were crossed to obtain the lines listed in Table 2.1. To detect T-DNA in these lines, genomic DNA solutions were prepared from cauline leaves of those plants as previously described (Tsugama et al., 2018). PCR was run with these solutions as templates, the KOD FX Neo DNA polymerase (Toyobo, Osaka, Japan), and the primers listed in Table 2.2. Plants were grown for 14 days on an agar medium and further grown on rockwool cubes with regular watering to collect their seeds.

Table 2.1. T-DNA insertion lines used in this study.

Line name	Description
ndr4 (SALK_035906C)	*NDR4* knockout line with T-DNA insertion in the first exon corresponding to the 5' untranslated region of *NDR4*
ndr6 (SALK_130076C)	*NDR6* knockout line with T-DNA insertion in the ninth intron of *NDR6*
ndr7 (SALK_037043C)	*NDR7* knockout line with T-DNA insertion in the first exon corresponding to the 5' untranslated region of *NDR7*
ndr8 (SALK_075540C)	*NDR8* knockout line with T-DNA insertion in the eleventh intron of *NDR8*
ndr47	*NDR4 NDR7* double knockout line obtained by the cross between *ndr4* and *ndr7* plants
ndr68	*NDR6 NDR8* double knockout line obtained by the cross between *ndr6* and *ndr8* plants
ndr467	*NDR4 NDR6 NDR7* triple knockout line obtained by the cross between *ndr47* and

	ndr6 plants
ndr478	*NDR4 NDR7 NDR8* triple knockout line obtained by the cross between *ndr47* and *ndr8* plants
ndr46+-78	Line that is homozygous for T-DNA insertion in *NDR4*, *NDR7* and *NDR8* and that is heterozygous for T-DNA insertion in *NDR6*
ndr4678+-	Line that is homozygous for T-DNA insertion in *NDR4*, *NDR6* and *NDR7* and that is heterozygous for T-DNA insertion in *NDR8*

Table 2.2. Primers used for genomic PCR.

Primer name	Sequence (5' > 3')	Target*
NDR4_G_F	TGACCAAGGAAAGAGAAATGCG	*NDR4*
NDR4_G_R	CCCAACGCCTGCAAATCAAA	*NDR4*
NDR6_G_F	TGCAACGTTGACCATAGGCT	*NDR6*
NDR6_G_R	TCACCATCATCACCAGTGGC	*NDR6* and T-DNA-*NDR6*
NDR7_G_F	TCCGTTCAATCGTGCTGTCA	*NDR7*
NDR7_G_R	ATACGCACAAACACCATGCG	*NDR7*
NDR8_G_F	GACGTCCAAGGACACCAACT	*NDR8* and T-DNA-*NDR8*
NDR8_G_R	CTCTCCATTGCCTCTGCCAA	*NDR8*
T-DNA_LBb1.3	ATTTTGCCGATTTCGGAAC	T-DNA-*NDR6* and T-DNA-*NDR8*

2.2.2 Quantitative reverse transcription-PCR (qRT-PCR)

To analyze expression levels of *NDR1-8*, roots, leaves, flower stalks, and flowers from mature wild-type plants and 10-day-old wild-type seedlings were sampled. Total RNA was extracted from these samples with the NucleoSpin RNA Plant kit (Macherey-Nagel GmbH & Co., Düren, Germany). cDNA was synthesized from 1 μg of the total RNA with the ReverTra

Ace reverse transcriptase (Toyobo, Osaka, Japan) and the oligo (dT)15 primer. Resulting cDNA solutions were diluted 20 times with distilled water and used as PCR templates. qRT-PCR was run with the Step One Real-Time PCR System (Applied Biosystems, Waltham, MA, USA). Primer pairs used are listed in Table 2.3. Relative expression levels were calculated with the comparative cycle threshold method using *UBQ5* as the internal control gene. Experiments were performed with three biological replicates.

Table 2.3. Primer pairs used for qRT-PCR.

Gene		Sequence (5'>3')
NDR1	Fw	TCACCCTTGGTTTAGAGGCAC
	Rv	ATGGACCTGACTTGGCTGAC
NDR2	Fw	AAGTCCCCGGTATAGCCGAA
	Rv	CACGAGGCGTCGGATTAGAA
NDR3	Fw	GCCAAAGCGGCCATCAATTA
	Rv	CGAAACGTGTGGTGGAAGATG
NDR4	Fw	CGATGAGGTGGAGTGTCCAA
	Rv	GTGGAGGTGAAACGCTTCCT
NDR5	Fw	CCTGGAATGGCGGAGTTGAA
	Rv	TTCCCTGAACAACCGGAGGA
NDR6	Fw	GGTTCAAGGATGTTGTGTGGG
	Rv	GCATCTTCCTGGAGAGTCCTG
NDR7	Fw	CGGAACTGAAGCGGAAGAGTA
	Rv	TGGTGATCCGGAAGACCCTC
NDR8	Fw	GCATCCATGGTTCAAAGGCA
	Rv	GGACCAACTTGTGGTGCTTC
UBQ5	Fw	GACGCTTCATCTCGTCC
	Rv	CCACAGGTTGCGTTAG

2.2.3. *In vitro* phosphorylation assays

Coding sequences (CDSs) of NDR2, NDR3, NDR8, and WAG2 were amplified by RT-PCR using KOD FX Neo and the cDNA from the seedlings (see the section 2.2.2 above). The resulting PCR products were cloned into the pMAL-c5E vector (New England Biolabs, Ipswich, MA, USA). Primers and restriction sites used to clone these genes are listed in Table 2.4. The resulting constructs were transformed into the *Escherichia coli* strain BL21 (DE3). Maltose-binding protein (MBP)-fused NDR2 (MBP-NDR2), MBP-fused NDR3 (MBP-NDR3), MBP-fused NDR8 (MBP-NDR8), and MBP-fused WAG2 (MBP-WAG2) as well as GST-fused VIP1 variants were expressed in the *E. coli* cells and purified as previously described (Tsugama et al., 2013, 2019). Purified MBP-fused protein solutions were mixed with purified GST-fused protein solutions, 20 mM $MgCl_2$, 10 mM $CaCl_2$, and 2 mM ATP, and incubated at room temperature for an hour. These reaction mixtures were mixed with 2× SDS sample buffer (125 mM Tris-HCl, pH 6.8, 10% (v/v) 2-mercaptoethanol, 4% (w/v) SDS, 10% (w/v) sucrose, and 0.01% (w/v) bromophenol blue), and incubated for 5 min at 100℃. The solutions were then subjected to SDS-PAGE followed by western blotting. Phosphorylated proteins were detected by western blotting with a phosphorylated protein probe, Phos-tag biotin BTL-104 (Fujifilm Wako, Osaka Japan), according to the manufacturer's instructions. MBP-fused proteins were detected with MBP-tag mAb (Medical & Biological Laboratories Co. Ltd. (MBL), Nagoya, Japan) as a primary antibody and an Anti-mouse IgG (H+L-chain) (MBL) as a secondary antibody. GST-fused proteins were detected with an anti-GST antibody (GE Healthcare, Chicago, IL, USA), SuperSignal West Pico Chemiluminescent Substrate (Thermo Fisher Scientific, Waltham, MA, USA) and an ImageQuant LAS 4000 mini image analyzer (Fuji Film Wako).

Table 2.4. Primers used for *in-vitro* phosphorylation assays.

Primer name	Sequence (5' > 3')*	Restriction sites(pMAL-c5E)
NDR2_CDS_NotI_F	CTGTGCGGCCGCATGGATTCTGCAAGAAGTTGGTTTC	*Not*I
NDR2_CDS_NotI_R	CACCGCGGCCGCGGATCCTACTCAGAATCTAGACGTCTCAG	
NDR3_CDS_NotI_F	CTGTGCGGCCGCATGGATACTGCCAGAGCATGGC	*Not*I
NDR3_CDS_NotI_R	AGGAGCGGCCGCGGATCCTTAGGATGTGGCATTGTCGAAACG	
NDR8_CDS_NotI_F	AAGAGCGGCCGCATGGACGGCGCCGATGGAACCGTTCG	*Not*I
NDR8_CDS_NotI_R	CCCTGCGGCCGCGGATCCTATGTCTTGTGGTTTAACTCACC	
WAG2_CDS_NcoI_F	CCCTCTAGAGCCATGGAACAAGAAGATTTCTATTTC	*Nco*I and *Sal*I
WAG2_CDS_SalI_R	CCCGTCGACCAACGCGTTTGCGACTCGCGTAGC	

2.2.4. Accession numbers and a phylogenetic analysis

Details about the sequences of the genes used in this chapter are available with the following Arabidopsis Genome Initiative accession numbers: AT4G14350 (*NDR1*), AT1G03920 (*NDR2*), AT3G23310 (*NDR3*), AT2G19400 (*NDR4*), AT2G20470 (*NDR5*), AT4G33080 (*NDR6*), AT1G30640 (*NDR7*), AT5G09890 (*NDR8*), AT3G14370 (*WAG2*), AT4G04720 (*CPK21*), AT3G62250 (*UBQ5*) and AT1G43700 (*VIP1*). A phylogenetic tree was generated on NGPhylogeny.fr (https://ngphylogeny.fr/) (Lemoine et al., 2019) with the amino acid sequences of NDR1-8 and CPK21 as input.

2.3. Results

2.3.1. NDR2, NDR3 and NDR8 phosphorylate VIP1 *in vitro*

Phos-tag biotin detected GST-fused VIP1 (GST-VIP1) when GST-VIP1 was reacted with MBP-NDR2, MBP-NDR3, or MBP-NDR8 *in vitro*, but did not when GST-VIP1 was reacted with MBP-fused WAG2, an Arabidopsis AGC superfamily protein kinase that does not belong to the NDR/LATS family (Figure 2.1B, C). Phos-tag biotin detected GST-fused N-terminal region of VIP1 (1-186 amino acids of VIP1, GST-VIP1N) as strong signals when GST-VIP1N was reacted with MBP-NDR8 but detected GST-fused C-terminal region of VIP1 (165-341 amino acids of VIP1, GST-VIP1C) as weaker signals (Figure 2.1D). GST-fused VIP1 S35 115A, where VIP1 S35 and S115 are both substituted by alanine, was hardly detected by Phos-tag biotin when reacted with either MBP-NDR3 or MBP-NDR8 (Figure 2.1E). These results suggest that VIP1 S35 and S115 can be phosphorylated by the NDR/LATS-family protein kinases *in vitro*.

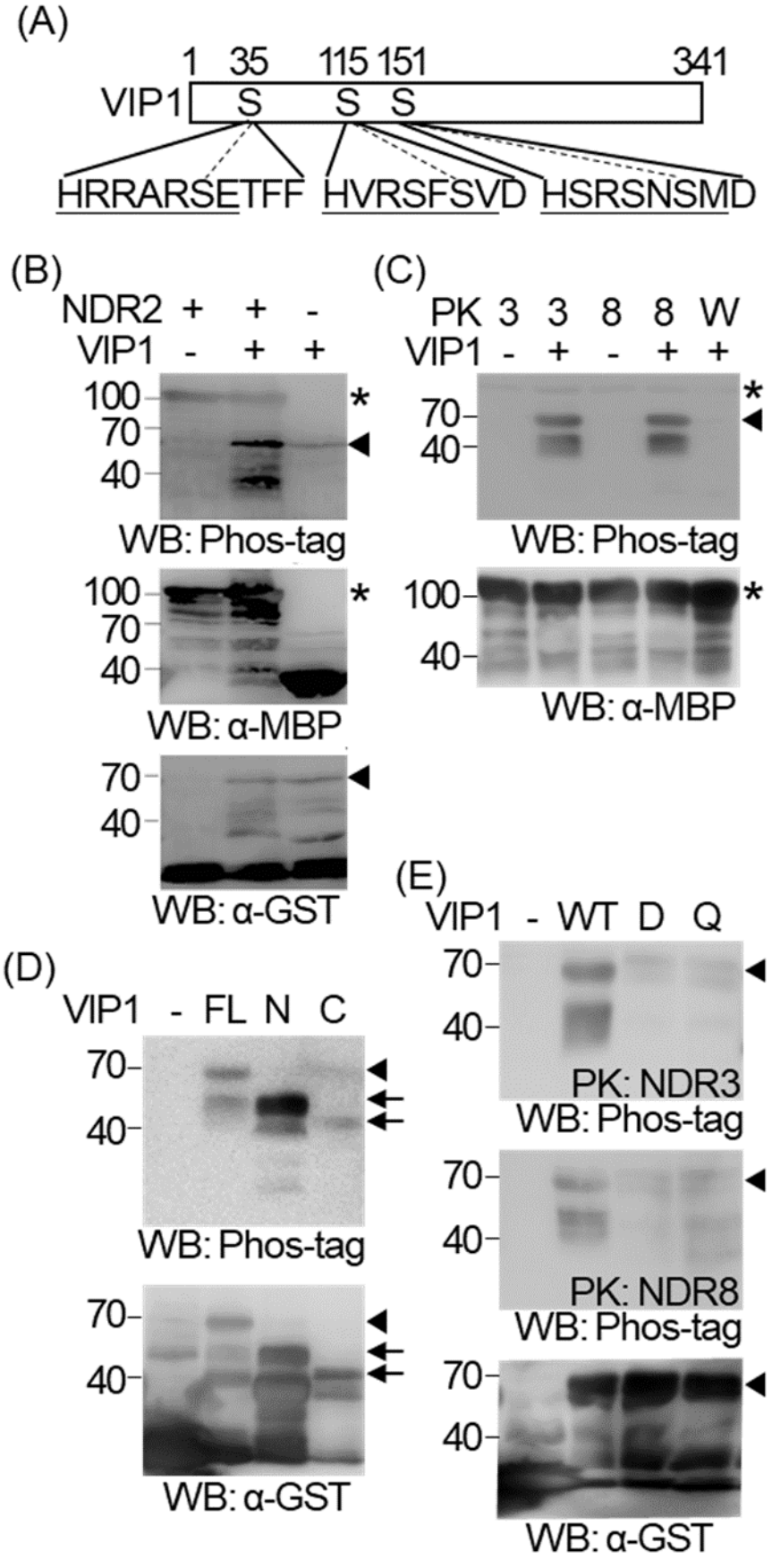
(A)
1 35 115 151 341
VIP1 S S S
HRRARSETFF HVRSFSVD HSRSNSMD
(B)
NDR2 + + -
VIP1 - + +
100
70
40
*
WB: Phos-tag
WB: α-MBP
WB: α-GST
(C)
PK 3 3 8 8 W
VIP1 - + - + +
WB: Phos-tag
WB: α-MBP
(D)
VIP1 - FL N C
WB: Phos-tag
WB: α-GST
(E)
VIP1 - WT D Q
PK: NDR3
WB: Phos-tag
PK: NDR8
WB: Phos-tag
WB: α-GST

Figure 2.1. NDR2, NDR3, and NDR8 phosphorylate VIP1 *in vitro*. (A) VIP1 contains putative NDR/LATS-family protein kinase phosphorylation sites. Amino acid positions in VIP1 are indicated at the top. S35, S115, S151 and their flanking sequences are presented at the bottom. The Hx[RK]xx[ST] consensus sequence for NDR/LATS-family protein kinase phosphorylation is underlined. (B-E) *In-vitro* phosphorylation assays with MBP-fused protein kinases and GST-VIP1. The proteins were analyzed by western blotting with Phos-tag biotin, an anti-MBP antibody or an anti-GST antibody ("WB: Phos-tag", "WB: α-MBP" or "WB: α-GST", respectively). Arrowheads indicate positions of GST-VIP1. Asterisks indicate positions of the MBP-fused protein kinases. The numbers on the left side of the images indicate molecular mass. The experiments were performed three times and a representative result is presented. (B) NDR2 phosphorylates VIP1 *in vitro*. MBP-NDR2 and GST-VIP1, which are indicated as "NDR2" and "VIP1", respectively, in the figure, were reacted, and analyzed by western blotting. The presence and absence of these proteins in the reaction mixtures are indicated as '+' and '-', respectively. For "NDR2 -", MBP alone was used instead of MBP-NDR2. For "VIP1 -", GST alone was used instead of GST-VIP1. (C) NDR3 and NDR8 also phosphorylate VIP1 but WAG2 does not. MBP-NDR3, MBP-NDR8 or MBP-WAG2, which is indicated as "3", "8" or "W", respectively, in the figure, was reacted with GST-VIP1, and these proteins were analyzed by western blotting. The presence and absence of GST-VIP1 in the reaction mixtures are indicated as '+' and '-', respectively. For "VIP1 -", GST alone was used instead of GST-VIP1. (D) NDR8 phosphorylates VIP1N yet hardly VIP1C. GST-VIP1, GST-VIP1N or GST-VIP1C, which is indicated as "FL", "N" or "C", respectively, in the figure, was reacted with MBP-NDR8, and analyzed by western blotting. For "VIP1 -", GST alone was used. Arrows indicate positions of GST-VIP1N and GST-VIP1C. (E) NDR3 and NDR8 phosphorylate S35 and S115 of VIP1. GST-VIP1, GST-VIP1D (GST-fused VIP1 variant that has Ser → Ala substitutions at the amino acid positions 35 and 115 of VIP1) or GST-VIP1Q (GST-fused VIP1 variant that has Ser → Ala substitutions at the amino acid positions 35, 115, 149 and 151 of VIP1), which is indicated as "WT", "D" or "Q", respectively, in the figure, was reacted with either MBP-NDR3 (for the top panel, "PK: NDR3") or MBP-NDR8 (middle, "PK: NDR8"), and analyzed by western blotting. For "VIP1 -", GST alone was used. For the panels B-E, experiments were performed three times, and a representative result is shown.

2.3.2. Transcript levels of *NDR1-8* in Arabidopsis tissues

In qRT-PCR, expression of *NDR1-8* was detected in seedlings, rosette leaves, roots, flower stalks and flowers. *NDR1*, *NDR3*, *NDR4*, *NDR6*, *NDR7*, and *NDR8* were expressed strongly in rosette leaves and flower stalks, and weakly in the other tissues. *NDR2* was expressed strongly in flower stalks and weakly in the other tissues. *NDR5* was expressed strongly in flowers and weakly in the other tissues (Figure 2.2).

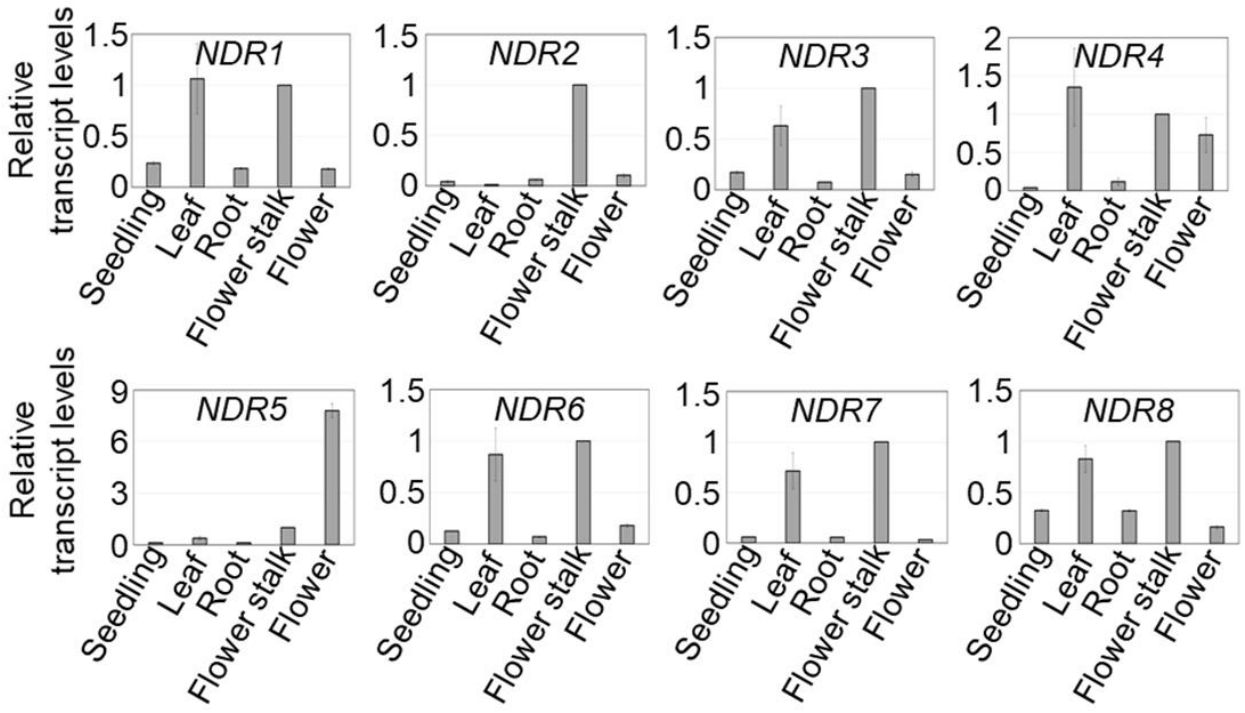

Figure 2.2. Expression levels of *NDR1-8* in various Arabidopsis tissues. Relative expression levels of *NDR1-8* were analyzed by quantitative RT-PCR using *UBQ5* as the internal control gene. Data are means ± SD of three biological replicates.

2.3.3. An *NDR4 NDR6 NDR7 NDR8* quadruple knockout causes embryonic lethality

Arabidopsis mutant lines where two or three of *NDR4 NDR6 NDR7* and *NDR8* were knocked out by T-DNA insertion were generated (Table 2.1 and Figure 2.3). These lines exhibited no defects in germination and grew just as the wild type under a normal growth condition. However, although selfing *ndr46+-78* plants is expected to generate *ndr46--78* (i.e., *NDR4 NDR6 NDR7 NDR8* quadruple-knockout), *ndr46+-78* and *ndr46++78* (i.e., *ndr478*) plants in the 1:2:1 ratio in the progeny, the numbers of these plants obtained were 0, 50 and 25, respectively. If an *NDR4 NDR6 NDR7 NDR8* quadruple-knockout causes lethality in either female or male gametes, the ratio of *ndr46--78*, *ndr46+-78* and *ndr46++78* plants is expected to be 0:1:1. If such a quadruple knockout causes embryonic (i.e., post-fertilization) lethality, the ratio of *ndr46--78*, *ndr46+-78* and *ndr46++78* plants is expected to be 0:2:1. The observed numbers of these plants (0, 50 and 25, respectively, as described above) could be different from the 0:1:1 ratio on the basis of a χ^2 test (P = 0.0039) but were consistent with the 0:2:1 ratio. Similarly, selfing *ndr4678+-* plants generated no *ndr4678--* (i.e., *NDR4 NDR6 NDR7 NDR8* quadruple knockout) plants, 48 *ndr4678+-* plants and 24 *ndr4678++* (i.e., *ndr467*) plants. These numbers (0, 48 and 24) could be different from the 0:1:1 ratio (P = 0.0047 in the χ^2 test) but were consistent with the 0:2:1 ratio. These results suggest that an *NDR4 NDR6 NDR7 NDR8* quadruple knockout does not cause gametophytic lethality but does cause embryonic lethality.

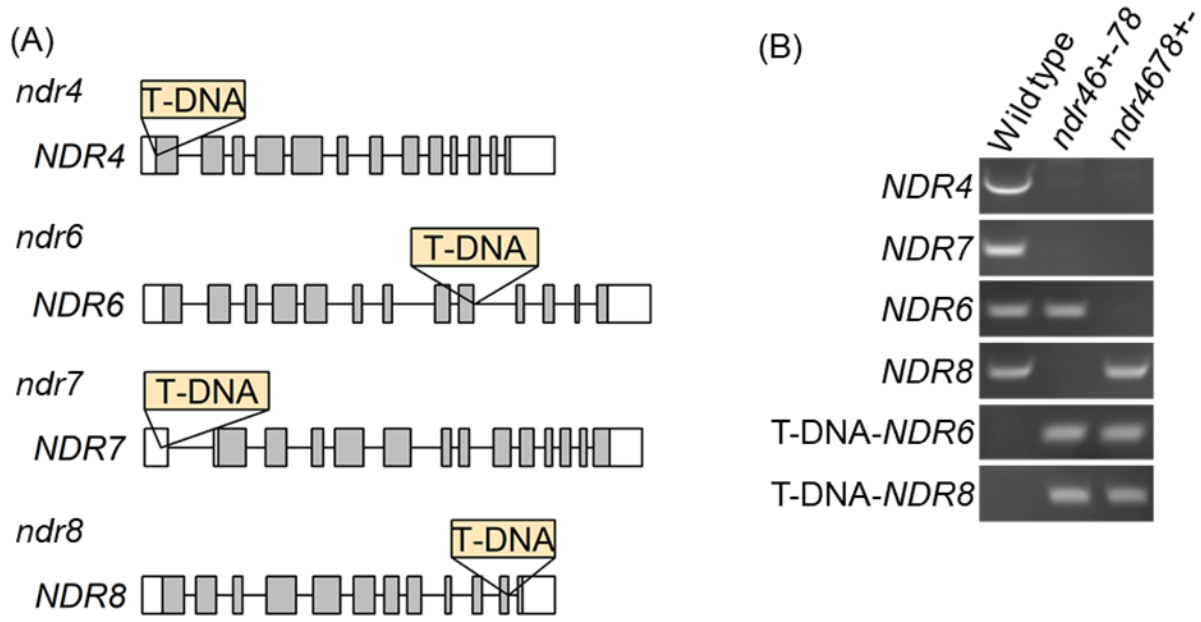

Figure 2.3. T-DNA insertion lines for *NDR4, NDR6, NDR7,* and *NDR8*. (A) T-DNA insertion positions in *NDR4*, *NDR6*, *NDR7*, and *NDR8*. Boxes indicate exons. White and grey regions in the boxes indicate untranslated regions and CDSs, respectively. (B) Genomic PCR analyses of T-DNA insertion in *ndr46+-78* and *ndr4678+-* plants. For "T-DNA-*NDR6*", T-DNA and its flanking sequence with *NDR6* were analyzed. For "T-DNA-*NDR8*", T-DNA and its flanking sequence with *NDR8* were analyzed.

2.4. Discussion

Our data indicate that at least NDR2, NDR3, and NDR8 can phosphorylate VIP1 *in vitro* but WAG2 cannot (Figure 2.1C). This supports the idea that, as animal and yeast NDR/LATS-family protein kinases (Kumar et al., 2020), plant NDR/LATS-family protein kinases differ in substrate specificity from the other plant AGC protein kinases. On the other hand, even though CPK21 is not an AGC protein kinase, it can also phosphorylate VIP1 *in vitro* (Tsugama et al., 2019). In human, the activity of Ndr, an NDR/LATS-family protein kinase, is increased in the presence of the PP2A inhibitor okadaic acid, raising the possibility that activities of NDR/LATS-family protein kinases are inhibited by PP2A (Millward et al., 1999). A human PP2A B-family B subunit, PR55α, is thought to be responsible for the PP2A-dependent inhibition of NDR/LATS-family protein kinases (Hein et al., 2019). Although the PP2A complex responsible for the VIP1 dephosphorylation is thought to contain the B''-family subunit but not the B-family subunit (Tsugama et al., 2019), it is interesting that PP2A can be involved in regulating both VIP1 and NDR/LATS-family protein kinases. Further studies are necessary to elucidate how the substrate specificity of CPK21 and plant NDR/LATS-family protein kinases is determined.

The *NDR4 NDR6 NDR7 NDR8* quadruple knockout was shown to cause embryogenic lethality. NDR4, NDR6, and NDR8 are phylogenetically closer to each other than to the other NDR/LATS-family protein kinases in Arabidopsis (i.e., NDR1, NDR2, NDR3, NDR5, and NDR7) (Zhou et al., 2021; Figure 2.4). The expression level of *NDR4* as well as the expression levels of *NDR2* and *NDR5* is higher in pollen grains than in other tissues, whereas the expression levels of the other NDR/LATS-family protein kinase genes are high in leaves and other vegetative tissues (Zhou et al., 2021; Figure 2.2). Together, it is likely that, although at least NDR2, NDR3, and NDR8 can phosphorylate VIP1 *in vitro* (Figure 2.1), NDR6, NDR7, and NDR8 differ in physiological roles from the other NDR/LATS-family protein kinases. VIP1 is

unlikely involved in the embryogenic lethality caused by the *NDR4 NDR6 NDR7 NDR8* quadruple knockout. This is because, although the *NDR4 NDR6 NDR7 NDR8* quadruple knockout is expected to promote the nuclear localization of VIP1, overexpression of nuclear-localized variants of VIP1 do not cause embryonic lethality (Tsugama et al., 2014; Takeo and Ito, 2017). MOB1A and MOB1B both interact with NDR2, NDR4 and NDR5 in the cytosol and are thought to be involved in regulating pollen development (Zhou et al., 2021). *MOB1A* and *MOB1B* are both expressed in vegetative tissues and also regulate vegetative growth (Pinosa et al., 2013). Thus, MOB1A and MOB1B may also be involved in the NDR4-, NDR6-, NDR7- and NDR8-dependent regulation of embryogenesis. Previous proteome analyses detected NDR1, NDR2, and NDR3 in both the plasma membrane and the cytosol, and NDR8 in the cytosol (Benschop et al., 2007, De la Fuente van Bentem et al., 2008). Thus, plasma membrane-localized proteins as well as cytosolic proteins such as MOB1A and MOB1B can be the embryogenesis regulators under the control of the NDR/LATS-family protein kinases. Further studies are necessary to identify such proteins and to elucidate physiological functions of plant NDR/LATS-family protein kinases.

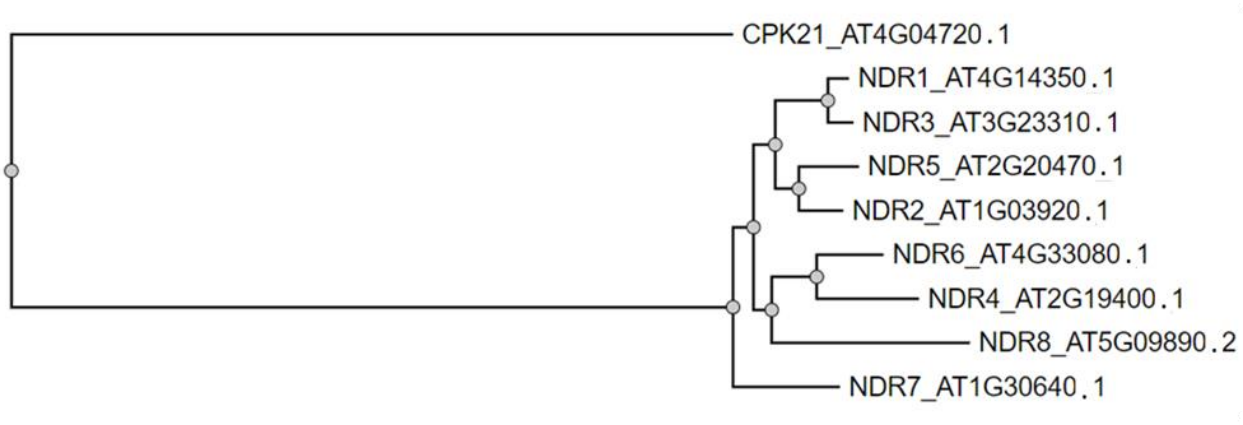

Figure 2.4. A rooted phylogenetic tree of NDR1-8. The tree was generated on NGPhylogeny.fr (https://ngphylogeny.fr/) using NDR1-8 and CPK21 amino acid sequences. CPK21 was used as an outgroup.

Chapter 3

The B”-family subunits of protein phosphatase 2A are indispensable for dephosphorylation of VIP1 *in vitro*

3.1. Introduction

PP2A is a serine/threonine protein phosphatase and acts as a heterotrimeric holoenzyme complex consisting of a scaffolding A subunit, a regulatory B subunit, and a catalytic C subunit (Janssens and Goris, 2001; Farkas et al., 2007; País et al., 2009). Arabidopsis has three PP2A A subunit genes, 17 PP2A B subunit genes, and five PP2A C subunit genes (Ballesteros et al., 2013). Substrate specificity of PP2A holoenzyme is determined by its B subunit (Farkas et al., 2007). Members of the B subunit are grouped into B, B’, B”, and B’’’ families based on their conserved domains (Farkas et al., 2007; País et al., 2009). PP2A therefore has broad substrate specificity and diverse roles in Arabidopsis (Farkas et al., 2007; País et al., 2009; Ballesteros et al., 2013). For example, a mutant lacking *ROOTS CURL IN NAPHTHYLPHTHALAMIC ACID1* (*RCN1*), which is one of the three PP2A A subunit genes, displays defects in root gravitropism (Rashotte et al., 2001; Xi et al., 2016) and abscisic acid (ABA) responses during germination (Kwak et al., 2002; Waadt et al., 2015). A mutant that lacks two PP2A C subunit genes, *PP2A-C3* and *PP2A-C4*, shows altered auxin distribution and growth defects (Ballesteros et al., 2013). A mutant lacking another PP2A C subunit gene, *PP2A-C5*, shows root growth retardation under a salinity-stressed condition (Hu et al., 2017; Sun et al., 2018). PP2A B”-family subunits have Ca^{2+}-binding EF-hand motifs and comprise six members, AtB”α-ε, and FASS (also known as “TONNEAU2” or “EMBRYO DEFECTIVE 40”), in Arabidopsis (Farkas et al., 2007; Leivar et al., 2011). AtB”α and AtB”β bind and regulate the activity of the enzyme 3-hydroxy-3-methylglutaryl-CoA reductase (HMGR), which is involved in the mevalonate pathway for

isoprenoid biosynthesis (Leivar et al., 2011). A mutant lacking *AtB"α* grows better than the wild type under salinity-stressed conditions (Leivar et al., 2011).

AtB"α and AtB"ε can both interact with bZIP29 (Van Leene et al., 2016). FASS and AtB"δ can both interact with VIP1, and VIP1 dephosphorylation in Arabidopsis is inhibited by either okadaic acid or cantharidin (Tsugama et al., 2019). These findings support the idea that PP2A regulates VIP1 and other group I bZIP proteins. However, it is unclear whether the PP2A B" subunits are involved in plant mechanical stress responses and/or the dephosphorylation of VIP1.

Here, PP2A B"-family subunits are shown to be indispensable for dephosphorylation of VIP1 *in vitro* and that PP2A B"-family subunits have functional redundancy.

3.2. Materials and methods

3.2.1. Plant materials and growth conditions

Arabidopsis ecotype Col-0 was used as the wild-type control in all experiments. *rcn1-6* (SALK_059903, an *RCN1* knockout line) was obtained from ABRC. To generate the quadruple-knockout mutant for PP2A B"-family subunit genes, seeds of *atb"α* (SALK_135978C, an *ATB"α* knockout line), *atb"β-1* (SAIL_1233_B02.V1, *ATB"β* knockout), *atb"γ* (SALK_032713C, *ATB"γ* knockout), and *atb"δ* (SALK_051304, *ATB"δ* knockout) were obtained from ABRC. Seeds were surface-sterilized with 10% (v/v) HClO solution with 0.05% (v/v) Tween 20, chilled at 4℃ for 3 days, and sown on the MS agar medium (0.8% (w/v) agar, 0.5× MS salts, 1 % (w/v) sucrose and 0.5 g l^{-1} MES, pH 5.8). Plants were grown at 22℃ with the 16-h light/8-h dark photoperiod. Plants were grown for 14 days on an agar medium and further grown on rockwool cubes with regular watering.

atb"β-1 and *atb"γ* were crossed to obtain the *atb"β-1 atb"γ* (*atb"βγ*) double-knockout

mutant. *atb"α* and *atb"δ* were crossed to obtain the *atb"α atb"δ* (*atb"αδ*) double-knockout mutant. The *atb"β atb"γ* mutant and the *atb"α atb"δ* mutant were crossed to obtain the *atb"α atb"β atb"γ atb"δ* (*atb"αβγδ*) quadruple-knockout mutant. T-DNA insertions in these mutant lines were confirmed by genomic PCR with KOD FX Neo (Toyobo) and primer pairs listed in Table 3.1.

To express the VIP1-GFP in *AtB"β AtB"δ* double-knockout background, *atb"β-2* (SALK_151964) was obtained from ABRC and crossed with either a transgenic line overexpressing VIP1-GFP in the wild-type background (VIP1-GFPox/WT) (Tsugama et al., 2012a) or a line overexpressing VIP1-GFP in the *atb"δ* background (VIP1-GFPox/*atb"δ*) (Tsugama et al., 2019) as the pollen parents. The resulting F2 and F3 plants were subjected to GFP detection with a BX50 epifluorescence microscope (Olympus, Tokyo, Japan) as described previously (Tsugama et al., 2012a). These plants were also subjected to genomic PCR with KOD FX Neo (Toyobo) and primer pairs in Table 3.1 to examine T-DNA insertions in *AtB"β* and *AtB"δ* and to select plants expressing VIP1-GFP in either the *atb"β* background (VIP1-GFPox/*atb"β*) or the *atb"βδ* background (VIP1-GFPox/*atb"βδ*).

To examine root vertical growth indices (VGIs), wild-type, VIP1-SRDXox #7, *rcn1-6*, and *atb"αβγδ* plants were grown for 5 days on an agar medium (1.6% (w/v) agar, 0.5× MS salts, 1 % (w/v) sucrose and 0.5 g l^{-1} MES, pH 5.8) tilted at a 75° as described previously (Tsugama et al., 2016). Five-day-old seedlings were photographed, and then the lengths of the primary roots and the lengths of vertical projections from those roots were measured by ImageJ software (Schneider et al., 2012). To obtain root VGIs, the vertical projection lengths were divided by the primary root lengths as previously described (Grabov et al., 2005).

To examine plant responses to Ca^{2+} deficiency, plants were grown on the MS agar

medium lacking $CaCl_2$. To examine plant responses to ABA or abiotic stress, plants were grown on the MS agar medium supplemented with 1 μM ABA, 100 mM NaCl or 200 mM mannitol.

Table 3.1. Primer pairs used for genotyping.

Primers	Sequence (5'>3')
gDNA bppa(670)_Fw	GCTTCCCGGTTTGTCTCCTG
gDNA bppa(1600)_Rv	CAACTGTCAAGCAAGGTAGTGC
atbppb_gDNA(338)Fw	AGCCGCTGTTGTCGAATTTTG
atbppb_gDNA(1337)Rv	AGGCAGCTTGCAGACTTGT
atbppg_gDNA(502)Fw	CCGGACGGTAACACAACGAA
atbppg-gDNARv	CATGCTGCATTGCGTCAACTA
atbppd_gDNA(1019)Fw	TGACAATGATGCCTTAGGTGGT
atbppd_gDNA(2300)Rv	AGTACATCATACCAAAGTGGCA
gDNA rcn1-6_Fw	GTCAAGTACCTCACCTATAAC
gDNA rcn1-6_Rv	CATAGCCAGCAACCAAAATGG
T-DNA_LBTR3	CAGCTGTTGCCCGTCTCACTGG
pp2abppb-2g_F	TCATTTCCTGCCTCTGGACC
pp2abppb-2g_R	ACTGGTTTGAAGTCTGCCTGT
pDAP101LB1	GCCTTTTCAGAAATGGATAAATAGCCTTGCTTCC

3.2.2 qRT-PCR

To analyze expression levels of *AtB"α-ε* and *FASS*, roots, leaves, flower stalks, and flowers from matured wild-type plants and 10-day-old wild-type seedlings were sampled. RNA extraction, cDNA synthesis, and qRT-PCR were performed as described above in the section 2.2.2. Standard curves were obtained with the pGADT7-Rec constructs with the PP2A B"-family subunit genes (see the section 3.2.4 below) and were used to obtain the absolute expression

levels of *AtB"α-ε* and *FASS*. *UBQ5* was used as the internal control gene to normalize those expression levels. Primer pairs are listed in Table 3.2.

Table 3.2. Primer pairs used for qRT-PCR.

Genes		Sequence (5'>3')
AtB"α	Fw	AACCCGTGACCCTTTTCTCA
	Rv	ACTTCCTCCACATCTTCCTCCA
AtB"β	Fw	CCGAGAAGGAGAACTGTATCAC
	Rv	CTGAGCAAATCGATCCCACT
AtB"γ	Fw	GAAACGCGTGATCCCTTCCT
	Rv	AGTCGTCCCATGCTTCAGCA
AtB"δ	Fw	AGAGAACCCTACATTGACAGAT
	Rv	AAAGGGAGCCTCCAGCGACGAC
AtB"ε	Fw	CGAGAACCCGACATTGACAGAC
	Rv	GAAGGGAGCCTCCAGTGACGAG
FASS	Fw	GACGAGATCTGGGACATGGT
	Rv	GAAGGTTCTCACGGTTGTCATG
UBQ5	Fw	GACGCTTCATCTCGTCC
	Rv	CCACAGGTTGCGTTAG

3.2.3. Subcellular localization of VIP1-GFP

VIP1-GFPox/WT, VIP1-GFPox/*atb"β*, VIP1-GFPox/*atb"δ*, and VIP1-GFPox/*atb"βδ* plants were grown on the MS agar medium for seven days. Resulting seedlings were either submerged in distilled water or touched with tweezers. Signals of VIP1-GFP in their roots were detected with the BX50 fluorescence microscope as described previously (Tsugama et al., 2012a). Images were processed with ImageJ.

3.2.4. Yeast two-hybrid (Y2H) assays

For Y2H assays, the CDSs of RCN1, PP2A-A2, PP2A-C3, PP2A-C5, AtB”α, AtB”β, PosF21C (172-398 amino acids of PosF21, which contain its bZIP domain), bZIP29C (364-553 amino acids of bZIP29, which contain its bZIP domain), and bZIP30C (341-525 amino acids of bZIP30, which contain its bZIP domain) were amplified by the RT-PCR with leaf cDNA (see the section 3.2.2 above) and cloned into pGBKT7 vector, generating pGBK-RCN1, pGBK-PP2A-A2, pGBK-PP2A-C3, pGBK-PP2A-C5, pGBK-AtB”α, pGBK-AtB”β, pGBK-PosF21C, pGBK-bZIP29C, and pGBK-bZIP30C, respectively. The CDSs of AtB”α-ε, and FASS were also amplified by the RT-PCR and cloned into pGADT7-Rec, generating pGAD-AtB”α-ε, and pGAD-FASS. Primers and restriction sites used to generate these constructs are shown in Table 3.3. pGBKT7 constructs with AtB”δ, FASS and VIP1C (165-341 amino acids of VIP1, which contain its bZIP domain) (pGBK-AtB”δ, pGBK-FASS and pGBK-VIP1C, respectively) and the pGADT7-Rec construct with CDSs of VIP1FL (native, full-length version with 341 amino acids), VIP1N (1-186 amino acids of VIP1, which contain its phosphorylation sites), and VIP1C were prepared as previously described (Tsugama et al., 2019). The yeast strain AH109 was co-transformed with one of the pGBKT7 constructs and one of the pGADT7 constructs as previously described (Tsugama et al., 2014). At least four colonies of the transformed yeast cells for each combination of the constructs were streaked on a moderately-stringent selection medium (triple-dropout medium (TDO), which lacks leucine, tryptophan, and histidine and which was supplemented with 5 mM 3-amino-1,2,4-triazole (3-AT, a histidine biosynthesis inhibitor)) and highly stringent selection medium (quadruple-dropout medium (QDO), which lacks leucine, tryptophan, histidine, and adenine) as previously described (Yoon et al., 2020). These transformed yeast cells were then incubated for 5 days at 28°C, and photographed. The images were processed by GIMP and ImageJ.

Table 3.3. Primer pairs used for Y2H assay.

Gene (Restriction sites)		Sequence (5'>3')	Vectors (Restriction sites)
AtB"α	Fw	GGGAGATCT**CCATGG**AAATCGATGGTGGAAACG	pGADT7-Rec
(NcoI-BglII)	Rv	GGG**AGATCT**AAAATGGAGATTCGAGTGG	(NcoI-BamHI)
AtB"β	Fw	GAG**CATATG**GATATTGACGGAGTAGACG	pGADT7-Rec
(NdeI-BglII)	Rv	GGG**AGATCT**AAAATGGAGGTTCGAGTGG	(NdeI-BamHI)
AtB"γ	Fw	CTC**CATATG**GAGTCGATAACGTTAGATATAGAGC	pGADT7-Rec
(NdeI-XhoI)	Rv	CG**CTCGAG**AAAAGGGGACCTCAAGTGAGTCGTC	(NdeI-XhoI)
AtB"δ	Fw	GGG**CCATGG**TGGATACGGTTATTCCCGGAGATAT	pGADT7-Rec
(NdeI-XhoI)	Rv	GGG**CTCGAG**TCAAAAGGGAGCCTCCAGCGACG	(NdeI-XhoI)
AtB"ε	Fw	CCA**CCATGG**TGGATACGGTTATTCCCGGAGATAT	pGADT7-Rec
(NcoI-XhoI)	Rv	GG**CTCGAG**GAAGGGAGCCTCCAGTGACGAGTCAT	(NdeI-XhoI)
FASS	Fw	GAG**GAATTC**ATGTATAGCGGATCTAGCGATG	pGADT7-Rec
(EcoRI-SalI)	Rv	GAG**GTCGAC**TCACTGAGACTCTTCCTCAGG	(EcoRI-XhoI)
AtB"α	Fw	GGGAGATCT**CCATGG**AAATCGATGGTGGAAACG	pGBKT7
(NcoI-BglII)	Rv	GGG**AGATCT**AAAATGGAGATTCGAGTGG	(NcoI-BamHI)
AtB"β	Fw	GAG**CATATG**GATATTGACGGAGTAGACG	pGBKT7
(NdeI-BglII)	Rv	GGG**AGATCT**AAAATGGAGGTTCGAGTGG	(NdeI-BamHI)
RCN1	Fw	GGG**CTCGAG**CCATGGCTATGGTAGATGAACCG	pGBKT7
(XhoI)	Rv	CTC**CTCGAG**CGGATTGTGCTGCTGTGGAACC	(SalI)
PP2A-A2	Fw	GGG**CTCGAG**CCATGTCTATGATCGATGAGCCG	pGBKT7
(XhoI-SalI)	Rv	CCC**GTCGAC**CGCTAGACATCATCACATTGTC	(SalI)
PP2A-C3	Fw	GGG**CTCGAG**CCATGGGCGCGAATTCTATTCCG	pGBKT7
(XhoI)	Rv	CCT**CTCGAG**CCAGGAAATAGTCTGGAGTCC	(SalI)
PP2A-C5	Fw	GGG**CTCGAG**CCATGCCGCCGGCGACCGGAGA	pGBKT7
(XhoI-SalI)	Rv	GAG**GTCGAC**CATCTGGAGTCTTGCGAGTGG	(SalI)
PosF21	Fw	GGT**GAATTC**ATGCTTATGTCGGGAAATGAAGA	pGBKT7
(EcoRI-BamHI)	Rv	CCC**GGATCC**AGTTCTCTTTCTGGGCTTGTGAA	(EcoRI-BamHI)
bZIP29	Fw	GGT**GAATTC**AGCATCGAGTTCAATAACGGTGA	pGBKT7
(EcoRI-BamHI)	Rv	CCC**GGATCC**ATTCATTTGATTCAGATTTTGTTGC	(EcoRI-BamHI)
bZIP30	Fw	GGT**GAATTC**AGTGTTGAATTTGGAAACAGTGA	pGBKT7
(EcoRI-BamHI)	Rv	CCC**GGATCC**AGTCGTTTGAAGTGTGCTTTGCTTT	(EcoRI-BamHI)

3.2.5. *In-vitro* pull-down assays

The CDSs of the PP2A B”-family subunits (AtB”α-ε and FASS respectively), PP2A-C3, and RCN1 were amplified by RT-PCR as described above in the section 3.2.2, and inserted into the pRSETB vector (Thermo Fisher Scientific) and the pGEX-6P-3 vector (GE Healthcare). Primers and restriction sites used are shown in Table 3.4. To examine Ca^{2+} effects on interactions between PP2A B”-family subunits and PP2A A subunits, His-tagged AtB”γ (His-AtB”γ) and His-tagged AtB”δ (His-AtB”δ) were expressed in BL21 (DE3) and purified with the Ni-NTA agarose (Qiagen) as previously described (Tsugama et al., 2019). Either GST alone or GST-fused RCN1 (GST-RCN1) was fixed on the Glutathione Sepharose 4B resin (GE Healthcare) and washed three times with Tris-buffered saline with Tween-20 (TBST: 150mM NaCl and 20 mM Tris-HCl, pH 7.5 with 0.1% (v/v) Tween-20) according to the manufacturer’s instructions. The resin was resuspended in a solution with purified His-AtB”γ or purified His-AtB”δ. Either $CaCl_2$ or EGTA was added to the solution to make 10 mM final concentration. The solution and resin were incubated at room temperature for an hour. The resin was precipitated by brief centrifugation, washed three times with TBST, resuspended in 2× SDS sample buffer, and incubated for 5 min at 100℃. The supernatant was then subjected to SDS-PAGE followed by western blotting. His-tagged proteins and GST-fused proteins were detected by western blotting with an anti-GST antibody (GE Healthcare), HisProbe-HRP (Thermo Fisher Scientific), SuperSignal West Pico Chemiluminescent Substrate (Thermo Fisher Scientific) and an ImageQuant LAS 4000 mini image analyzer (Fuji Film). To examine Ca^{2+} effects on interactions between PP2A C subunits and a PP2A A subunit, Myc-tagged PP2A-C3 (Myc-PP2A-C3) or Myc-tagged PP2A-C5 (Myc-PP2A-C5) was expressed *in vitro* by the TNT Quick Master Mix (Promega) with the pGBK-PP2A-C3 or pGBK-PP2A-C5 construct, respectively. Either GST alone or GST-RCN1 was immobilized by the Glutathione Sepharose 4B resin according to the manufacturer’s instructions

and reacted with the crude protein solution containing either Myc-PP2A-C3 or Myc-PP2A-C5. Either $CaCl_2$ or EGTA was added to the solution to make the 10 mM final concentration. The solution and resin were incubated at room temperature for an hour. The resin was precipitated by brief centrifugation, washed three times with TBST, resuspended in 2× SDS sample buffer, and incubated for 5 min at 100℃. The supernatant was then used for western blotting. Signals of GST-fused proteins were detected as described above. Myc-tagged proteins were detected with anti-Myc-tag pAb (MBL) as a primary antibody and Anti-Rabbit IgG (H+L-chain) (MBL) as a secondary antibody. To examine Ca^{2+} effects on interactions between PP2A B”-family subunits and the complex of RCN1 and PP2A-C5, either GST alone or GST-RCN1 was fixed on Glutathione Sepharose 4B and reacted with Myc-PP2A-C5 as described above. The resin was washed three times with TBST and resuspended in the solution containing purified His-AtB”γ or His-AtB”δ, which was prepared as described above. Either $CaCl_2$ or EGTA was added to the solution to make the 10 mM final concentration. To examine stabilities of the recombinant proteins, a solution with purified a His-tagged PP2A B”-family subunit, GST-RCN1, GST-VIP1, Myc-PP2A-C3, or Myc-PP2A-C5 was incubated in the presence and absence of 10 mM $CaCl_2$, 10 mM EDTA, or 10 mM EGTA. Signals of His-tagged proteins, Myc-tagged proteins, and GST-fused proteins were detected by western blotting as described above.

To examine Ca^{2+} effects on interactions between PP2A B”-family subunits and VIP1, GST-fused VIP1 variants were prepared as previously described (Tsugama et al., 2013, 2019). The His-tagged forms of the PP2A B”-family subunits and the GST-fused forms of VIP1 were reacted and detected as described above for the interactions between those PP2A B”-family subunits and GST-RCN1.

To examine interactions of VIP1 variants with PP2A A and C subunits, Myc-tagged RCN1 (Myc-RCN1), His-tagged PP2A-A2 (His-PP2A-A2), His-tagged PP2A-C3 (His-PP2A-

C3) and Myc-tagged PP2A-C5 (Myc-PP2A-C5) were prepared as previously described (Yoon et al., 2020, 2021). The GST-fused VIP1 variants were fixed on Glutathione Sepharose 4B and reacted with purified His-PP2A-A2 or His-PP2A-C3 and/or a crude protein solution containing Myc tag alone, Myc-RCN1 or Myc-PP2A-C5. Signals of His-tagged proteins, Myc-tagged proteins and GST-fused proteins were detected by western blotting as described above.

To examine the interaction between His-AtB”δ and rabbit PP2A C subunits, His-AtB”δ was immobilized on Ni-NTA agarose, and resuspended in the TNT Quick Master Mix. The resulting solution was incubated at room temperature for an hour. The agarose was precipitated by brief centrifugation, washed three times with TBST, resuspended in 2× SDS sample buffer, and incubated for 5 min at 100℃. The supernatant was subjected to SDS-PAGE followed by western blotting using an anti-PP2A C subunit antibody (Anti-PP2A Antibody, C subunit, clone 1D6 (Merck Millipore)) as a primary antibody and an anti-Mouse IgG (H+L-chain) antibody (MBL) as a secondary antibody. A431 Cell Lysate (Merck Millipore) was used as a positive control for the western blotting. For a control, His-tagged mVenus (His-Venus) was expressed in BL21(DE3) cells transformed with the mVenus/pRSETB vector (Nagai et al., 2002), which was obtained from the RIKEN Brain Science Institute, and purified with the Ni-NTA agarose as described above. To examine interactions between Arabidopsis PP2A B subunits and rabbit PP2A C subunits, Myc-tagged forms of AtB”δ, FASS, and AtB”α were expressed from pGBK-AtB”δ, pGBK-FASS (Tsugama et al., 2019), and pGBK-AtB”α, respectively, with the TNT Quick Master Mix. Myc-tagged proteins were fixed on Anti-Myc-tag mAb-Magnetic Beads (MBL) according to the manufacturer’s instructions. Resulting beads were washed three times with TBST, resuspended in 2× SDS sample buffer, and incubated for 5 min at 100℃. The supernatant was subjected to SDS-PAGE followed by western blotting to detect the Myc-tagged

proteins and rabbit PP2A C subunits as described above. All images were processed with ImageJ.

Table 3.4. Primer pairs used for *in-vitro* pull down assay.

Gene (Restriction sites)		Sequence (5'>3')	Vectors (Restriction sites)
AtB"α (BglII-HindIII)	Fw	CCC**AGATCT**AATGGAAATCGATGGTGGAAACGAT	pRSET B (BamHI-HindIII)
	Rv	CCC**AAGCTT**AAATGGAGATTCGAGTGGTTCATCC	
AtB"β (BamHI-XhoI)	Fw	CCC**GGATCC**AATGGATATTGACGGAGTAGACGAC	pRSET B (BamHI-XhoI)
	Rv	CCC**CTCGAG**AAATGGAGGTTCGAGTGGTTCATCC	
AtB"γ (NcoI-XhoI)	Fw	GGG**CCATGG**AGTCGATAACGTTAGATATAGAGCT	pRSET B (NcoI-XhoI)
	Rv	CG**CTCGAG**AAAAGGGGACCTCAAGTGAGTCGTC	
AtB"δ (NcoI-XhoI)	Fw	GGG**CCATGG**TGGATACGGTTATTCCCGGAGATAT	pRSET B (NcoI-XhoI)
	Rv	GGG**CTCGAG**TCAAAAGGGAGCCTCCAGCGACG	
AtB"ε (NcoI-XhoI)	Fw	GGG**CCATGG**TGGATACGGTTATTCCCGGAGATAT	pRSET B (NcoI-XhoI)
	Rv	GG**CTCGAG**GAAGGGAGCCTCCAGTGACGAGTCAT	
FASS (SpeI-SalI)	Fw	GAC**ACTAGT**GCCATGGCAATGTATAGCGGATCTAGCGATGG	pRSET B (BamHI-XhoI)
	Rv	CGC**GTCGAC**TCACTGAGACTCTTCCTCAGGTGG	
RCN1 (BamHI-XhoI)	Fw	CCC**GGATCC**ATGGCTATGGTAGATGAACCGTTGT	pGEX-6P-3 (BamHI-XhoI)
	Rv	CCC**CTCGAG**GGATTGTGCTGCTGTGGAACCATCG	
PP2A-A2 (XhoI-SalI)	Fw	GGG**CTCGAG**CCATGTCTATGATCGATGAGCCG	pRSET C (XhoI-SalI)
	Rv	CCC**GTCGAC**CGCTAGACATCATCACATTGTC	
PP2A-C3 (XhoI-SalI)	Fw	GGG**CTCGAG**CCATGGGCGCGAATTCTATTCCG	pRSET B (XhoI-SalI)
	Rv	CCT**CTCGAG**CCAGGAAATAGTCTGGAGTCC	

3.2.6 Bimolecular fluorescence complementation (BiFC) assays

The CDSs of AtB''α-ε, FASS, RCN1, PP2A-A2, PP2A-C3, and PP2A-C5 were amplified by RT-PCR as described in the section 3.2.4 and inserted into pBS-35SMCS-cYFP and pBS-35SMCS-nYFP-2 (Tsugama et al., 2012b), generating constructs to express these proteins as C-terminal half of yellow fluorescent protein (cYFP)-fused forms and N-terminal half of YFP (nYFP)-fused forms. Primers and restriction sites used to generate these constructs are shown in Table 3.5. pBS-35SMCS-cYFP and pBS-35SMCS-nYFP containing *VIP1* were prepared as previously described (Tsugama et al., 2014). One of the pBS-35SMCS-cYFP constructs and one of pBS-35SMCS-nYFP constructs were co-introduced into Arabidopsis mesophyll protoplasts as previously described (Yoo et al., 2007; Wu et al., 2009). Signals of YFP were detected by fluorescence microscopy as previously described (Tsugama et al., 2014). Images were processed with ImageJ.

Table 3.5. Primer pairs used for BiFC assays.

Gene (Restriction sites)		Sequence (5'>3')	Vector (Restriction sites)
AtB"α (XbaI-KpnI)	Fw	CCC**TCTAGA**AATGGAAATCGATGGTGGAAACGA	pBS-35SMCS-cYFP (XbaI-KpnI)
	Rv	CCC**GGTACC**AAAATGGAGATTCGAGTGGTTCAT	
AtB"β (SpeI-SpeI)	Fw	CCC**ACTAGT**ATGGATATTGACGGAGTAGACGA	pBS-35SMCS-cYFP (SpeI-SpeI)
	Rv	GGG**ACTAGT**AAATGGAGGTTCGAGTGGTTCAT	
AtB"γ (XbaI-XbaI)	Fw	CCC**TCTAGA**AATGGAGTCGATAACGTTAGATAT	pBS-35SMCS-cYFP (XbaI-XbaI)
	Rv	GGG**TCTAGA**GCAAAGGGGACCTCAAGTGAGTCG	
AtB"δ	Fw	CCC**ACTAGT**ATGGTGGATACGGTTATTCCCGG	pBS-35SMCS-

(SpeI-SpeI)	Rv	GGG**ACTAGT**AAAGGGAGCCTCCAGCGACGACT	cYFP (SpeI-SpeI)
AtB”ε (XbaI-KpnI)	Fw	CCC**TCTAGA**AATGGTGGATACGGTTATTCCCGG	pBS-35SMCS-cYFP (XbaI-KpnI)
	Rv	CCC**GGTACC**AGAAGGGAGCCTCCAGTGACGAGT	
FASS (SpeI-SpeI)	Fw	CCC**ACTAGT**ATGTATAGCGGATCTAGCGATGG	pBS-35SMCS-cYFP (SpeI-SpeI)
	Rv	GGG**ACTAGT**CTGAGACTCTTCCTCAGGTGGTT	
RCN1 (KpnI-SpeI)	Fw	CCC**GGTACC**TTATGGCTATGGTAGATGAACCGTT	pBS-35SMCS-nYFP (KpnI-SpeI)
	Rv	GGG**ACTAGT**GGATTGTGCTGCTGTGGAACCATCG	
PP2A-A2 (KpnI-SpeI)	Fw	CCC**GGTACC**TTATGTCTATGATCGATGAGCCGTTG	pBS-35SMCS-nYFP (KpnI-SpeI)
	Rv	GGG**ACTAGT**GCTAGACATCATCACATTGTCAATA	
PP2A-C3 (KpnI-SpeI)	Fw	CCC**GGTACC**TTATGGGCGCGAATTCTATTCCGAC	pBS-35SMCS-nYFP (KpnI-SpeI)
	Rv	GGG**ACTAGT**CAGGAAATAGTCTGGAGTCCTTCGG	
PP2A-C5 (KpnI-SpeI)	Fw	CCC**GGTACC**TTATGCCGCCGGCGACCGGAGATAT	pBS-35SMCS-nYFP (KpnI-SpeI)
	Rv	GGG**ACTAGT**CAAAAAATAATCTGGAGTCTTGCGA	

3.2.7. *In-vitro* dephosphorylation assays

A solution that contained purified MBP-fused CPK21 (MBP-CPK21) and 20 mM maltose in TBST was prepared as previously described (Tsugama et al., 2019). GST-VIP1FL and GST-fused bZIP29 (GST-bZIP29FL) were prepared as previously described (Tsugama et al., 2016). GST, GST-VIP1FL, or GST-bZIP29FL was immobilized on the Glutathione Sepharose 4B resin according to the manufacturer’s instructions. The resin was resuspended in the solution containing the purified MBP-CPK21 supplemented with 20 mM $MgCl_2$, 10 mM $CaCl_2$, and 2 mM ATP, and incubated at room temperature for an hour. The resin was washed three times with TBST. The solution containing purified His-AtB”δ was mixed with the TNT Quick Master Mix containing pGBKT7, pGBK-RCN1, or pGBK-PP2A-C5, and added to the resin as described previously (Yoon et al., 2021). $CaCl_2$ and $MnCl_2$ were added to this solution to make 10 mM and 1 mM final concentrations, respectively. The resin was resuspended in this solution, incubated at

room temperature for an hour, washed three times with TBST, resuspended in 2× SDS sample buffer, and incubated for 5 min at 100℃. The supernatant was subjected to SDS-PAGE followed by western blotting to detect the His-tagged and Myc-tagged proteins as described above in the section 3.2.5. Phosphorylated proteins were detected with Phos-tag biotin BTL-104 (Fujifilm Wako) according to the manufacturer's instructions. MBP-CPK21 was detected with MBP-tag mAb (MBL) as a primary antibody and an Anti-mouse IgG (H+L-chain) (MBL) as a secondary antibody. To confirm the presence of GST-fused proteins, the membrane used for the western blotting was incubated in a Ponceau S staining solution (0.2% (w/v) Ponceau S in 5% (v/v) acetic acid) for 1 min at room temperature and washed several times with distilled water.

To further examine PP2A B"-family subunit-induced dephosphorylation of VIP1 and bZIP29 *in vitro*, either GST-VIP1FL or GST-bZIP29FL was fixed on the Glutathione Sepharose 4B resin and phosphorylated by purified MBP-CPK21 as described above. The resin was washed three times with TBST and then resuspended in the TNT Quick Master Mix containing pGBKT7, pGBK-AtB"α, pGBK-AtB"δ, or pGBK-FASS. $CaCl_2$ and $MnCl_2$ were added to this solution to make 10 mM and 1 mM final concentrations, respectively. The resin was resuspended in this solution, incubated at room temperature for an hour, washed three times with TBST, resuspended in 2× SDS sample buffer, and incubated for 5 min at 100℃. The supernatant was subjected to SDS-PAGE followed by western blotting to detect phosphorylated proteins and GST-fused proteins as described above. Images were processed with GIMP and ImageJ.

3.2.8. Accession numbers

Details regarding the sequences of the genes used in this chapter are available with the following Arabidopsis Genome Initiative accession numbers: AT1G43700 (*VIP1*), AT2G31370 (*PosF21*), AT4G38900 (*bZIP29*), AT2G21230 (*bZIP30*), AT1G25490 (*RCN1*), AT3G25800

(*PP2A-A2*), AT2G42500 (*PP2A-C3*), AT1G69960 (*PP2A-C5*), AT5G44090 (*AtB"α*), AT1G03960 (*AtB"β*) AT1G54450 (*AtB"γ*), AT5G28900 (*AtB"δ*), AT5G28850 (*AtB"ε*), AT5G18580 (*FASS*), AT4G04720 (*CPK21*) and AT3G62250 (*UBQ5*).

3.3. Results

3.3.1. Expression of PP2A B"-family subunit genes in various Arabidopsis tissues

AtB"α-ε and *FASS* were expressed in seedlings, leaves, roots, flower stalks and flowers (Yoon et al., 2021; Figure 3.1). These expression patterns were similar to those reported for three PP2A A subunit genes (Zhou et al., 2004) and five PP2A C subunit genes (Ballesteros et al., 2013). *VIP1* and its close homologs are also expressed in various tissues (Tsugama et al., 2012a, 2014). These results support the idea that the PP2A B"-family subunit genes as well as PP2A A and C subunit genes can regulate functions of VIP1 and its close homologs in various Arabidopsis tissues.

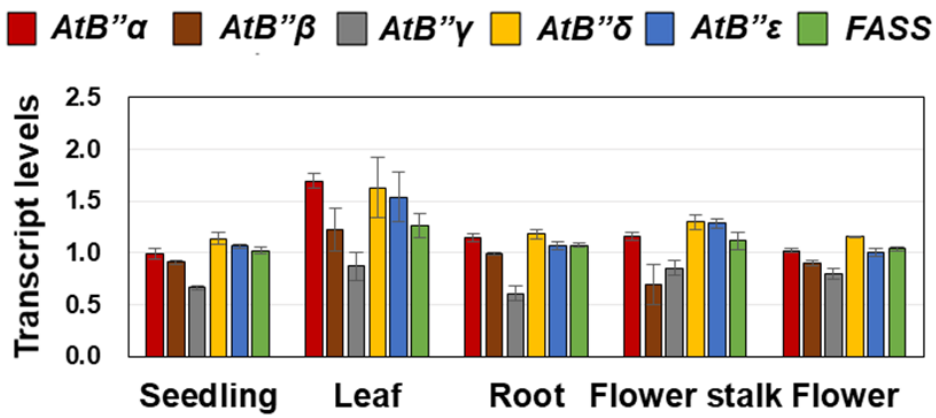

Figure 3.1. Expression levels of the PP2A B"-family subunit genes in Arabidopsis tissues. The absolute amounts of cDNA of the six PP2A B"-family subunit genes were quantified by RT-PCR using the standard curve method. The values were normalized by the amount of DNA for the internal control gene *UBQ5*. Data are means ± SD of three biological replicates.

3.3.2. PP2A B”-family subunits interact with VIP1 and its close homologs in a Y2H system.

To examine interactions between PP2A B”-family subunits and VIP1, Y2H assays were performed. Expression of GAL4 DNA-binding domain (BD)-fusion proteins, BD-AtB”α, BD-AtB”β, BD-AtB”δ, and BD-FASS, all enabled yeast cells to survive on the highly stringent quadruple-dropout (QDO) selection medium even in the absence of any putative interacting partner for them (Yoon et al., 2021; Figure 3.2). This result suggests that these proteins can self-activate reporter genes in this Y2H system and thus cannot be used to examine protein-protein interactions by this system. BD-fused VIP1N and BD-fused full-length forms of VIP1, PosF21, bZIP29, and bZIP30 also self-activate reporter genes in this Y2H system and cannot be used for this system, either (Tsugama et al., 2012a, 2014). However, none of AtB”α-ε and FASS self-activated the reporter genes in yeast when fused to the GAL4 activation domain (AD), and all of them (as AD-fused forms) enabled yeast cells to survive on either the moderately stringent TDO/3-AT medium or stringent QDO medium when co-expressed with BD-fused VIP1C (Yoon et al., 2021; Figure 3.3A). This result suggests that AtB”α-ε and FASS interact with VIP1 in the Y2H system. In similar Y2H assays, co-expression of those AD-fused PP2A B”-family subunits with BD-fused forms of PosF21C (172-398 amino acids of PosF21), bZIP29C (364-553 amino acids of bZIP29), and bZIP30C (341-525 amino acids of bZIP30) enabled yeast cells to survive on the TDO/3-AT medium (Figure 3.3B), suggesting that AtB”α-ε and FASS also interact with the close VIP1 homologs in the Y2H system. However, some of these combinations did not enable yeast cells to survive on the QDO medium (Figure 3.3B). This may be because VIP1 and its close homologs differ in affinity to the PP2A B”-family subunits.

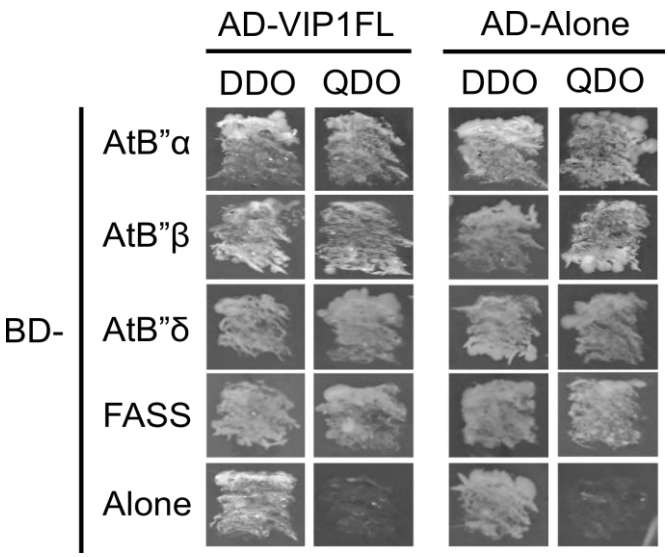

Figure 3.2. GAL4 DNA-binding domain (BD)-fused AtB"α, AtB"β, AtB"δ, and FASS activate reporter genes in yeast. The pGBKT7 vector containing no insert (BD-Alone), *AtB"α* (BD-AtB"α), *AtB"β* (BD-AtB"β), *AtB"δ* (BD-AtB"δ), or *FASS* (BD-FASS) was co-introduced with the pGADT7-Rec vector containing either no insert (AD-Alone) or *VIP1* (AD-VIP1FL) into the yeast strain AH109. The transformed yeast cells were grown for five days at 28 °C on the double-dropout medium (DDO: synthetic dextrose (SD) medium that lacks leucine and tryptophan) and the quadruple-dropout medium (QDO: SD medium that lacks leucine, tryptophan, histidine, and adenine), and photographed. The experiments were performed with four individual colonies for each combination of the constructs, and a representative result is shown.

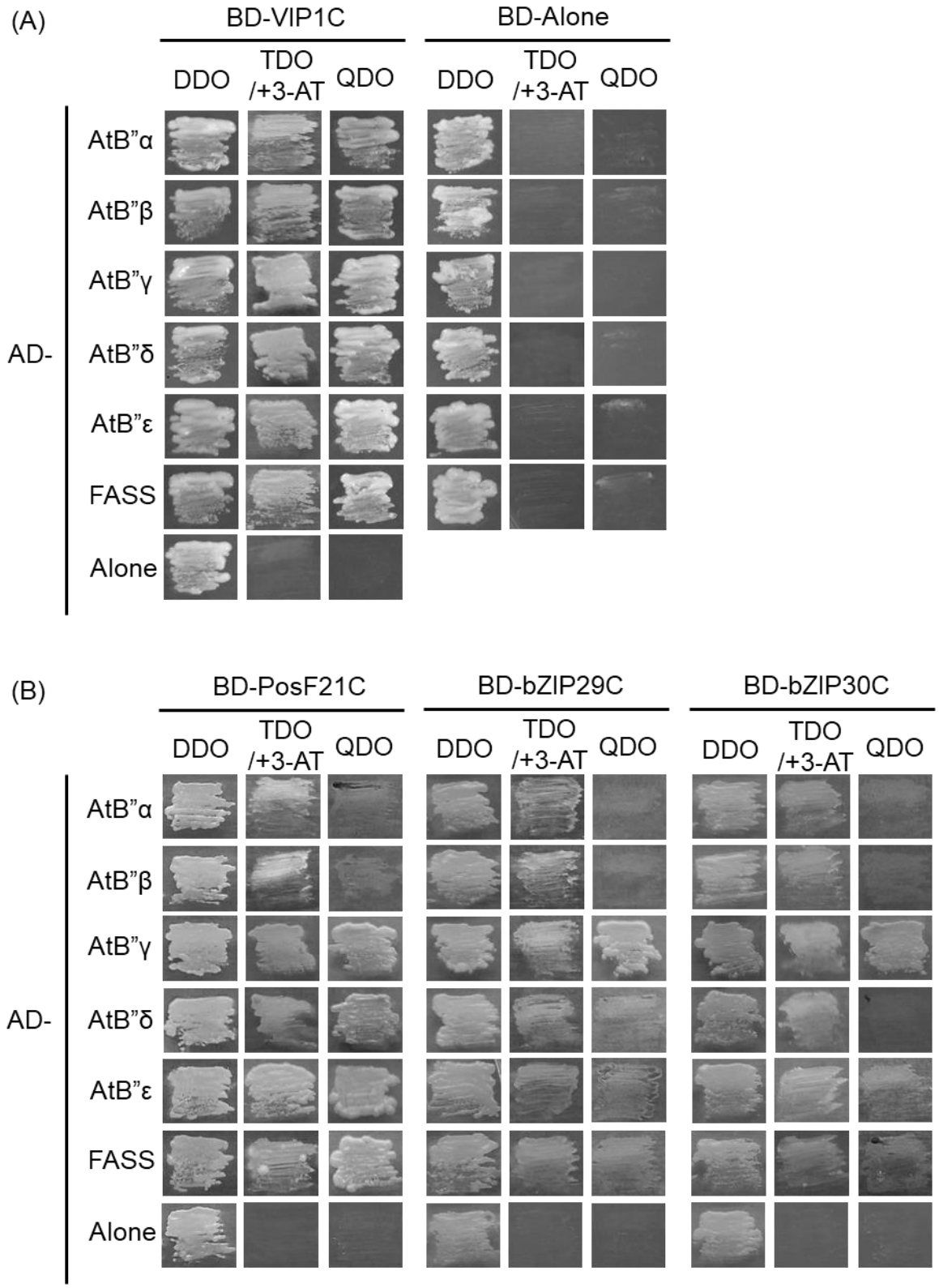

Figure 3.3. Interactions of PP2A B"-family subunits with VIP1 and its close homologs in yeast. (A) Y2H assays with all the six PP2A B"-family subunits (AtB"α-ε and FASS) and VIP1. The pGBKT7 vector containing no insert (BD-Alone) or the CDS of the C-terminal region of

VIP1 (BD-VIP1C) was co-introduced with the pGADT7-Rec vector containing no insert (AD-Alone) or one of the six PP2A-B" family subunit genes (*AtB"α-ε* and *FASS*, AD-AtB"α-ε and AD-FASS in the figure) into the yeast strain AH109. The transformed yeast cells were grown on the DDO medium, the TDO/+3-AT medium, and the QDO medium. (B) Y2H assays with AtB"α-ε, FASS, and three close VIP1 homologs. The pGBKT7 vector containing the CDS of the C-terminal region of PosF21 (BD-PosF21C), bZIP29 (BD-bZIP29C), or bZIP30 (BD-bZIP30C) was co-introduced with one of the above pGADT7-Rec constructs into the yeast strain AH109, and resulting yeast cells were grown on selection media as in the panel A to assess reporter gene expression. The experiments were performed with four individual colonies for each combination of the constructs for both the panels A and B, and a representative result is shown.

3.3.3. PP2A C subunits also interact with VIP1 in yeast.

To examine interactions of VIP1 with either PP2A A subunits or PP2A C subunits, Y2H assays were performed. Neither BD-fused RCN1 nor BD-fused PP2A-A2 enabled yeast cells to survive on the TDO/3-AT medium or the QDO medium when co-expressed with AD-VIP1FL (Yoon et al., 2020; Figure 3.4A). However, co-expression of either BD-fused PP2A-C3 (BD-PP2A-C3) or BD-fused PP2A-C5 (BD-PP2A-C5) with either AD-VIP1FL or AD-VIP1C did enable yeast cells to survive on the TDO/3-AT medium and the QDO medium (Yoon et al., 2020; Figure 3.4B). These results suggest that the Arabidopsis PP2A C subunits also interact with VIP1 in the Y2H system.

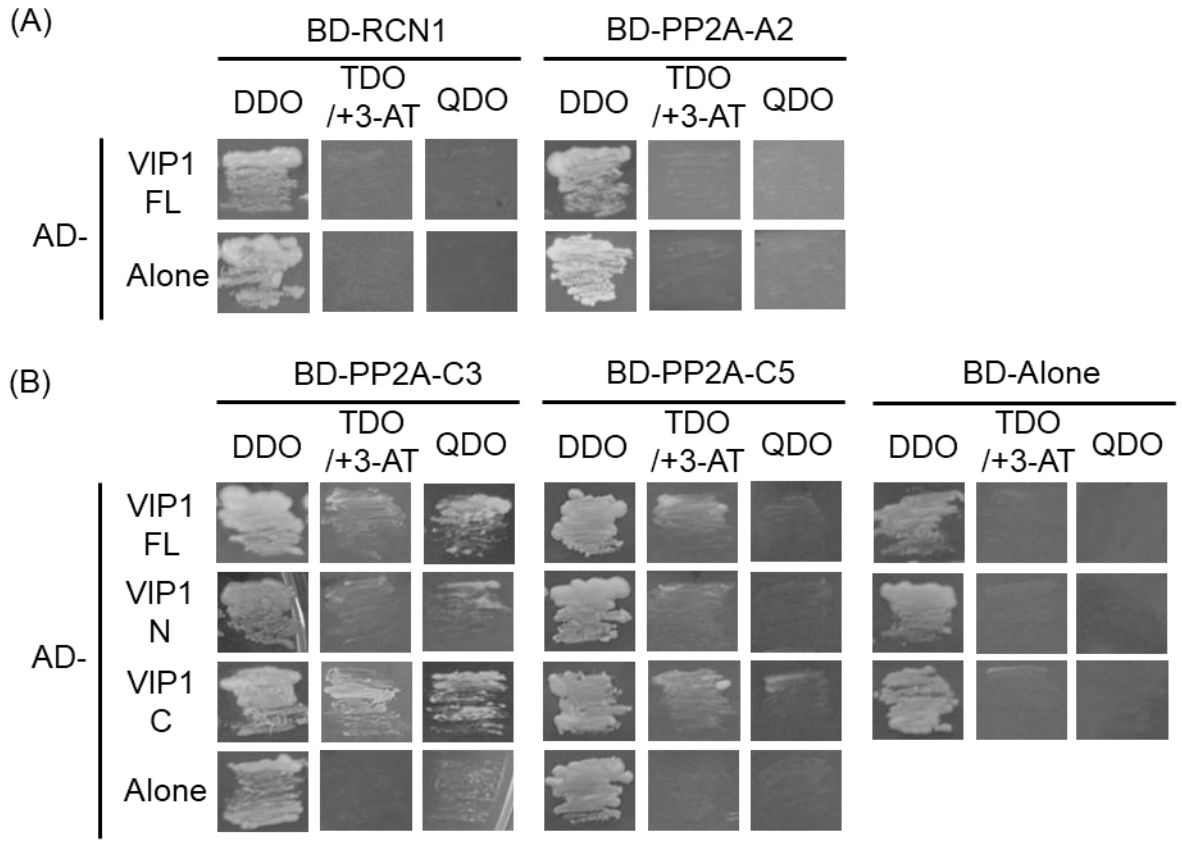

Figure 3.4. PP2A C subunits interact with VIP1 in yeast. (A) Y2H assays with VIP1 and two PP2A A subunits, RCN1 and PP2A-A2. The pGADT7-Rec vector containing no insert (AD-Alone) or *VIP1* (AD-VIP1FL) was co-introduced with the pGBKT7 vector containing either *RCN1* (BD-RCN1) or *PP2A-A2* (BD-PP2A-A2) into the yeast strain AH109. (B) Y2H assays with VIP1FL, VIP1N, VIP1C and two PP2A C subunits, PP2A-C3 and PP2A-C5. The pGADT7-Rec vector containing no insert (AD-Alone) or *VIP1* (AD-VIP1FL) was co-introduced with the pGBKT7-vector containing either *PP2A-C3* (BD-PP2A-C3) or *PP2A-C5* (BD-PP2A-C5) into the yeast strain AH109. For both the panels A and B, the transformed yeast cells were cultured on the DDO medium, the TDO/+3-AT medium, and the QDO medium for five days at 28°C, and photographed. The experiments were performed with four individual colonies for each combination of the constructs, and a representative result is shown.

3.3.4. PP2A B”-family subunits interact with either PP2A A subunits or PP2A C subunits in the Y2H system

To confirm interactions of the Arabidopsis PP2A B”-family subunits with either PP2A A subunits or PP2A C subunits, Y2H assays were performed. AD-fused AtB”α-ε and FASS all enabled yeast cells to survive on the TDO/3-AT medium and the QDO medium when they were co-expressed with BD-fused forms of RCN1 and PP2A-A2 (Yoon et al., 2021; Figure 3.5A). These results suggest that the Arabidopsis PP2A B”-family subunits interact with the Arabidopsis PP2A A subunits in the Y2H system. In similar assays, when either BD-PP2A-C3 or BD-PP2A-C5 was co-expressed in yeast cells with one of those AD-fused PP2A B’’-family subunits, the cells grew rapidly on the TDO/3-AT medium, and grew slowly on the QDO medium (Yoon et al., 2021; Figure 3.5B). These results suggest that the Arabidopsis PP2A B”-family subunits can also interact with the Arabidopsis PP2A C subunits in the Y2H system. These results also support the idea that the Y2H interactions of the PP2A B”-family subunits with the PP2A C subunits are not as strong as the Y2H interactions between the PP2A B”-family subunits and the PP2A A subunits. Yeast cells also have PP2A A subunits and these may mediate those Y2H interactions between the Arabidopsis PP2A B’’-family B subunits and C subunits.

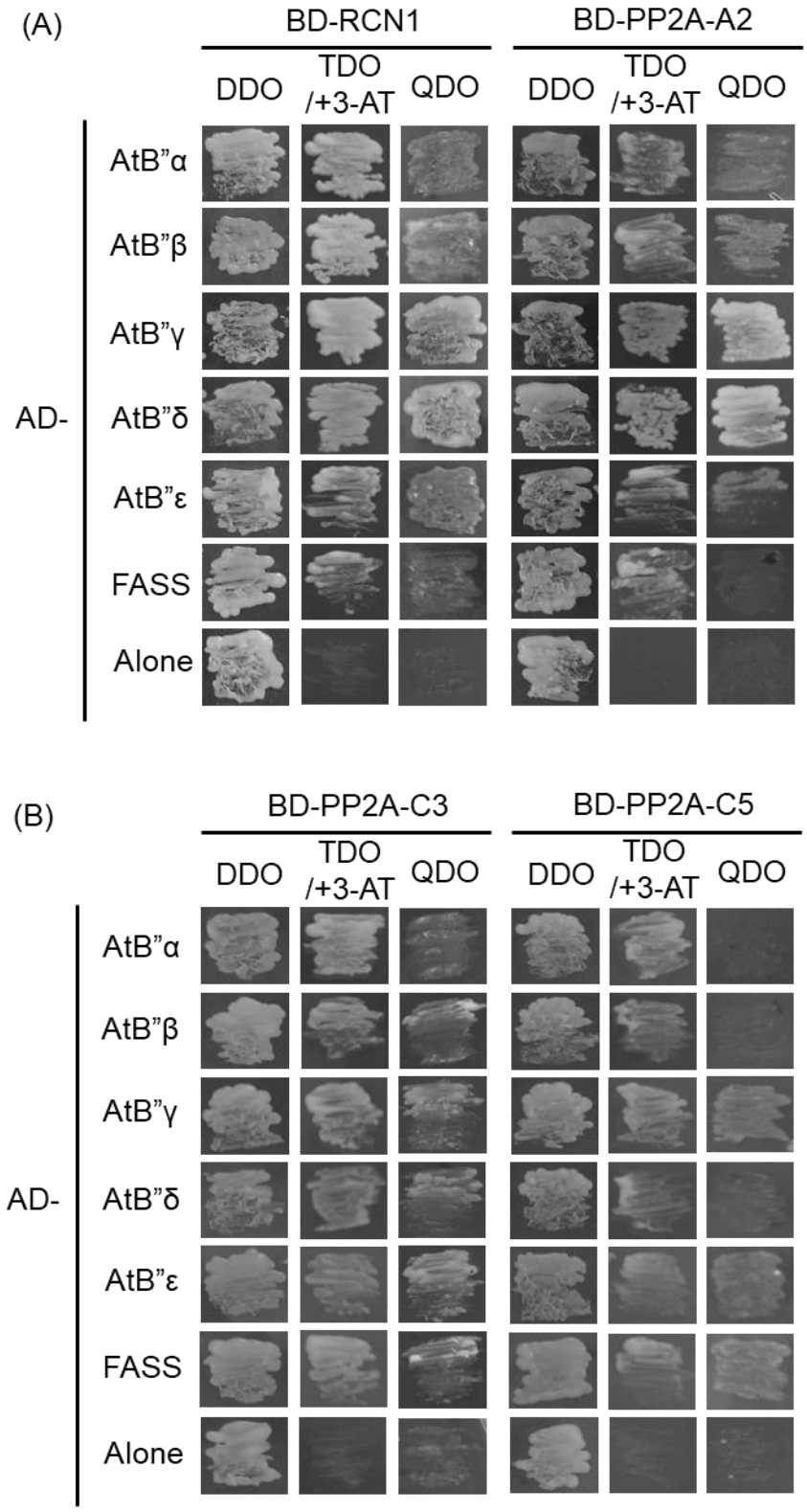

Figure 3.5. Arabidopsis PP2A B"-family subunits interact with PP2A A subunits and PP2A C subunits in a Y2H system. (A) Y2H assays with PP2A B"-family subunits and PP2A A subunits. The pGADT7-Rec vector containing no insert (AD-Alone) or the CDS of one of the six

PP2A B”-family subunit genes (*AtB”α-ε* and *FASS*, AD-AtB”α-ε and AD-FASS in the figure) was co-introduced with the pGBKT7 vector containing either *RCN1* or *PP2A-A2* (BD-RCN1 or BD-PP2A-A2, respectively) into the yeast strain AH109. (B) Y2H assays with PP2A B’’-family subunits and PP2A C subunits. One of the above pGADT7-Rec constructs was co-introduced with the pGBKT7- vector containing either *PP2A-C3* or *PP2A-C5* (BD-PP2A-C3 or BD-PP2A-C5, respectively) into the yeast strain AH109. The transformed yeast cells were grown on the DDO medium, the TDO/+3-AT medium, and the QDO medium for five days at 28 °C, and photographed. The experiments were performed with four individual colonies for each combination of the constructs, and a representative result is shown.

3.3.5. Ca^{2+} promotes interactions of PP2A B”-family subunits with VIP1 *in vitro*

AtB’’α-ε and FASS all have Ca^{2+}-binding EF-hand motifs (Farkas et al., 2007). This led us to examine effects of Ca^{2+} on the interactions of PP2A B”-family subunits with VIP1. The intensity of signals of His-tagged AtB”δ and His-tagged FASS pulled down by GST-VIP1FL was higher in the presence of 10 mM $CaCl_2$ in the reaction mixture than in the presence of 10 mM EDTA (a Ca^{2+} chelator) (Yoon et al., 2021; Figure 3.6A). In similar assays, the intensities of signals of His-tagged AtB”α-ε and His-tagged FASS pulled down by GST-VIP1FL were also higher in the presence of 10 mM $CaCl_2$ in the reaction mixtures than in the presence of 10 mM EGTA (another Ca^{2+} chelator) (Yoon et al., 2021; Figure 3.6B). These results suggest that Ca^{2+} promotes interactions between PP2A B”-family subunits and VIP1. His-tagged AtB”α-ε and His-tagged FASS were all pulled down by GST-VIP1C but hardly by GST-VIP1N (Figure 3.6C). These results suggest that all of the six PP2A B’’-family B subunits interact with the C-terminal half of VIP1.

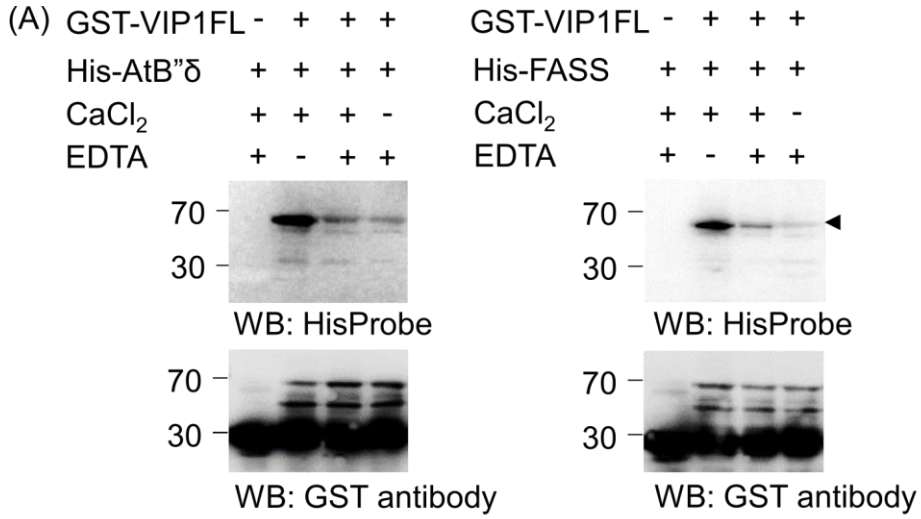
(A)
GST-VIP1FL - + + +
His-AtB"δ + + + +
CaCl2 + + + -
EDTA + - + +
70
30
WB: HisProbe
WB: GST antibody
GST-VIP1FL - + + +
His-FASS + + + +
CaCl2 + + + -
EDTA + - + +
70
30
WB: HisProbe
WB: GST antibody

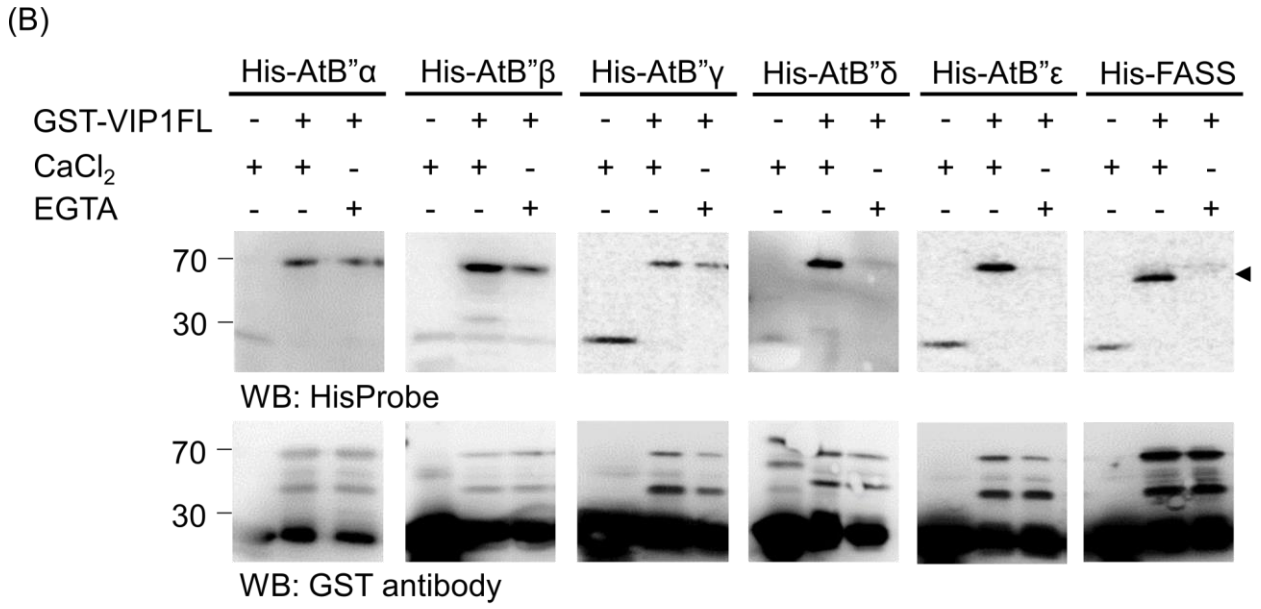
(B)
His-AtB"α
His-AtB"β
His-AtB"γ
His-AtB"δ
His-AtB"ε
His-FASS
GST-VIP1FL
CaCl2
EGTA
70
30
WB: HisProbe
WB: GST antibody

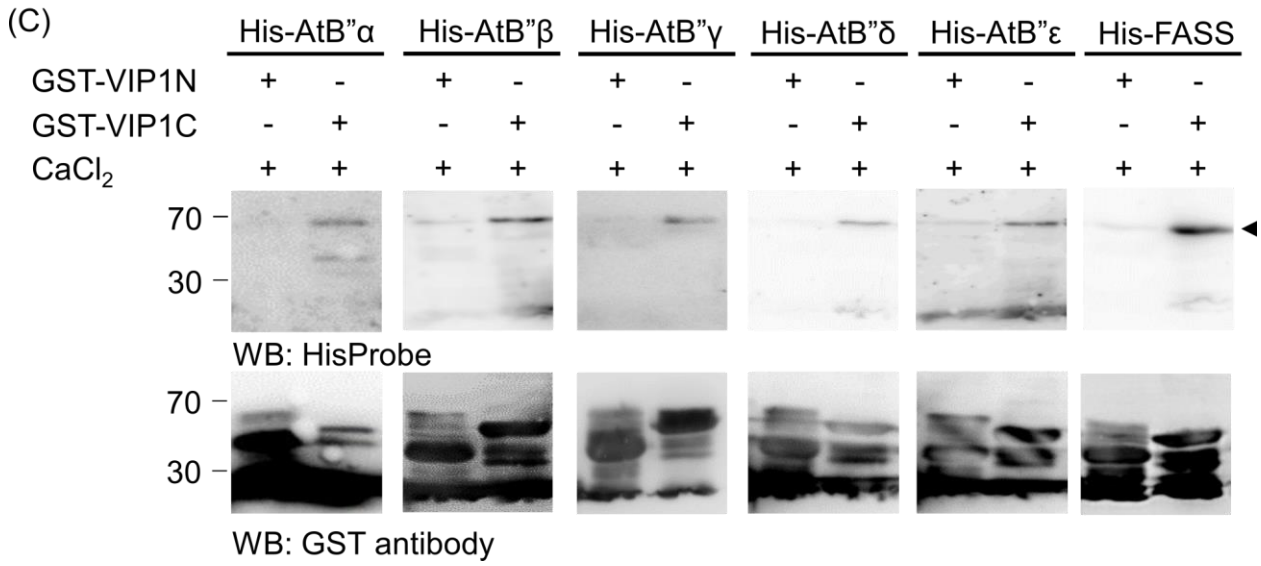
(C)
His-AtB"α
His-AtB"β
His-AtB"γ
His-AtB"δ
His-AtB"ε
His-FASS
GST-VIP1N
GST-VIP1C
CaCl2
70
30
WB: HisProbe
WB: GST antibody

Figure 3.6. AtB”α-ε and FASS interact with VIP1 in a Ca^{2+}-dependent manner. (A) *In-vitro* pull-down assays with VIP1 and PP2A B”-family subunits in the presence and absence of $CaCl_2$ and EDTA. GST-VIP1FL was immobilized on the glutathione resin and incubated in a solution containing purified His-AtB"δ or His-FASS in the presence or the absence of either 20 mM $CaCl_2$ or 20 mM EDTA. The presence and absence of GST-VIP1FL, His-AtB"δ, His-FASS, $CaCl_2$, and EDTA in reaction mixtures are indicated as ‘+’ and ‘-’, respectively. GST (GST-Alone) was used as a negative control. Signals of His-AtB"δ and His-FASS were detected by western blotting with HisProbe-HRP (WB: HisProbe), and signals of GST-VIP1FL were detected by western blotting with an anti-GST antibody (WB: GST antibody). (B) *In-vitro* pull-down assays with VIP1 and PP2A B”-family subunits in the presence and absence of $CaCl_2$ and EGTA. GST-VIP1FL was immobilized on the glutathione resin and incubated in a solution containing His-tagged one of the six PP2A B”-family subunits (His-AtB”α-ε and His-FASS) in the presence or the absence of either 10 mM $CaCl_2$ or 10 mM EGTA. Signals of GST-VIP1FL and His-tagged proteins were detected as in the panel A. (C) *In-vitro* pull-down assays with VIP1N, VIP1C and PP2A B”-family subunits. Either GST-VIP1N or GST-VIP1C was immobilized on the glutathione resin and incubated in a solution containing one of His-AtB”α-ε and His-FASS in the presence of $CaCl_2$. The presence and absence of GST-VIP1N and GST-VIP1C in reaction mixtures are indicated as ‘+’ and ‘-’, respectively. Signals of GST-fused and His-tagged proteins were detected as in the panel A. The experiments were performed three times and the representative result is shown for the panels A-C. His-tagged proteins are indicated by arrowheads.

3.3.6. PP2A C subunits interact with VIP1 *in vitro*

PP2A C subunits interact with bZIP29 in Arabidopsis suspension cell cultures and seedlings (Van Leene et al., 2016). This is consistent with our Y2H data (Figure 3.4). To confirm the interactions between VIP1 and either PP2A A or C subunits, His-tagged PP2A-A2 (His-PP2A-A2) and His-tagged PP2A-C3 (His-PP2A-C3) were expressed in *E. coli*, purified, and used for *in-vitro* pull-down assays. Neither His-tagged RCN1 nor His-tagged PP2A-C5 could be expressed in *E. coli*. However, Myc-tagged RCN1 (Myc-RCN1) and Myc-tagged PP2A-C5 (Myc-PP2A-C5) could be prepared by an *in-vitro* transcription and translation system and were also used for pull-down assays. Neither Myc-RCN1 nor His-PP2A-A2 was pulled down by GST-VIP1FL *in vitro* (Yoon et al., 2020; Figure 3.7A). However, both His-PP2A-C3 and Myc-PP2A-C5 were pulled down by GST-VIP1FL (Yoon et al., 2020; Figure 3.7B). These results suggest that VIP1 does not interact with PP2A A subunits *in vitro* but that VIP1 interacts with PP2A C subunits. His-PP2A-C3 and Myc-PP2A-C5 were also pulled down by GST-VIP1C, but were not by GST-VIP1N (Yoon et al., 2020; Figure 3.7C), suggesting that, as well as the PP2A B''-family subunits, PP2A C subunits interact with the C-terminal half with the bZIP domain of VIP1. These results are all consistent with the Y2H data (Figure 3.4). The VIP1 interactions with PP2A C subunits may contribute to stabilizing the interaction between VIP1 and the PP2A complex containing the B"-family subunits.

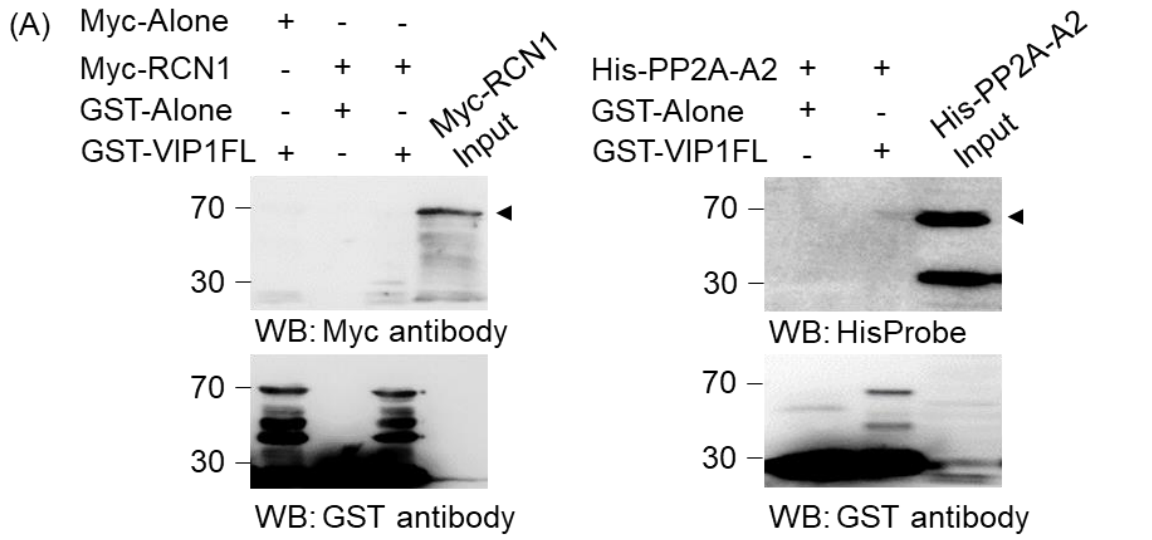
(A)
Myc-Alone + - -
Myc-RCN1 - + +
GST-Alone - + -
GST-VIP1FL + - +
Myc-RCN1 Input
70
30
WB: Myc antibody
70
30
WB: GST antibody
His-PP2A-A2 + +
GST-Alone + -
GST-VIP1FL - +
His-PP2A-A2 Input
70
30
WB: HisProbe
70
30
WB: GST antibody

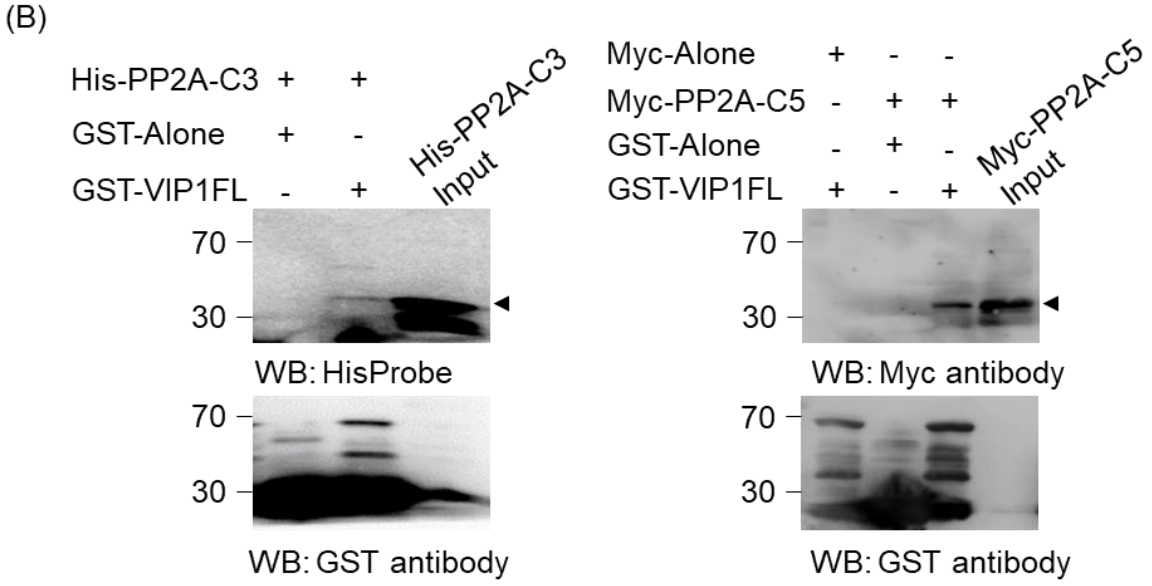
(B)
His-PP2A-C3 + +
GST-Alone + -
GST-VIP1FL - +
His-PP2A-C3 Input
70
30
WB: HisProbe
70
30
WB: GST antibody
Myc-Alone + - -
Myc-PP2A-C5 - + +
GST-Alone - + -
GST-VIP1FL + - +
Myc-PP2A-C5 Input
70
30
WB: Myc antibody
70
30
WB: GST antibody

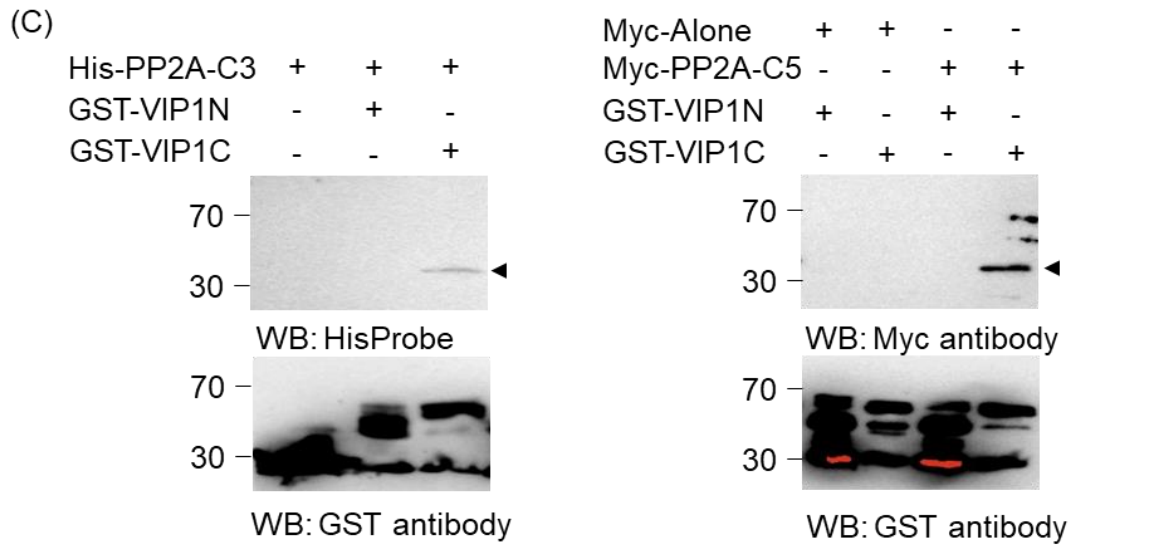
(C)
His-PP2A-C3 + + +
GST-VIP1N - + -
GST-VIP1C - - +
70
30
WB: HisProbe
70
30
WB: GST antibody
Myc-Alone + + - -
Myc-PP2A-C5 - - + +
GST-VIP1N + - + -
GST-VIP1C - + - +
70
30
WB: Myc antibody
70
30
WB: GST antibody

Figure 3.7. PP2A C subunits interact with VIP1. (A) *In-vitro* pull-down assays with VIP1 and PP2A A subunits (RCN1 and PP2A-A2). Either GST alone (GST-Alone) or GST-VIP1FL was immobilized on the glutathione resin and incubated in a solution containing His-PP2A-A2, the Myc tag alone (Myc-Alone, a negative control), or Myc-RCN1. The resin was used for western blotting to analyze the His-tagged, Myc-tagged, and GST-fused proteins ("WB: HisProbe", "WB: Myc antibody", and "WB: GST antibody", respectively). The presence and absence of the His-tagged, Myc-tagged, and GST-fused proteins are indicated as '+' and '-', respectively. (B) *In-vitro* pull-down assays with VIP1 and two PP2A C subunits (PP2A-C3 and PP2A-C5). Either GST or GST-VIP1FL was immobilized on the glutathione resin and incubated in a solution containing His-PP2A-C3, Myc-Alone, or Myc-PP2A-C5. These proteins were detected as in the panel A. The presence and absence of His-tagged and Myc-tagged proteins in the reaction mixtures are indicated as '+' and '-', respectively. (C) *In-vitro* pull-down assays with VIP1N, VIP1C, PP2A-C3 and PP2A-C5. GST-VIP1N and GST-VIP1C were immobilized on the glutathione resin and incubated in a solution containing His-PP2A-C3, Myc-Alone, or Myc-PP2A-C5. These proteins were detected as in the panel A. The presence and absence of His-tagged and Myc-tagged proteins in the reaction mixtures are indicated as '+' and '-', respectively. All experiments were performed three times, and a representative result is shown for the panels A-C. Myc-tagged proteins and His-tagged proteins are indicated by arrowheads.

3.3.7. Arabidopsis PP2A B”-family interacts with PP2A A subunits in the presence of Ca^{2+} *in vitro*

Human PP2A B” subunits interact with the PP2A A and C subunits in the presence of Ca^{2+} (Wlodarchak et al., 2013). Similarly, AtB”α and AtB”β interact with PP2A-A2 of Arabidopsis in the presence of Ca^{2+} (Leivar et al., 2011). In agreement with these findings, in pull-down assays, His-AtB”γ and His-AtB”δ were pulled down by GST-RCN1 *in vitro* in the presence of 0 or 10 mM $CaCl_2$, but not in the presence of 10 mM EGTA (Yoon et al., 2021; Figure 3.8A). Myc-PP2A-C3 and Myc-PP2A-C5 were pulled down by GST-RCN1 in the presence of 0 or 10 mM $CaCl_2$, or in the presence of 10 mM EGTA. However, the signals of Myc-PP2A-C3 and Myc-PP2A-C5 pulled down by GST-RCN1 were weaker in the presence of 10 mM EGTA than its absence (Yoon et al., 2021; Figure 3.8B). This result raises the possibility that metal ions that could be bound by EGTA mediate the interaction between RCN1 and either PP2A C3 or PP2A-C5. To examine Ca^{2+} effects on interactions between the PP2A B”-family subunits and the complex of RCN1 and PP2A-C5, GST-RCN1 was preincubated with Myc-PP2A-C5 and then reacted with a solution containing purified His-AtB”γ or His-AtB”δ in the presence of either 10 mM $CaCl_2$ or 10 mM EGTA. The preincubation of GST-RCN1 with Myc-PP2A-C5 did not affect the signal intensity of either His-AtB”γ or His-AtB”δ pulled down by GST-RCN1 (Yoon et al., 2021; Figure 3.8C). $CaCl_2$, EDTA, and EGTA did not affect the stability of these proteins *in vitro* (Yoon et al., 2021; Figure 3.9). These results suggest that the interactions between Arabidopsis PP2A B”-family subunits and A subunits are neither stabilized nor attenuated by PP2A C subunits.

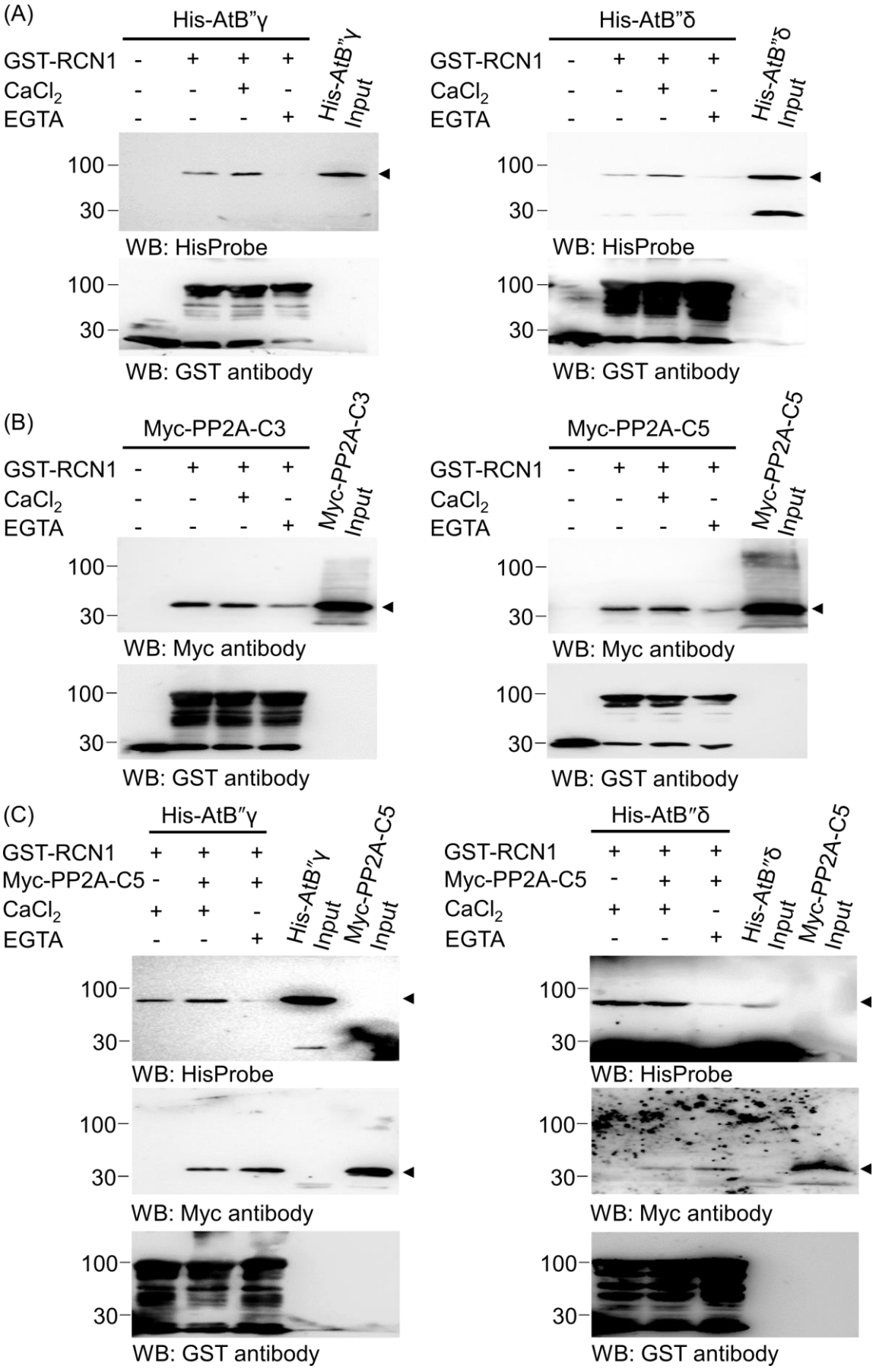
(A)
His-AtB"γ
GST-RCN1 - + + +
CaCl2 - - + -
EGTA - - - +
His-AtB"γ Input
100
30
WB: HisProbe
100
30
WB: GST antibody
His-AtB"δ
GST-RCN1 - + + +
CaCl2 - - + -
EGTA - - - +
His-AtB"δ Input
100
30
WB: HisProbe
100
30
WB: GST antibody
(B)
Myc-PP2A-C3
GST-RCN1 - + + +
CaCl2 - - + -
EGTA - - - +
Myc-PP2A-C3 Input
100
30
WB: Myc antibody
100
30
WB: GST antibody
Myc-PP2A-C5
GST-RCN1 - + + +
CaCl2 - - + -
EGTA - - - +
Myc-PP2A-C5 Input
100
30
WB: Myc antibody
100
30
WB: GST antibody
(C)
His-AtB"γ
GST-RCN1 + + +
Myc-PP2A-C5 - + +
CaCl2 + + -
EGTA - - +
His-AtB"γ Input
Myc-PP2A-C5 Input
100
30
WB: HisProbe
100
30
WB: Myc antibody
100
30
WB: GST antibody
His-AtB"δ
GST-RCN1 + + +
Myc-PP2A-C5 - + +
CaCl2 + + -
EGTA - - +
His-AtB"δ Input
Myc-PP2A-C5 Input
100
30
WB: HisProbe
100
30
WB: Myc antibody
100
30
WB: GST antibody

Figure 3.8. Ca^{2+} promotes interactions of PP2A B”-family subunits with PP2A A subunits. (A) *In-vitro* pull-down assays with His-tagged AtB’’γ, His-tagged AtB’’δ, and GST-fused RCN1 (His-AtB’’γ, His-AtB’’δ, and GST-RCN1, respectively). Either GST alone or GST-RCN1 was fixed on the glutathione resin and incubated with either His-AtB”γ (left panel) or His-AtB”δ (right panel) in the presence or absence of either 10 mM $CaCl_2$ or 10 mM EGTA. The resulting resin was used for western blotting to analyze the His-tagged proteins with HisProbe-HRP (WB: HisProbe) and to analyze GST-fused proteins with an anti-GST antibody (WB: GST antibody). The presence and absence of GST-fused proteins, $CaCl_2$, and EGTA are indicated as ‘+’ and ‘-’, respectively. For ‘GST-RCN1 -’, GST alone was used instead of GST-RCN1. (B) *In-vitro* pull-down assays with Myc-tagged PP2A-C3 (Myc-PP2A-C3), Myc-tagged PP2A-C5 (Myc-PP2A-C5) and GST-RCN1. Either GST or GST-RCN1 was immobilized on the glutathione resin and incubated in a solution containing either Myc-PP2A-C3 or Myc-PP2A-C5 in the presence or the absence of 10 mM $CaCl_2$ or 10 mM EGTA. The resulting resin was subjected to western blotting to analyze the Myc-tagged proteins with an anti-Myc antibody (WB: Myc antibody) and to analyze GST-fused proteins with an anti-GST antibody (WB: GST antibody). The presence and absence of GST-fused proteins, $CaCl_2$, and EGTA are indicated as ‘+’ and ‘-’, respectively. (C) *In-vitro* pull-down assays with His-ATB’’γ, His-ATB’’δ, GST-RCN1 and Myc-PP2A-C5. Either GST or GST-RCN1 was fixed on the glutathione resin and reacted with Myc-PP2A-C5 as in the panel B. The resin was then reacted with either His-AtB”γ or His-AtB”δ in the presence or absence of either 10 mM $CaCl_2$ or 10 mM EGTA. The resulting resin was used for western blotting to analyze the His-tagged, Myc-tagged, and GST-fused proteins as in the panels A and B. The presence and absence of GST-RCN1, Myc-PP2A-C5, $CaCl_2$, and EGTA are indicated as ‘+’ and ‘-’, respectively. All experiments were performed three times, and a representative result is shown for the panels A-C. Myc-tagged proteins and His-tagged proteins are indicated by arrowheads.

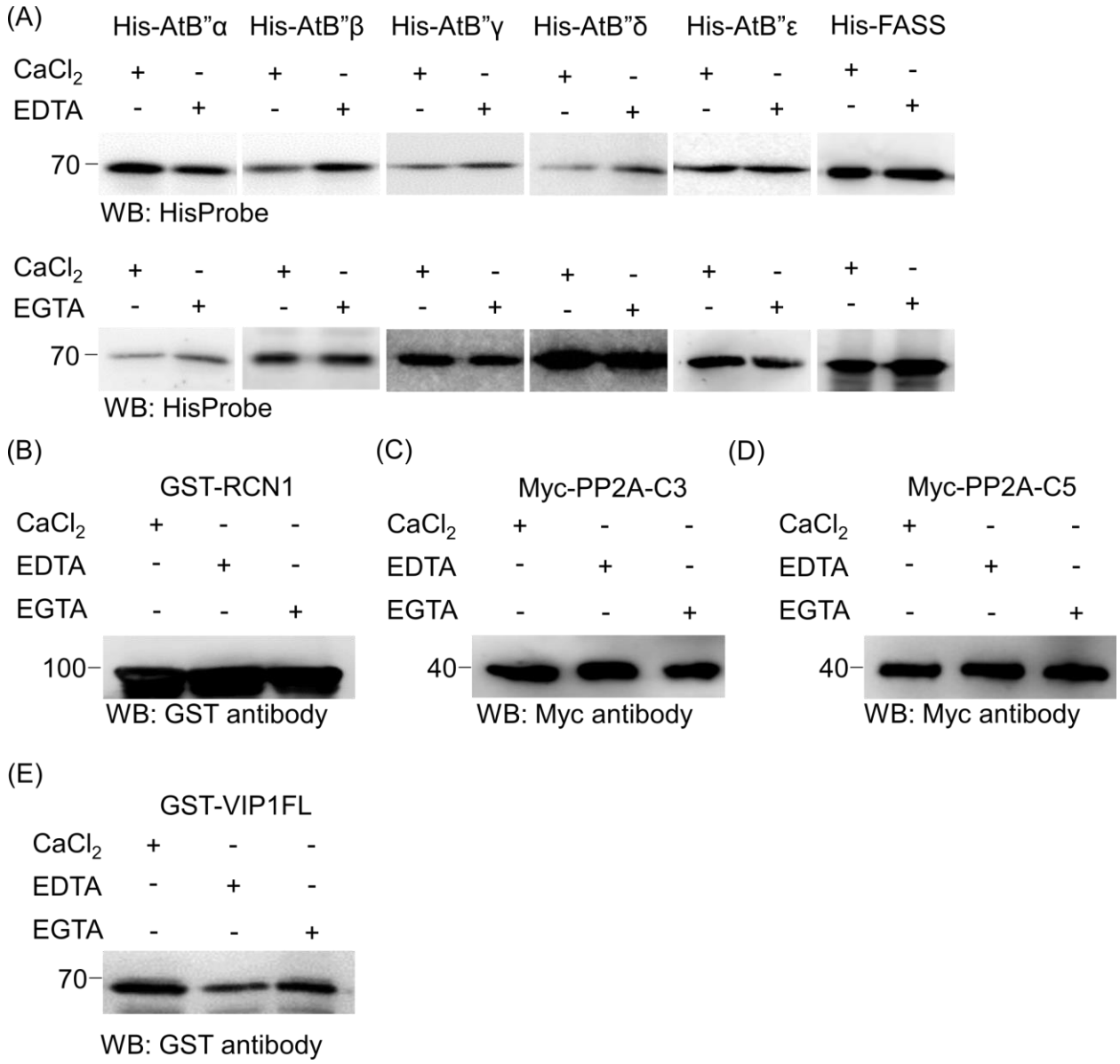

Figure 3.9. Stabilities of recombinant proteins in the presence of $CaCl_2$, EDTA, or EGTA *in vitro*. (A) His-tagged proteins indicated on the top of the images were incubated in the presence ('+') or absence ('-') of 10 mM $CaCl_2$, 20 mM EDTA, or 10 mM EGTA and were detected by western blotting with HisProbe-HRP ("WB: HisProbe"). (B) GST-RCN1 was fixed on the glutathione resin and incubated in the presence ('+') or the absence ('-') of 10 mM $CaCl_2$, 10 mM EDTA, or 10 mM EGTA, eluted from the resin, and detected by western blotting with an anti-GST antibody ("WB: GST antibody"). (C) Myc-PP2A-C3 was fixed on the Anti-Myc-tag mAb-Magnetic Beads (MBL) and incubated in the presence ('+') or the absence ('-') of 10 mM $CaCl_2$, 10 mM EDTA, or 10 mM EGTA, was eluted from the beads and was detected by western blotting with an anti-Myc tag antibody ("WB: GST antibody"). (D) Myc-PP2A-C5 was

incubated with 10 mM $CaCl_2$, 10 mM EDTA, or 10 mM EGTA, and detected as in the panel C. (E) GST-VIP1FL was incubated with 10 mM $CaCl_2$, 10 mM EDTA, or 10 mM EGTA, and detected as in the panel B. The experiments were performed three times, and a representative result is shown for the panels A-E. Molecular mass (kDa) is indicated on the left of each panel.

3.3.8. Arabidopsis PP2A B”-family B subunits and C subunits interact with VIP1 in plant cells

The interactions of VIP1 with PP2A B”-family subunits were also examined by BiFC. The YFP fluorescence was observed when one of the six members of the PP2A B’’-family subunit was as a cYFP-fused form coexpressed with nYFP-fused VIP in Arabidopsis mesophyll protoplasts (Yoon et al., 2021; Figure 3.10A). The YFP fluorescence was also observed when a cYFP-fused form of VIP1 (VIP1-cYFP) was coexpressed with either nYFP-fused PP2A-C3 or nYFP-fused PP2A-C5 in the Arabidopsis mesophyll protoplasts, but not when VIP1-cYFP was coexpressed with either nYFP-fused RCN1 or nYFP-fused PP2A-A2 (Figure 3.10B). These results are consistent with the results of Y2H (Figure 3.2, 3.3 and 3.4) and *in-vitro* pull-down assays (Figure 3.6 and 3.7), and suggest that VIP1 interacts with PP2A B’’-family B subunits and C subunits in plant cells.

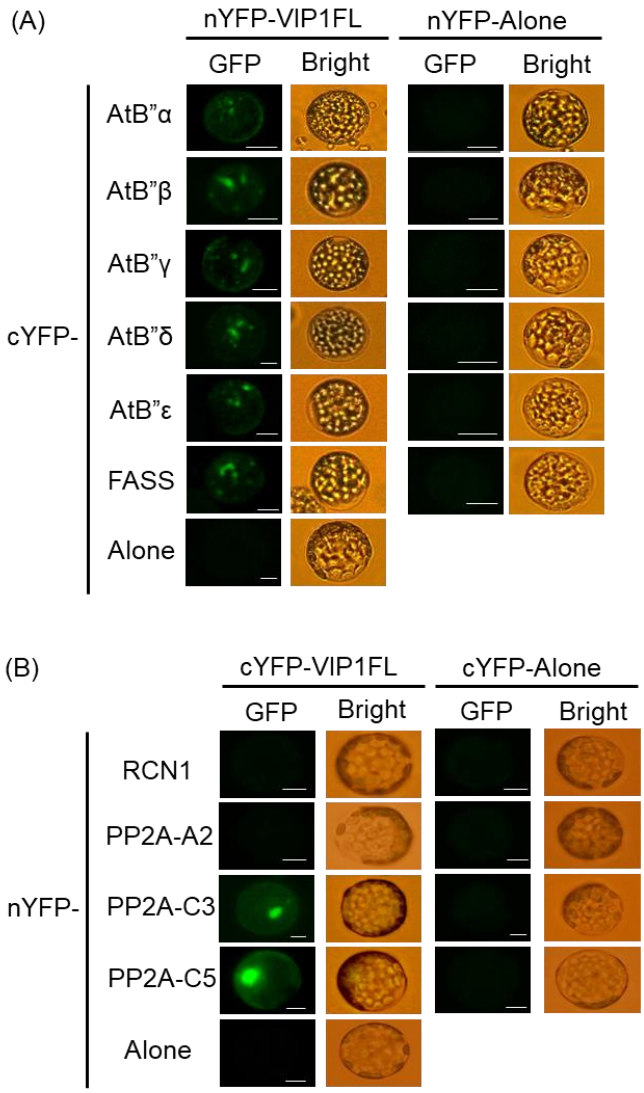

Figure 3.10. PP2A B"-family subunits and C subunits interact with VIP1 in plant cells. (A) BiFC assays with PP2A B"-family subunits and VIP1. nYFP-fused VIP1 (nYFP-VIP1FL) and cYFP-fused forms of PP2A-B" family subunits (cYFP-AtB"α-ε and cYFP-FASS) were co-expressed in Arabidopsis mesophyll protoplasts. YFP signals were detected by fluorescence microscopy. (B) BiFC assays with VIP1, PP2A A subunits (RCN1 and PP2A-A2) and PP2A C subunits (PP2A-C3 and PP2A-C5). nYFP-fused forms of RCN1, PP2A-A2, PP2A-C3 and PP2A-C5 (nYFP-RCN1, nYFP-PP2A-A2, nYFP-PP2A-C3, and nYFP-PP2A-C5, respectively) were coexpressed with cYFP-fused VIP1 (cYFP-VIP1FL) in Arabidopsis mesophyll protoplasts. The pBS-35S-nYFP and pBS-35S-MCS-cYFP empty vectors were used for negative controls (nYFP-Alone and cYFP-Alone, respectively). Signals were observed 16 hours after transformation. Scale bars = 20 μm.

3.3.9. Arabidopsis PP2A B”-family subunits are necessary for de-phosphorylation of VIP1 and its homolog *in vitro*

GST-VIP1FL in a solution can be phosphorylated by purified MBP-CPK21 *in vitro* (Tsugama et al., 2019). In agreement, when GST-VIP1FL was bound by the glutathione resin and was reacted with MBP-CPK21, GST-VIP1FL signals could be detected by western blotting with the phosphorylated protein probe Phos-tag biotin (Yoon et al., 2021; Figure 3.11A). To determine whether PP2A can dephosphorylate VIP1 *in vitro*, the resin-bound phosphorylated form of GST-VIP1FL was incubated in solutions containing Myc-RCN1, Myc-PP2A-C5 and His-AtB”δ and subjected to western blotting with Phos-tag biotin. For this system, the Myc-tagged proteins were expressed in a rabbit reticulocyte lysate-based solution (TNT Quick Master Mix), and His-AtB”δ was expressed in *E.coli* and eluted by 100 mM imidazole. Phos-tag biotin-derived GST-VIP1FL signals were decreased when both the His-AtB”δ solution and the rabbit reticulocyte lysate-based solution were added to GST-VIP1 FL, regardless of the Myc-tagged proteins present in the solution (Yoon et al., 2021; Figure 3.11B). Western blotting with an anti-human PP2A C subunit antibody, which is supposed to cross-react with rabbit PP2A C subunits, detected signals in the rabbit reticulocyte lysate-based solution (Yoon et al., 2021; Figure 3.11C), suggesting that this solution contains rabbit PP2A C subunits. These rabbit PP2A C subunits were pulled down by His-AtB”δ but hardly by His-Venus, a His-tagged protein unrelated to PP2A (Yoon et al., 2021; Figure 3.11D). These results support the idea that AtB”δ interacts with the rabbit PP2A C subunits and induces the VIP1 dephosphorylation *in vitro*.

Myc-tagged AtB”α (Myc-AtB”α), Myc-tagged AtB”δ (Myc-AtB”δ), and Myc-tagged FASS (Myc-FASS) were also expressed in the rabbit reticulocyte lysate-based solution and reacted with phosphorylated GST-VIP1FL. In agreement with the above result with His-AtB”δ, Phos-tag biotin-derived GST-VIP1FL signals were decreased when those Myc-tagged proteins

were present in the reaction mixture (Figure 3.12A). When those Myc-tagged proteins in the rabbit reticulocyte lysate-based solution were immunoprecipitated, the rabbit PP2A C subunits were co-precipitated. The level of the co-precipitated PP2A C subunits was higher when Myc-AtB”δ was used than when either Myc-AtB”α or Myc-FASS was used (Figure 3.12B). GST-fused bZIP29 (GST-bZIP29FL) could also be detected by Phos-tag biotin when reacted with MBP-CPK21 (Figure 3.12C). Phos-tag biotin-derived GST-bZIP29FL signals were also decreased when GST-bZIP29FL was incubated in the rabbit reticulocyte lysate-based solution containing Myc-AtB”α, Myc-AtB”δ, or Myc-FASS (Figure 3.12D). Together, these results suggest that, although AtB”α, AtB”δ, and FASS may differ from each other in affinity to PP2A C subunits, all of them mediate dephosphorylation of VIP1 and bZIP29 *in vitro*.

(A)

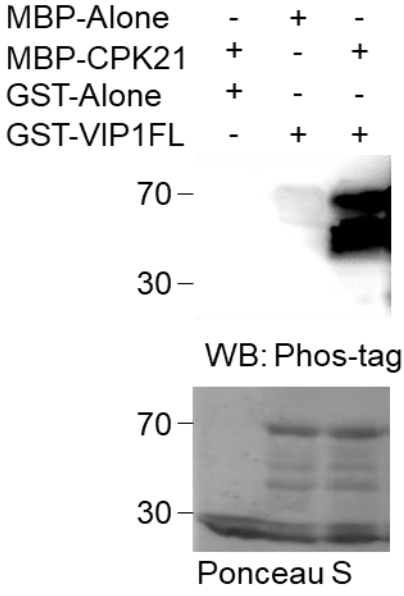
MBP-Alone - + -
MBP-CPK21 + - +
GST-Alone + - -
GST-VIP1FL - + +
70
30
WB: Phos-tag
70
30
Ponceau S

(B)

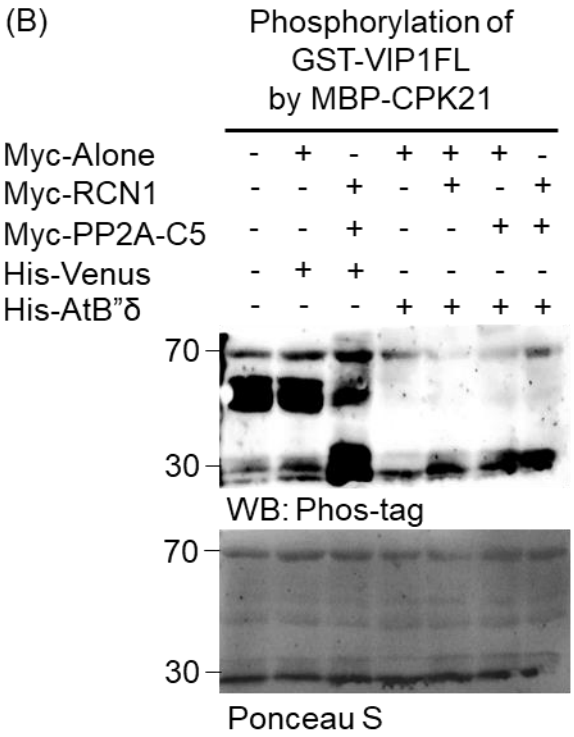
Phosphorylation of GST-VIP1FL by MBP-CPK21
Myc-Alone - + - + + + -
Myc-RCN1 - - + - + - +
Myc-PP2A-C5 - - + - - + +
His-Venus - + + - - - -
His-AtB"δ - - - + + + +
70
30
WB: Phos-tag
70
30
Ponceau S

(C)

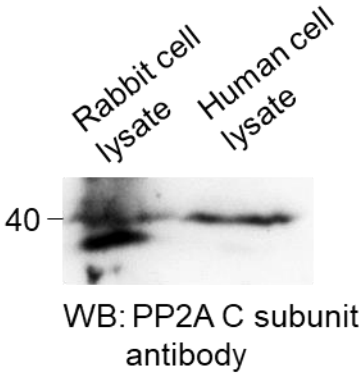
Rabbit cell lysate
Human cell lysate
40
WB: PP2A C subunit antibody

(D)

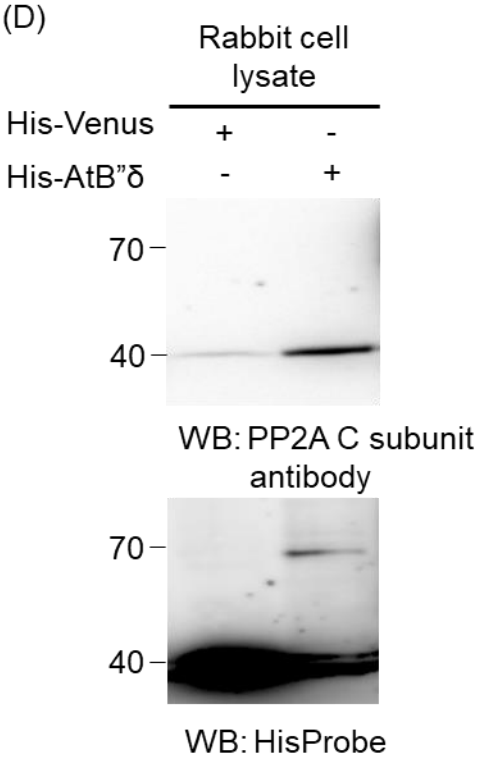
Rabbit cell lysate
His-Venus + -
His-AtB"δ - +
70
40
WB: PP2A C subunit antibody
70
40
WB: HisProbe

Figure 3.11. AtB”δ-dependent dephosphorylation of VIP1 *in vitro*. (A) *In-vitro* phosphorylation assays. Either GST (GST-Alone) or GST-VIP1FL was immobilized on the glutathione resin and incubated with purified MBP-CPK21. MBP (MBP-Alone) was used for a negative control. The presence and absence of GST-fused proteins and MBP-fused proteins are indicated as ‘+’ and ‘-’, respectively. Signals of phosphorylated GST-VIP1 were detected by western blotting with Phos-tag biotin (WB: Phos-tag). The presence of the GST-fused proteins was confirmed by a Ponceau S staining solution. (B) GST-VIP1 FL was fixed on the glutathione resin and phosphorylated by MBP-CPK21. A TNT Quick Master Mix solution containing the Myc tag alone (Myc-Alone), Myc-tagged PP2A-C5 (Myc-PP2A-C5), or Myc-tagged RCN1 (Myc-RCN1) was added to the resin and incubated for one hour at room temperature. Signals of phosphorylated GST-VIP1 were detected as in the panel A. (C) Detection of rabbit PP2A C subunits. The TNT Quick Master Mix solution was subjected to western blotting with an anti-PP2A C subunits antibody (“WB: PP2A C subunit antibody”). A human A431 cell lysate was used as a positive control. (D) AtB”δ interacts with rabbit PP2A C subunits *in vitro*. Either His-Venus or His-AtB”δ was immobilized on the Ni-NTA agarose and reacted with the TNT Quick Master Mix solution. The presence and the absence of His-Venus and His-AtB”δ in the reaction mixtures are indicated as ‘+’ and ‘-’, respectively. Rabbit PP2A C subunits and the His-tagged proteins were detected by western blotting with an anti-PP2A C subunit (“WB: PP2A C subunit”) and HisProbe-HRP (“WB: HisProbe”), respectively. The experiments were performed three times, and a representative result is shown for the panels A-D. Molecular mass (kDa) is indicated on the left in each panel.

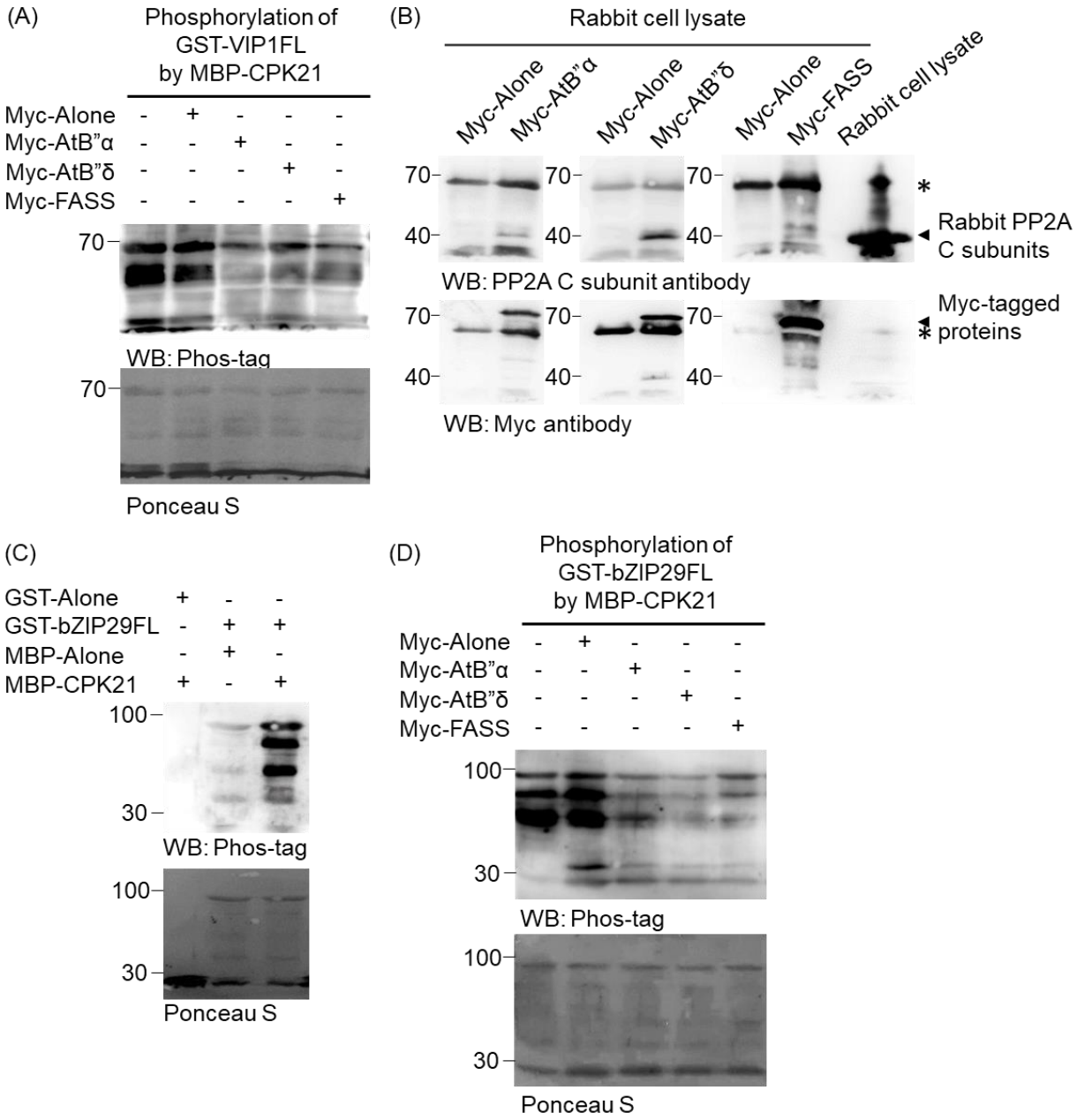

Figure 3.12. Arabidopsis PP2A B"-family subunits are necessary for *in-vitro* dephosphorylation of VIP1 and bZIP29. (A) *In-vitro* dephosphorylation assays with GST-VIP1FL. GST-VIP1FL was fixed on the glutathione beads and phosphorylated by MBP-CPK21. Myc tag alone (Myc-Alone), Myc-tagged AtB"α (Myc-AtB"α), Myc-tagged AtB"δ (Myc-AtB"δ) or Myc-tagged FASS (Myc-FASS) in the TNT Quick Master Mix solution was added to the resin and incubated for one hour at room temperature. Signals of phosphorylated GST-VIP1FL was detected by western blotting with Phos-tag biotin ("WB: Phos-tag biotin"). The presence of GST-VIP1FL was confirmed by a Ponceau S staining solution. (B) *In-vitro* pull-down assays. Myc-

Alone, Myc-AtB”α, Myc-AtB”δ, or Myc-FASS was expressed in the TNT Quick Master Mix solution and was immobilized on Anti-Myc-tag mAb-Magnetic Beads (MBL). Rabbit PP2A C subunits and Myc-tagged proteins were detected by western blotting with an anti-PP2A C subunit (“WB: PP2A C subunit”) and an anti-Myc tag antibody (“WB: Myc antibody”), respectively. Asterisks indicate positions of nonspecific signals. (C) An *in-vitro* phosphorylation assay with GST-bZIP29FL. Either GST (“GST-Alone”) or GST-bZIP29FL was immobilized on the glutathione resin and phosphorylated by purified MBP-CPK21. MBP (MBP-Alone) was used for a negative control. The presence and absence of GST-fused proteins and MBP-fused proteins are indicated as ‘+’ and ‘-’, respectively. Signals of phosphorylated GST-bZIP29FL were detected by western blotting with Phos-tag biotin (WB: Phos-tag). GST-fused proteins were confirmed by a Ponceau S staining solution. (D) *In-vitro* dephosphorylation assays with GST-bZIP29FL. GST-bZIP29FL was fixed on the glutathione resin and phosphorylated by MBP-CPK21. Myc-Alone, Myc-AtB”α, Myc-AtB”δ, or Myc-FASS in the TNT Quick Master Mix solution was added to the resin and incubated for one hour at room temperature. Signals of phosphorylated GST-bZIP29FL were detected as in the panel A. The experiments were performed three times, and a representative result is shown for the panels A-D. Molecular mass (kDa) is indicated on the left in each panel.

3.3.10. *AtB"β AtB"δ* double knockout does not affect the subcellular localization of VIP1

VIP1-GFP was expressed in the wild-type (VIP1-GFPox/WT), *AtB"β* single knockout (VIP1-GFPox/*atb"β*), *AtB"δ* single-knockout (VIP1-GFPox/*atb"δ*), and *AtB"β AtB"δ* double-knockout (VIP1-GFPox/*atb"βδ*) backgrounds (Figure 3.13A). When these plants were incubated in the hypotonic solution or when their roots were touched by tweezers, VIP1-GFP signals were detected in the nucleus and then in the cytoplasm, regardless of their genetic backgrounds (Yoon et al., 2021; Figure 3.13B, C). This may be because the PP2A B''-family subunits other than AtB"β and AtB"δ can induce VIP1 dephosphorylation and the subsequent VIP1 nuclear accumulation.

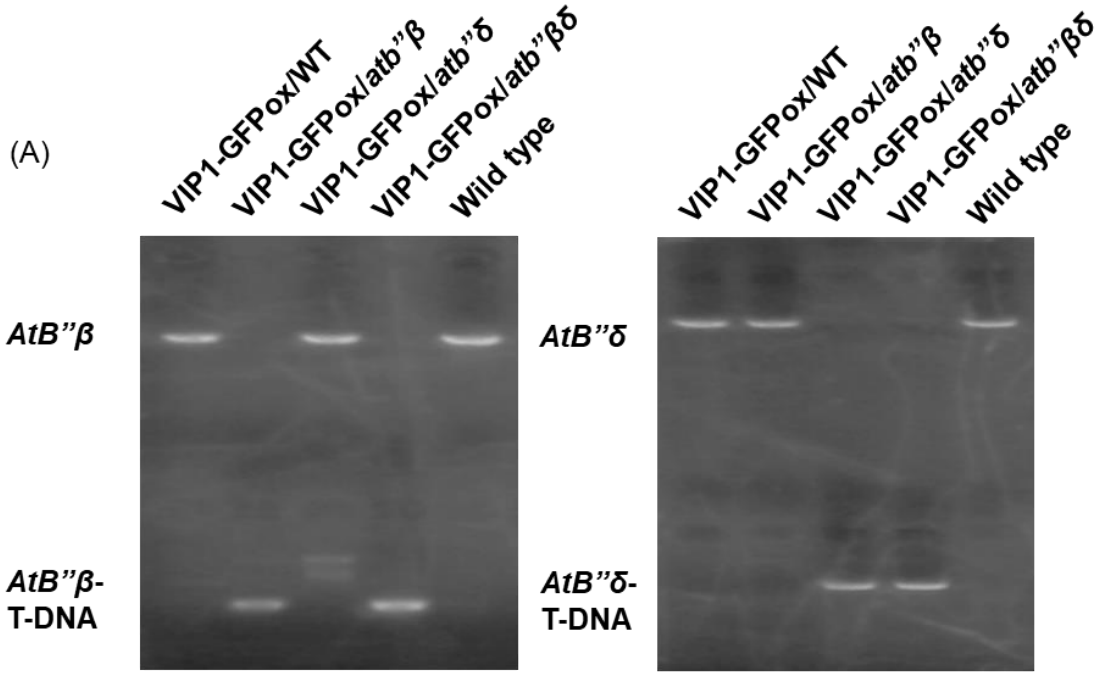
(A)
VIP1-GFPox/WT
VIP1-GFPox/atb"β
VIP1-GFPox/atb"δ
VIP1-GFPox/atb"βδ
Wild type
AtB"β
AtB"β-
T-DNA
VIP1-GFPox/WT
VIP1-GFPox/atb"β
VIP1-GFPox/atb"δ
VIP1-GFPox/atb"βδ
Wild type
AtB"δ
AtB"δ-
T-DNA

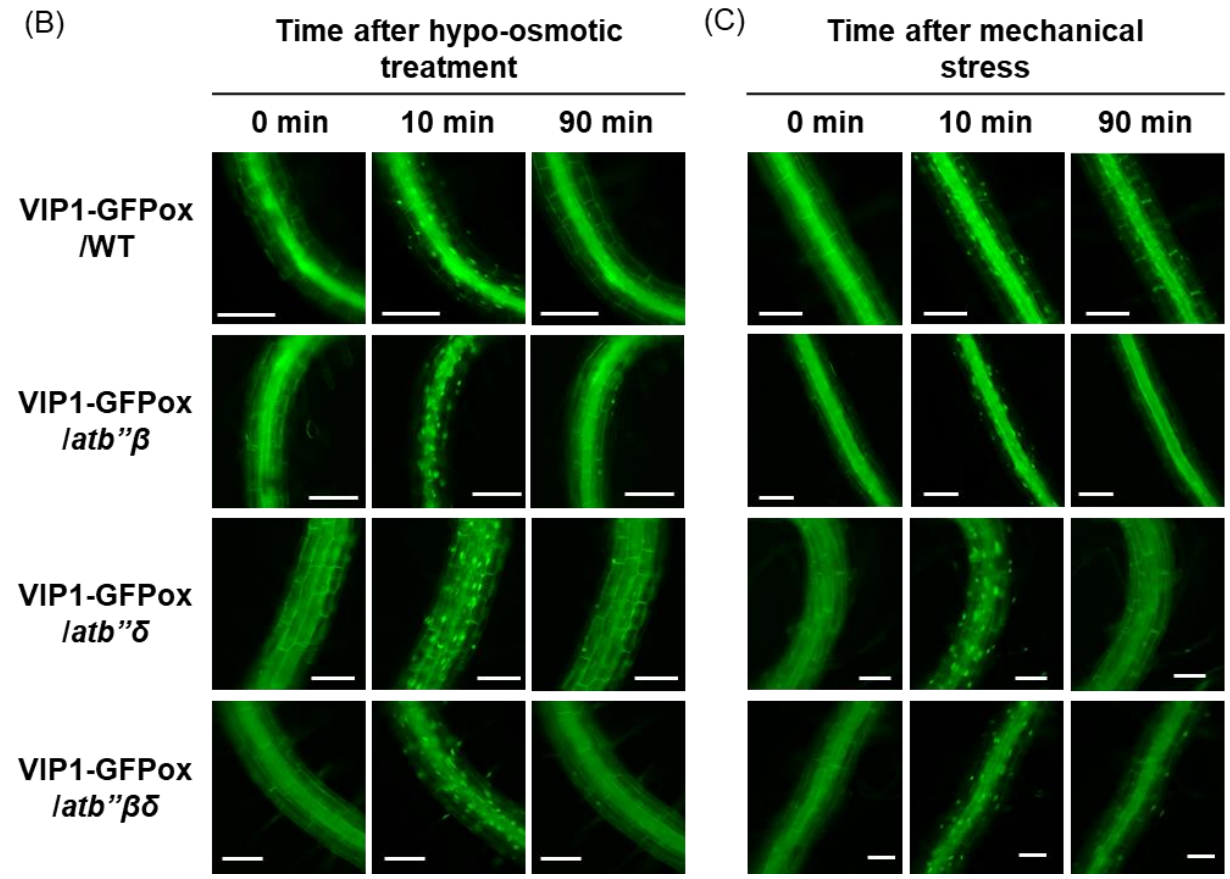
(B)
Time after hypo-osmotic treatment
0 min
10 min
90 min
VIP1-GFPox /WT
VIP1-GFPox /atb"β
VIP1-GFPox /atb"δ
VIP1-GFPox /atb"βδ
(C)
Time after mechanical stress
0 min
10 min
90 min

Figure 3.13. An *AtB"β AtB"δ* double knockout does not affect the subcellular localization of VIP1-GFP under hypo-osmotic stress and mechanical stress. (A) Genotyping of VIP1-GFP-overexpressing lines. Genomic DNA was extracted from wild-type plants and plants overexpressing VIP1-GFP (VIP1-GFPox) in the wild type background (VIP1-GFPox/WT), the *AtB"β* single-knockout background (VIP1-GFPox/*atb"β*), the *AtB"δ* single-knockout background (VIP1-GFPox/*atb"δ*) and the *AtB"β AtB"δ* double-knockout background (VIP1-GFPox/*atb"βδ*). (B) Patterns of VIP1-GFP signals under a hypo-osmotically stressed condition. VIP1-GFPox/WT, VIP1-GFPox/*atb"β*, VIP1-GFPox/*atb"δ*, and VIP1-GFPox/*atb"βδ* plants were incubated in distilled water to induce hypo-osmotic stress. VIP1-GFP signals in roots were detected by fluorescence microscopy at the indicated time points. (C) Patterns of VIP1-GFP signals in touch-stressed plants. Roots of VIP1-GFPox/WT, VIP1-GFPox/*atb"β*, VIP1-GFPox/*atb"δ*, and VIP1-GFPox/*atb"βδ* plants were touched and VIP1-GFP signals in these roots were detected by fluorescence microscopy at the indicated time points. For the panels B and C, ten seedlings were used for the analyses and a representative result is shown for each genotype. Scale bars=100 μm.

3.3.11. Quadruple knockout of PP2A B”-family subunit genes does not affect plant responses to abiotic stresses.

ATB”α ATB”β ATB”γ ATB”δ quadruple-knockout (*atb”αβγδ)* plants were generated (Figure 3.14A). In agreement with previous studies (Waadt et al., 2015; Tsugama et al., 2016; Xi et al., 2016), root VGIs of *RCN1* knockout (*rcn1-6*; Figure 3.14B) plants and the VIP1-SRDXox #7 (VIP1-SRDX-overexpressing line #7) plants were both significantly lower than the VGI of the wild type. However, the VGI of *atb”αβγδ* plants was similar to the VGI of the wild-type plants (Figure 3.14C, D). No difference was observed between *atb”αβγδ* and wild-type plants in germination rates under a Ca^{2+}-deficient, mannitol-stressed, NaCl-stressed, or ABA-supplemented condition (Figure 3.15). No difference was observed in their subsequent growth, either. It is possible that *FASS* and *ATB”ε* have functional redundancy with the other four PP2A B”-family subunit genes and cause the wild type-like phenotypes of the *atb”αβγδ* plants. Further studies are necessary to better understand the physiological functions of the PP2A B”-family subunits in plants.

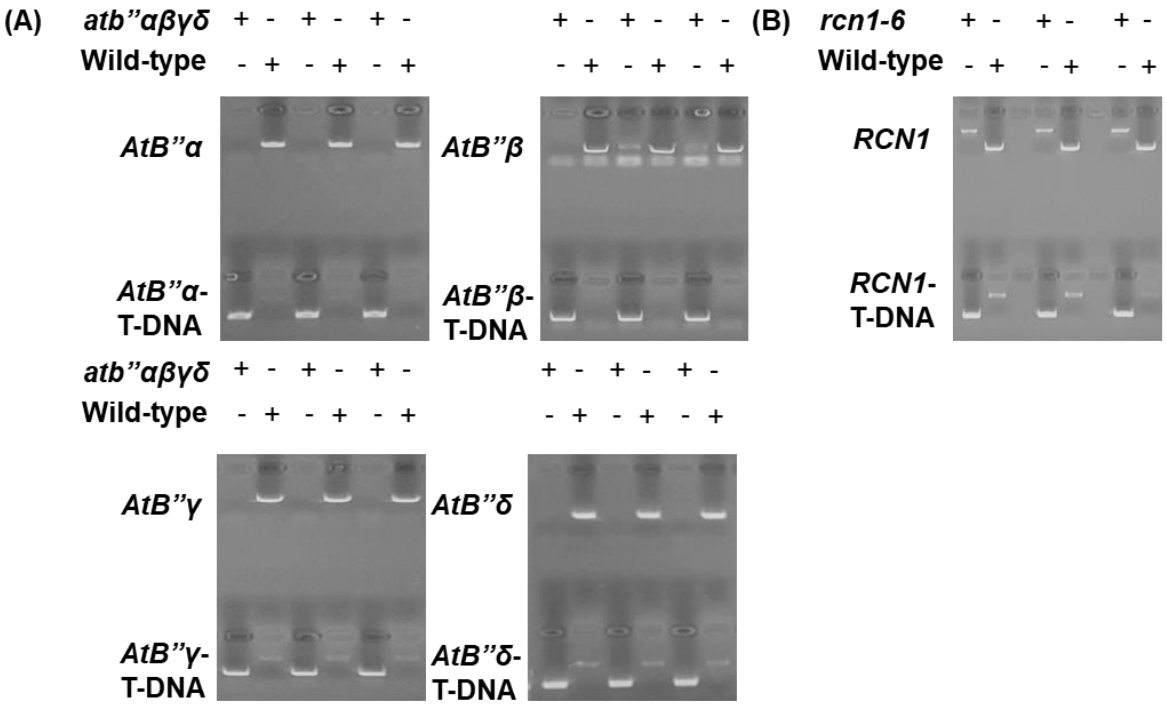
(A)
atb"αβγδ + - + - + -
Wild-type - + - + - +
AtB"α
AtB"α-
T-DNA
AtB"β
AtB"β-
T-DNA
atb"αβγδ + - + - + -
Wild-type - + - + - +
AtB"γ
AtB"γ-
T-DNA
AtB"δ
AtB"δ-
T-DNA
(B)
rcn1-6 + - + - + -
Wild-type - + - + - +
RCN1
RCN1-
T-DNA


(C)
Wild type
VIP1-SRDXox #7
rcn1-6
atb"αβγδ

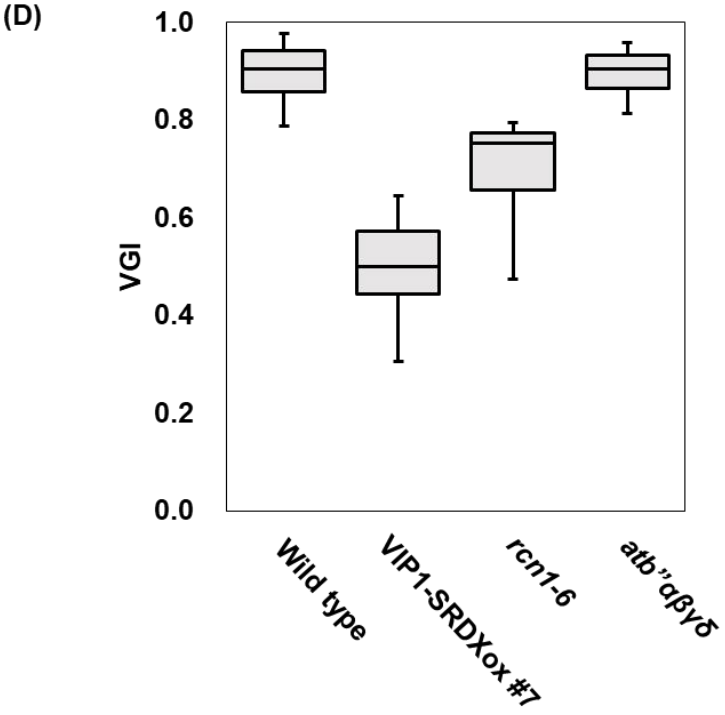
(D)
VGI
1.0
0.8
0.6
0.4
0.2
0.0
Wild type
VIP1-SRDXox #7
rcn1-6
atb"αβγδ

Figure 3.14. Touch-induced root bending in the *atb"αβγδ* quadruple-knockout mutant. (A) Genotyping of *atb"αβγδ* plants. Genomic DNA was extracted from wild-type and *atb"αβγδ* plants and used as templates for PCR to analyze T-DNA insertions in *AtB"α*, *AtB"β*, *AtB"γ* and *AtB"δ*. (B) Genomic DNA was extracted from the wild-type and *rcn1-6* plants and used as templates for PCR to confirm the T-DNA insertion in *RCN1*. (C) Phenotypes of wild-type, VIP1-SRDXox #7, *rcn1-6*, and *atb"αβγδ* seedlings. These plants were grown on an agar medium containing tilted at a 75° angle for 5 days. A representative image is presented for each genotype. Bars = 5 mm. (D) Root VGIs of wild-type, VIP1-SRDXox #7, *rcn1-6*, and *atb"αβγδ* seedlings. The top and bottom edges and the line in the middle of each box indicate quartiles, and the bar corresponds to the data range (n = 50/each line).

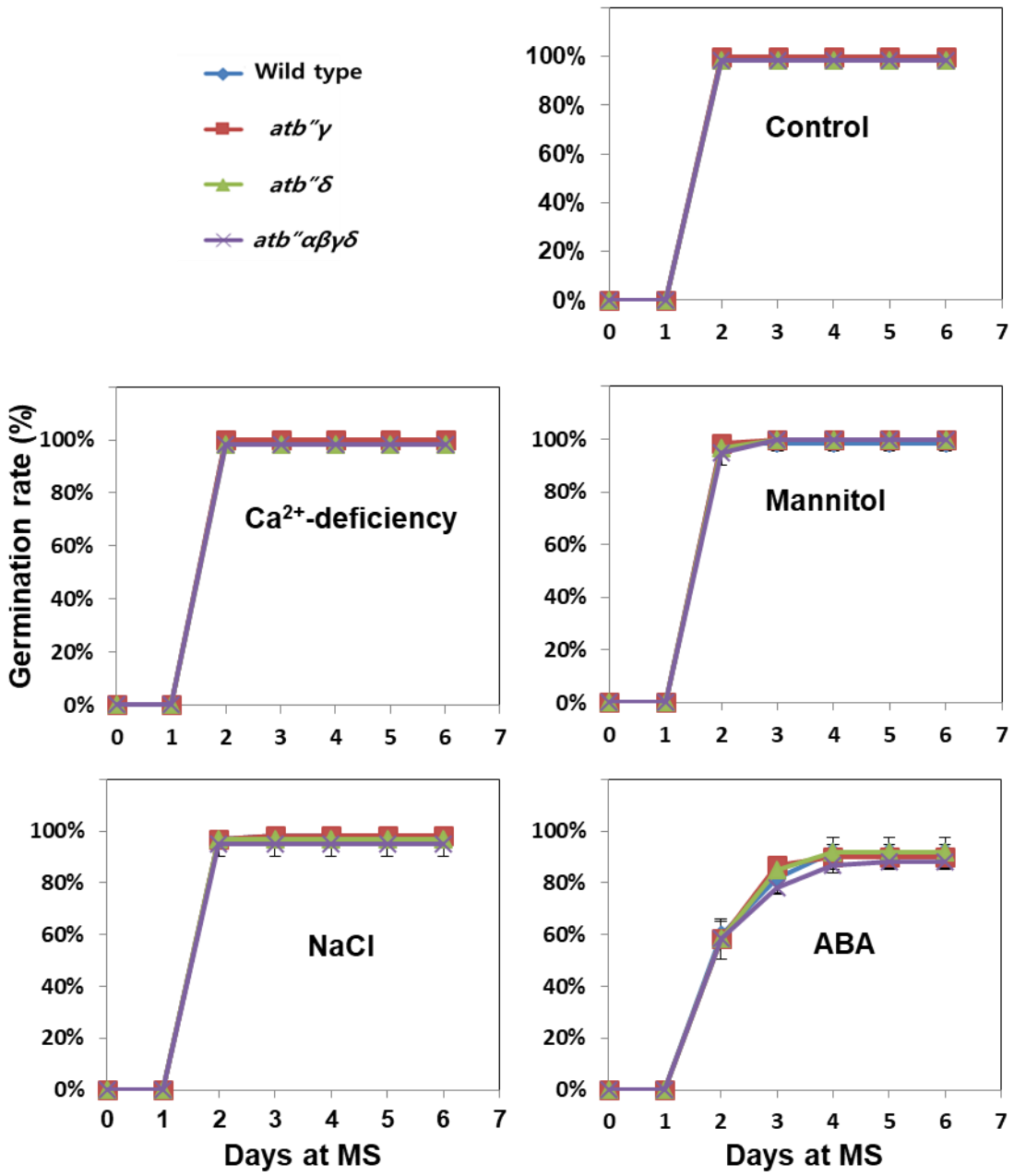

Figure 3.15. Germination rates of the *atb"αβγδ* quadruple-knockout mutant under stressed and ABA-supplemented conditions. Wild-type, *atb"γ*, *atb"δ*, and *atb"αβγδ* plants were grown on a medium lacking $CaCl_2$ ("Ca^{2+}-deficiency"), a medium containing 200 mM mannitol, a medium containing 100 mM NaCl, and a medium containing 1 μM ABA for 6 days to obtain their germination rates. Data are means ± SD of three biological replicates. Twenty plants were used to obtain the germination rate for each line and each condition.

3.4. Discussion

VIP1 was previously shown to interact with ATB''δ and FASS (Tsugama et al., 2019). Here VIP1 was also shown to interact with all the other Arabidopsis B''-family B subunits of PP2A (Yoon et al., 2021; Figure 3.3, 3.6 and 3.10). Here we also showed that VIP1-GFP is localized in the nucleus even in the *AtB"β AtB"δ* double-knockout background (Yoon et al., 2021; Figure 3.13B and C), and that the *AtB"α AtB"β AtB"γ AtB"δ* quadruple knockout does not affect growth under various growth conditions (Figure 3.14C, D and 3.15). Because a *FASS* knockout causes embryonic lethality (Mayer et al., 1991), FASS may play more significant physiological roles than the other PP2A B''-family B subunits. Nevertheless, our results suggest that those B''-family B subunits, or ATB''α-ε, function redundantly. Further studies with new materials such as an *AtB"α AtB"β AtB"γ AtB"δ AtB"ε* quintuple-knockout mutant is necessary to elucidate the physiological roles for those ATB''α-ε.

Not only the B''-family B subunits of PP2A but also its C subunits (PP2A-C3 and PP2A-C5) were shown to interact with VIP1 (Yoon et al., 2020; Figure 3.4B, 3.7B and 3.7C). PP2A-C5 alone cannot dephosphorylate VIP1 *in vitro* (Yoon et al., 2021; Figure 3.11B), but this does not rule out the possibility that those PP2A C subunits contribute to the PP2A-dependent dephosphorylation of VIP1. In human, proteins such as α4 and leucine carboxyl methyltransferase 1 (LCMT-1) can directly interact with PP2A C subunits and change their structure and activity (Stanevich et al., 2011; Jiang et al., 2013). Thus, VIP1 might also affect the PP2A C subunit activity.

In agreement with a previous study with ATB''α and ATB''β (Leivar et al., 2011), ATB''δ and ATB''γ interacted with RCN1 in the presence of Ca^{2+} (Figure 3.8A), confirming that ATB''δ and ATB''γ function as PP2A components. PP2A-C3 and PP2A-C5 were also shown to interact with RCN1. Unexpectedly, EGTA attenuated the interactions between these

PP2A C subunits and RCN1 (Yoon et al., 2021; Figure 3.8B). Rabbit PP2A C subunits require Mn^{2+} and Co^{2+} as a cofactor (Yu, 1998). Such Mn^{2+} ions are present at the active, catalytic site of PP2A C subunits and stabilize the structure of this site (Stanevich et al., 2011; Jiang et al., 2013). EGTA binds to Mn^{2+} and Co^{2+} with a higher affinity than Ca^{2+}, and this may lead to the destabilization of the interaction between PP2A A and C subunits.

Chapter 4

VIP1 and its close homologs confer the mechanical stress tolerance in Arabidopsis leaves

4.1. Introduction

PosF21, bZIP29, bZIP30, bZIP69, and bZIP52 are functionally redundant with VIP1: All of these proteins shuttle between the cytoplasm and nucleus when cells are exposed to hypo-osmotic stress; All of them interact with VIP1; All of them exhibit transcriptional activation potential in a yeast one-hybrid system; All of them bind promoter fragments of the hypo-osmotic stress-responsive genes *CYP707A1* and *CYP707A3* (Tsugama et al., 2014, 2016). Either AGCTGT or AGCTGG (AGCTG[GT]) in these promoter fragments is responsible for binding VIP1 (Tsugama et al., 2014). Previous studies identified AGCNGT as the VIP1 response element (Pitzschke et al., 2009), and AGCTG[GT] as the bZIP52-binding motif (O'Malley et al., 2016). PosF21, bZIP29, bZIP30, and bZIP69 are also likely to bind AGCTG[GT]. Phenotypes of *VIP1 bZIP29* double-knockout (*vip1-1 bzip29*) plants and *VIP1 bZIP29 PosF21* triple-knockout (*vip1-1 bzip29 posf21*) plants are similar to the phenotypes of wild-type plants under various growth conditions (Tsugama et al., 2016; Lapham et al., 2018). Although VIP1-SRDX-overexpressing (VIP1-SRDXox) plants exhibit enhanced touch-induced root bending, physiological relevance (especially to mechanical stress responses) of VIP1 and its close homologs remains to be examined.

Here, we show that *VIP1 PosF21 bZIP29 bZIP30* quadruple-knockout plants are hypersensitive to brushing-induced mechanical stress. By analyzing their transcriptomes, we also show that those proteins and AGCTG[GT] are relevant to controlling the mechanical stress-responsive gene expression.

4.2. Materials and method

4.2.1. Plant materials

Arabidopsis ecotype Col-0 was used as the wild type control in all experiments. *rcn1-6*, *atb"δ*, and *atb"αβγδ* plants were prepared as described in the section 3.2.1. VIP1-GFPox and VIP1-SRDXox (lines #7 and #11) plants were prepared as previously described (Tsugama et al., 2012a, 2016). To generate *VIP1 PosF21 bZIP29 bZIP30* quadruple-knockout lines, seeds of *vip1-1* (ABRC accession number: SALK_001014C, Li et al., 2005), *posf21* (SALK_043152, *PosF21* knockout), *bzip29* (SALK_065254C, *bZIP29* knockout; Tsugama et al., 2016), and *bzip30* (SALK_003886, *bZIP30* knockout) were obtained from ABRC. *vip1-1 bzip29 posf21* plants were generated as previously described (Lapham et al., 2018). Seeds of *vip1-2*, which has a 2-bp deletion in *VIP1* (Lapham et al., 2018), were provided by Dr. Stanton B. Gelvin (Purdue University). *vip1-1 bzip29 posf21* plants and *bzip30* plants were crossed to obtain the *vip1-1 posf21-1 bzip29-1 bzip30-1* quadruple-knockout mutant (QM1) line. *vip1-2* and QM1 plants were crossed to obtain the *vip1-2 posf21-1 bzip29-1 bzip30-1* quadruple-knockout mutant (QM2) line. T-DNA insertions in these mutant lines were confirmed by genomic PCR with KOD FX Neo (Toyobo). The 2-bp deletion in *vip1-2* and QM2 was confirmed by genomic PCR with HiDi Taq DNA polymerase (myPOLS Biotec), which is sensitive to one-base mismatch between a primer and a PCR template. Primer pairs used for the genomic PCR are listed in Table 4.1. Plant materials were maintained as described in the section 3.2.1.

Table 4.1. Primer pairs used for genomic PCR.

Primers	Sequence (5'>3')	Targets (Mutants)
VIP1WTgin450F	AGCTACAAGTTCAGGAGAGAAGAAGAA	*VIP1* and (*vip1-2* and QM2)
VIP1gin695R	GGATCAAGCAAAGCAAGCTCA	

VIP1mut2gin450F	AGCTACAAGTTCAGGAGAGAAGAAGAGG	
VIP1gF	CGGCGTCGTTTAATATCGAATC	*VIP1* (*vip1-1* and QM1)
VIP1gR	GGAGCGATGGCTGCCCGTTT	
PosF21_for_T-DNA_inner_Fw	GGGCCTCCTGGATCTCTCTCTC	*PosF21* (QM1 and QM2)
PosF21_for_T-DNA_inner_Rv	ACGCTGATGGAGCAACTTGGC	
bZIP29_for_genomic PCR_Fw	CCCGCTCCTTGAGAGTCGGTGAG	*bZIP29* (QM1 and QM2)
bZIP29_for_genomic PCR_Rv	CCCCGTTAGTCTTGGTCCCGCTT	
bzip30-2gFv2	TCTCGCTCTATGTCGCAACCGTC	*bZIP30* (QM1 and QM2)
bzip30-2gR	TTCCCACTCGCACTGCTATC	
T-DNA_LBTR3	CAGCTGTTGCCCGTCTCACTGG	T-DNA (QM1 and QM2)

4.2.2. Plant growth tests

To examine plant responses to mechanical stress, leaves were brushed as described previously (Verhertbruggen et al., 2013). Briefly, rosette leaves of three-week-old plants were brushed for 10 seconds. This brushing treatment was imposed on the same plants every day at 10:00 and 17:00 for another six days. To obtain survival rates and flower stalk lengths, the stressed plants (twenty plants per genotype) were photographed seven days after the brushing treatment was started. Plants with emerging green leaves were regarded as survivors. Experiments were independently performed three times.

To examine effects of planting density on plant growth, plants were grown on the MS agar medium as described in the section 2.2.1 and transferred to a soil with either a high density or a low density. For the low-density planting, four seedlings per genotype were planted on a pot with a 4 cm × 4 cm size. For the high-density planting, nine seedlings were planted on a pot with the same size. These plants were further grown for 2 weeks and photographed.

Root VGIs of wild-type, VIP1-GFPox, VIP1-SRDXox #7, QM1, and QM2 plants were examined as described in the section 3.2.1. These plants were also grown on the MS agar medium supplemented with 0.5 μM 1-aminocyclopropane-1-carboxylate (ACC), 0.2 μM 2,4-Dichlorophenoxyacetic acid (2,4-D), 0.5 μM ABA, 100 mM NaCl, or 200 mM mannitol.

4.2.3. RNA sequencing (RNA-Seq)

Two-week-old wild-type and QM2 plants were subjected to the brushing treatment for three days as described in the section 4.2.2. Their rosette leaves were sampled 20 minutes after the final brushing treatment. RNA was isolated from these leaves as described in the section 2.2.2. Resulting RNA samples were sent to Novogene Bioinformatics Institute (Beijing, China), where RNA-Seq libraries were prepared and sequenced with NovaSeq 6000 (Illumina, Inc., San Diego, CA). The brushing treatment and RNA isolation were performed three times for each genotype, and these were regarded as three biological replicates.

Clean reads obtained were mapped to the Arabidopsis cDNA (or mRNA) sequences (Araport11). Transcripts per million (TPM) values were obtained from the read counts and were used as expression values for each mRNA. mRNA with a TPM value more than 2 times higher in one sample than another was regarded as differentially expressed mRNA (or differentially expressed genes, DEGs). To analyze motifs in promoters of DEGs, 500-bp upstream sequences from the start codons for those genes were downloaded from The Arabidopsis Information Resource (TAIR, https://www.arabidopsis.org/) and used as the promoter sequences. Motifs enriched in these promoter sequences were extracted by HOMER (v. 4.11) (Heinz et al., 2010) with promoter sequences of 2000 randomly chosen genes of Arabidopsis as the background.

4.2.4. qRT-PCR

RNA was prepared as described in the section 4.2.3. cDNA was prepared and qRT-PCR was run as described in the section 2.2.2. Target genes and primers used are listed in Table 4.2. *UBQ5* was used as the internal control gene to obtain relative expression levels as described in the section 2.2.2. Experiments were performed three times independently and regarded as biological replicates.

Table 4.2. Primer pairs used for qRT-PCR.

Genes		Sequence (5'>3')
EXLA1	Fw	CCACCGGAGCTATCCAGTTC
	Rv	AAGATGTTTGTTTGTGTGCCACT
XTH23	Fw	TGGTTCGTGGTTGTCTCAGG
	Rv	CTAAGCACTCGCGTGGAAGA
UBQ5	Fw	GACGCTTCATCTCGTCC
	Rv	CCACAGGTTGCGTTAG

4.2.5. Reactive oxygen species (ROS) detection

ROS were detected with a fluorescent ROS probe, aminophenyl fluorescein (APF) as previously described (Tsugama et al., 2012c). Rosette leaves of four-week-old wild-type, VIP1-SRDXox #7, QM1, and QM2 plants were brushed for 10 seconds once, submerged into 20mM Tris-HCl, pH 6.8, containing 5 μM APF 1, 5 or 10 min after the treatment, and incubated for 10 min at room temperature. Leaves were then washed with distilled water, and APF fluorescence was detected by an epifluorescence microscope (BX51). APF signals were quantified with ImageJ as previously described (Shin et al., 2019).

4.2.6. DAPI staining

To examine brushing-induced damages in leaf cells, rosette leaves of four week-old wild-type, VIP1-SRDXox #7, QM1, QM2, and VIP1-GFPox plants were brushed for 10 seconds once and sampled 1 min, 5 min, 15 min, 60 min and 1 day after the treatment. Leaves were submerged into phosphate-buffered saline (PBS) (pH 7.4) containing 1 μg/ml of DAPI, incubated for 20 min at room temperature and washed twice by PBS. DAPI-stained areas in leaves were detected by an epifluorescence microscope (BX51).

4.2.7. Analysis of electrolyte leakage

Leaves of four-week-old wild-type, VIP1-SRDXox #7, QM1, QM2, and VIP1-GFPox plants were brushed once for 10 seconds and sampled 0 min, 5 min and 15 min after the treatment. Five (approximately 50 mg) rosette leaves were submerged into 5 ml distilled water and incubated overnight at room temperature. The electrical conductivity (EC) of the solution was measured by an EC meter (COMPACT CONDUCTIVITY METER LAQUAtwin-EC-33, HORIBA Scientific, Kyoto, Japan) before and after the samples were autoclaved for 15 min at 120℃ and designated as EC-I and EC-II, respectively. Electrolyte leakage was evaluated by the values obtained by 100 × EC-I/EC-II as previously described (Lu et al., 2008; Shakir et al., 2018).

4.2.8. Subcellular localization of VIP1-GFP

Rosette leaves of four-week-old VIP1-GFPox plants were brushed for 10 seconds and incubated for 10 min at room temperature. Signals of VIP1-GFP in these leaves were then detected with the fluorescence microscopy as described in the section 3.2.3.

4.2.9. Accession numbers

Details regarding the sequences of the genes used in this chapter are available with the following Arabidopsis Genome Initiative accession numbers: AT1G43700 (*VIP1*), AT2G31370 (*PosF21*), AT4G38900 (*bZIP29*), AT2G21230 (*bZIP30*), AT1G06070 (*bZIP69*), AT1G06850 (*bZIP52*), AT2G40620 (*bZIP18*), AT1G25490 (*RCN1*), AT5G44090 (*AtB"α*), AT1G03960 (*AtB"β*) AT1G54450 (*AtB"γ*), AT5G28900 (*AtB"δ*), AT4G25810 (*XTH23*), AT3G45970 (*EXLA1*), AT5G09410 (*CAMTA1*), AT5G64220 (*CAMTA2*), AT2G22300 (*CAMTA3*), AT1G67310 (*CAMTA4*), AT4G16150 (*CAMTA5*), AT3G16940 (*CAMTA6*), and AT3G62250 (*UBQ5*).

4.3. Results

4.3.1. Leaves of *VIP1 PosF21 bZIP29 bZIP30* quadruple mutant and VIP1-SRDXox lines are hypersensitive to mechanical stress

To further study physiological roles of VIP1 and its close homologs, QM1 and QM2, two lines with mutations in *VIP1*, *PosF21*, *bZIP29*, and *bZIP30*, were generated (Figure 4.1). In both QM1 and QM2 plants, *PosF21*, *bZIP29* and *bZIP30* are knocked out by T-DNA insertions. QM1 has T-DNA in *VIP1* as well but exhibits expression of *VIP1* 5' region that corresponds to the N-terminal 244 amino acids of the 341 amino acids of VIP1. QM2 has a 2-bp deletion in VIP1 5' region and should exhibit expression of N-terminal 140 amino acids of VIP1 (Lapham et al., 2018).

Under a normal, non-stressed growth condition, flower stalks of QM1 and QM2 plants were longer than the flower stalks of the wild-type plants (Figure 4.2). No difference was observed in either the time of the emergence of the first floral bud or the number of rosette leaves between the QM1, QM2 and wild-type plants. These results raise the possibility that the flower stalks grow faster in QM1 and QM2 plants than in the wild type.

No difference was observed in leaf shapes between QM1, QM2 and wild-type plants, either. However, leaves of QM1, QM2, and VIP1-SRDXox plants were appeared more severely damaged than did the leaves of wild-type, VIP1-GFPox, *atb"δ*, *atb"αβγδ*, and *rcn1-6* plants after they underwent a brushing treatment (Figure 4.3A). In agreement, survival rates of those QM1, QM2 and VIP1-SRDXox plants were significantly lower than the other lines (Figure 4.3B). These results support the idea that VIP1 and its homologs increase mechanical stress tolerance in leaves.

Mechanical stress can be induced by plants themselves, especially when their density is high (Masclaux et al., 2012; Benikhlef et al., 2013). However, no difference was observed in phenotypes between wild-type, QM1, QM2 and VIP1-SRDXox plants either under a low-density planting (4 plants/16 cm^2) condition or a high-density planting (9 plants/16 cm^2) condition (Figure 4.4). This result suggests that more severe mechanical stress such as brushing is necessary to induce responses dependent on VIP1 and its close homologs.

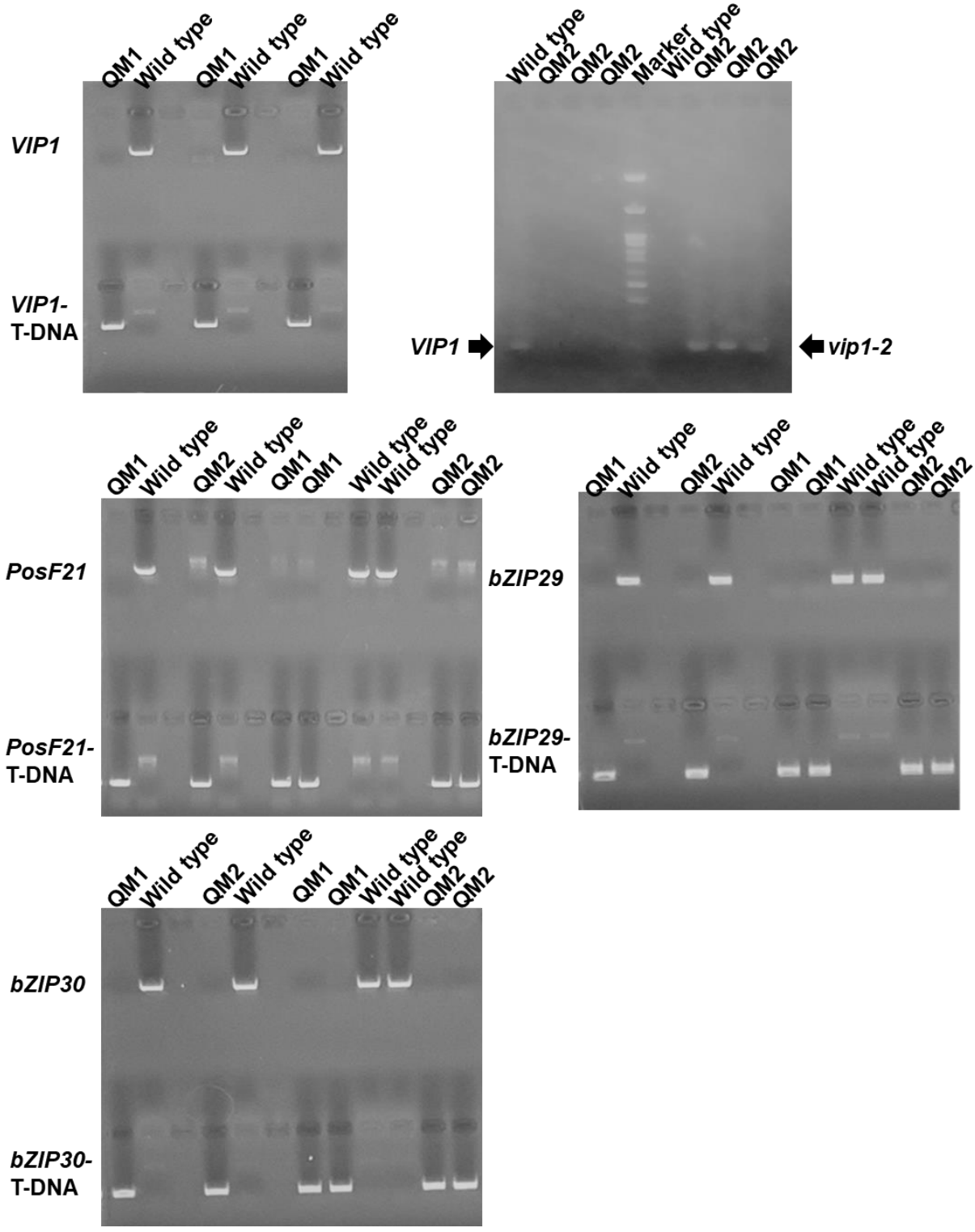

Figure 4.1. Generation of *VIP1 PosF21 bZIP29 bZIP30* quadruple-knockout mutants. Genotyping of QM1 and QM2 plants.

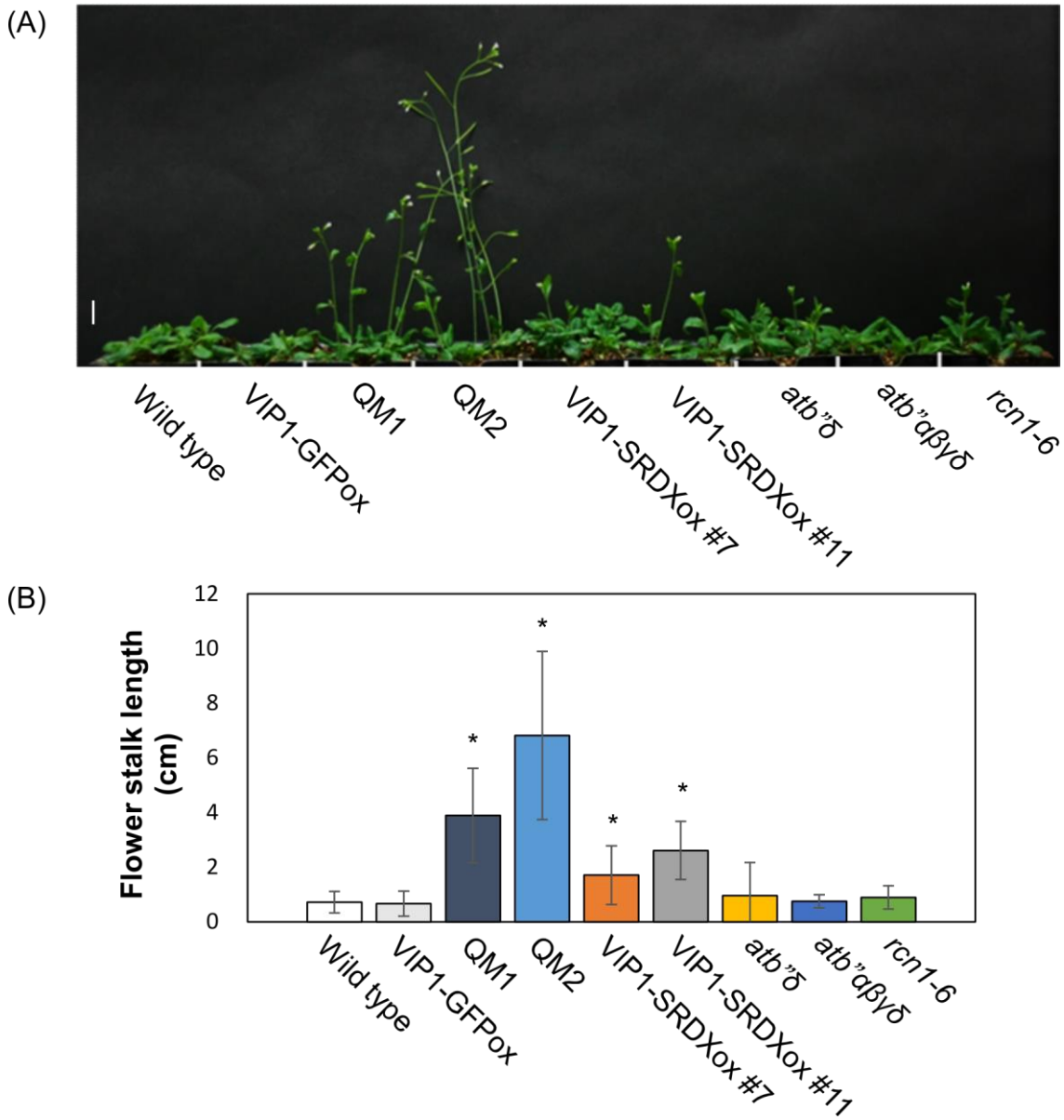

Figure 4.2. Flower stalk length of QM1, QM2, VIP1-SRDXox #7 and #11 plants. (A) Phenotypes of four-week-old plants grown under a normal growth condition. Four plants per genotype are shown. Scale bar = 1 cm. (B) Flower stalk length of the four-week-old plants. Data are means ± SD of three biological replicates. *, $P < 0.05$ according to the Student's t-test vs. the wild type.

(A)

atb" αβγδ	***atb"δ***	***rcn1-6***
VIP1-GFPox	**QM2**	**VIP1-SRDXox #7**
Wild type	**QM1**	**VIP1-SRDXox #11**

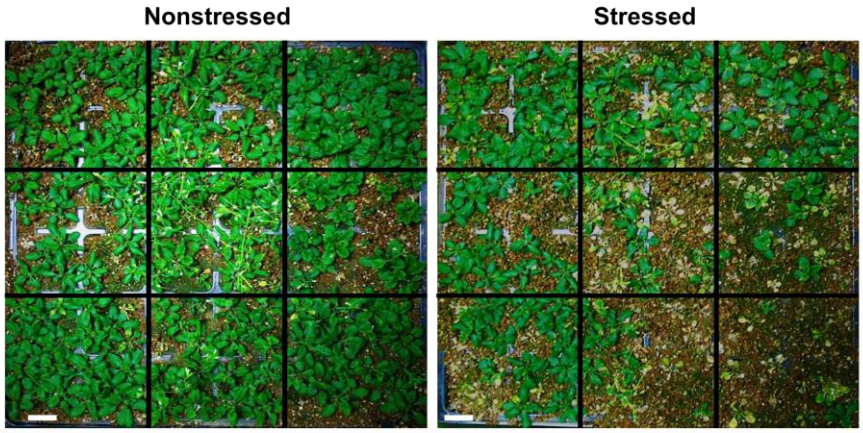

(B)

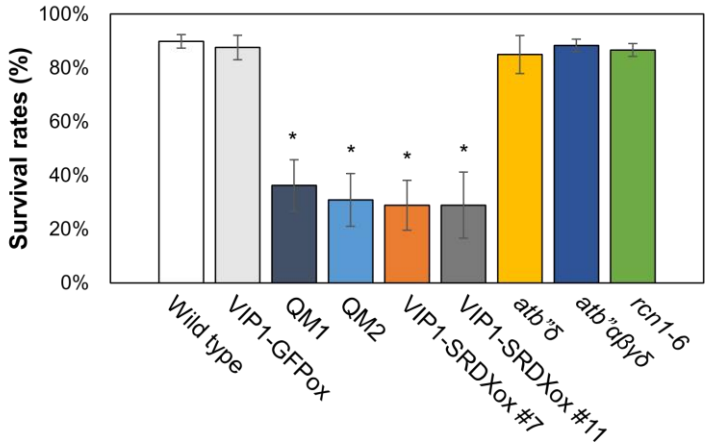

Figure 4.3. Leaves of QM1, QM2, VIP1-SRDXox #7 and #11 plants are hypersensitive to brushing-induced mechanical stress. (A) Phenotypes of four-week-old plants with leaves brushed. Plants were photographed seven days after the brushing treatment was started. A representative image is presented. Scale bars = 2 cm. (B) Survival rates of plants that underwent the brushing treatment. Data are means ± SD of three biological replicates. *, $P < 0.05$ according to the Student's t-test vs. the wild type.

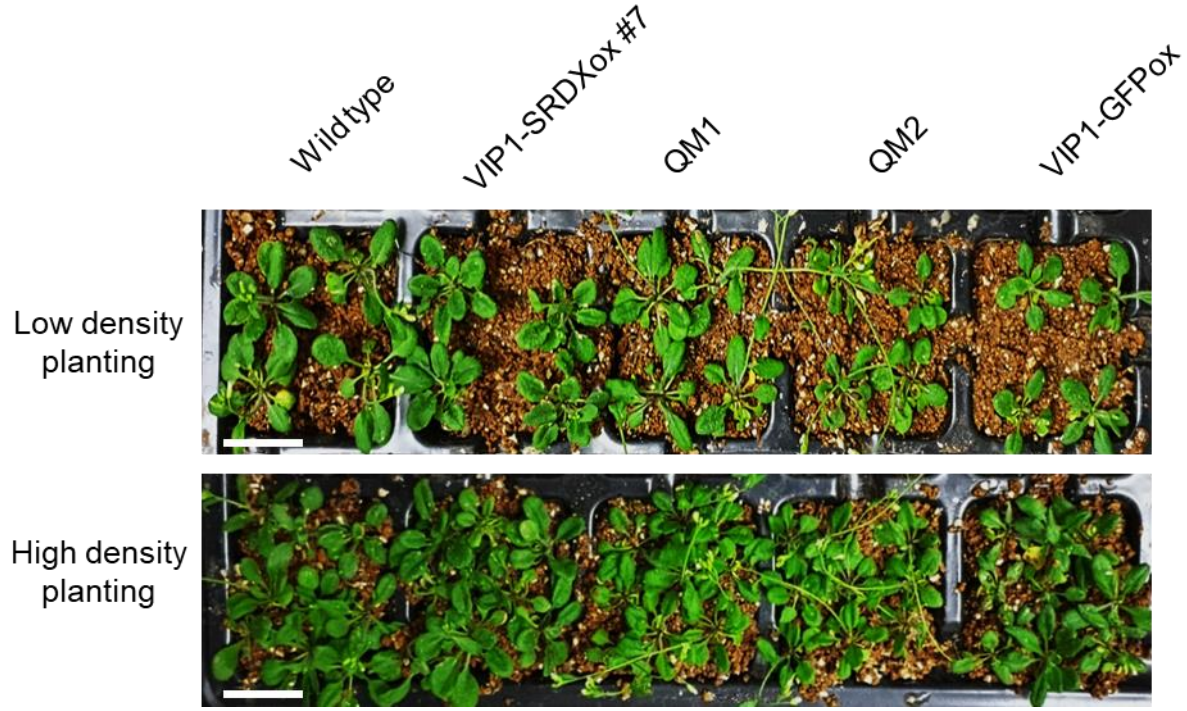

Figure 4.4. High-density planting does not affect the growth of QM1, QM2 and VIP1-SRDXox #7 plants. Two-week-old plants were transferred from the MS agar medium to the soil with either low or high planting density. These plants were further grown for two weeks and photographed. A representative image is presented. Scale bars = 2 cm.

4.3.2. Transcriptomes in brushed QM2 leaves

The brushing treatment that damaged QM1 and QM2 plants induced the nuclear localization of VIP1 (Figure 4.5), supporting the idea that this treatment can induce changes in gene expression mediated by VIP1 and its close homologs.

RNA-Seq was performed to analyze transcriptomes of the brushed wild-type and QM2 plants. TPM values for *VIP1*, *PosF21*, *bZIP29* and *bZIP30* were all lower in the QM2 plants than in the wild-type plants, validating the analysis (Table 4.3, the category "VIP1 and its homologs"). The RNA-Seq detected 1305 genes that were up-regulated by the brushing treatment, and 654 genes that were down-regulated by the brushing treatment in the wild-type plants. In QM2 plants, 1587 up-regulated genes and 1046 down-regulated genes were identified (Figure 4.6A). Of the up-regulated genes, 41.8% were shared between the wild-type and QM2 plants (Figure 4.6B). Of the down-regulated genes, 13.2% were shared between the wild-type and QM2 plants (Figure 4.6C).

TPM values of previously identified putative VIP1 target genes, *XYLOGLUCAN ENDO-TRANSGLYCOSYLASE/HYDROLASE 23* (*XTH23*) and *EXPANSIN-LIKE ALPHA 1* (*EXLA1*), were both lower in QM2 than in the wild type (Table 4.3, "Putative VIP1 target gene; Cell wall modifier" category). Consistent results were obtained in qRT-PCR for *XTH23* and *EXLA1* (Figure 4.7). These results further confirm the validity of the RNA-Seq. *De novo* motif scanning identified AGCTG[GT], which is bound by VIP1 and its close homologs (see the section 4.1), as a part of a sequence motif enriched in the promoters of the genes that were more weakly expressed in the stressed QM2 leaves than in the stressed wild-type leaves (Table 4.4, top two rows). This suggests that AGCTG[GT] is relevant to the mechanical stress-responsive gene expression. Such motif scanning also identified the CAMTA (calmodulin-binding transcription activator)-binding sequence ACGCGT as a part of a motif enriched in the promoters of the genes

that were upregulated by brushing in either the QM2 or wild-type plants (Table 4.4, bottom two rows). This raises the possibility that CAMTAs are also important for the mechanical stress-dependent induction of genes in Arabidopsis. None of the *CAMTA*s were not greatly induced by the brushing treatment (Table 4.3, “CAMTA” category).

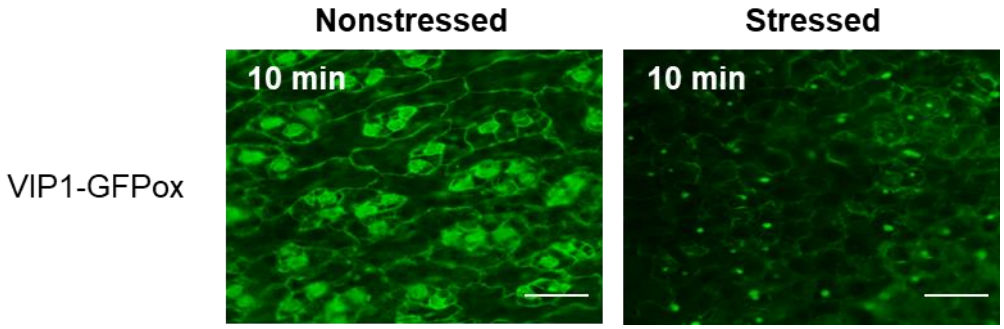

Figure 4.5. Brushing treatment induces nuclear localization of VIP1-GFP. Rosette leaves of four-week-old VIP1-GFPox plants were subjected to brushing treatment for 10 seconds. Nonstressed leaves of VIP1-GFPox plants were used as a control. VIP1-GFP signals were detected by fluorescence microscopy 10 minutes after the treatment. Ten leaves were used for the analysis and a representative result is shown. Scale bars = 50 μm.

Table 4.3. TPM values for selected genes.

			TPM in nonstressed				TPM in stressed			
			wild type		QM2		wild type		QM2	
Gene	AGI code	Category	Mean	SD	Mean	SD	Mean	SD	Mean	SD
VIP1	AT1G43700.1	VIP1 and its homolog	39.9	12.2	10.4	1.9	43.1	4.3	7.4	0.9
bZIP29	AT4G38900.3	VIP1 and its homolog	7.2	1.4	0.3	0.2	6.3	1.5	0.4	0.4
bZIP30	AT2G21230.1	VIP1 and its homolog	6.8	1.3	0.5	0.3	5.8	0.7	0.5	0.2
PosF21	AT2G31370.4	VIP1 and its homolog	4.2	0.5	0.8	0.2	3.3	0.3	0.5	0.2
bZIP69	AT1G06070.1	VIP1 and its homolog	11.7	1.0	13.6	2.0	12.6	1.8	10.7	1.2
bZIP52	AT1G06850.1	VIP1 and its homolog	8.8	2.2	13.3	2.3	9.8	1.4	11.6	0.8
bZIP18	AT2G40620.1	VIP1 and its homolog	7.0	1.3	7.4	2.0	7.0	1.2	7.8	2.0
EXLA1	AT3G45970.1	VIP1 target gene; Cell wall modifier	4.6	0.8	1.5	0.5	89.3	21.2	10.6	2.3
XTH23	AT4G25810.1	VIP1 target gene; Cell wall modifier	3.1	0.8	0.4	0.2	81.0	14.8	5.0	2.0
CAMTA1	AT5G09410.1	CAMTA	6.8	0.7	7.1	0.7	5.9	2.0	4.6	0.8
CAMTA2	AT5G64220.1	CAMTA	8.2	1.0	8.3	0.6	8.9	1.2	10.5	0.8
CAMTA3	AT2G22300.1	CAMTA	6.2	0.8	9.3	0.9	12.2	3.7	17.9	4.6
CAMTA4	AT1G67310.1	CAMTA	21.7	2.6	25.6	2.8	24.1	7.9	28.7	7.5
CAMTA5	AT4G16150.1	CAMTA	27.0	2.4	27.7	4.0	27.3	1.6	28.9	4.7
CAMTA6	AT3G16940.1	CAMTA	7.0	1.5	8.4	1.8	7.0	1.7	8.2	2.0

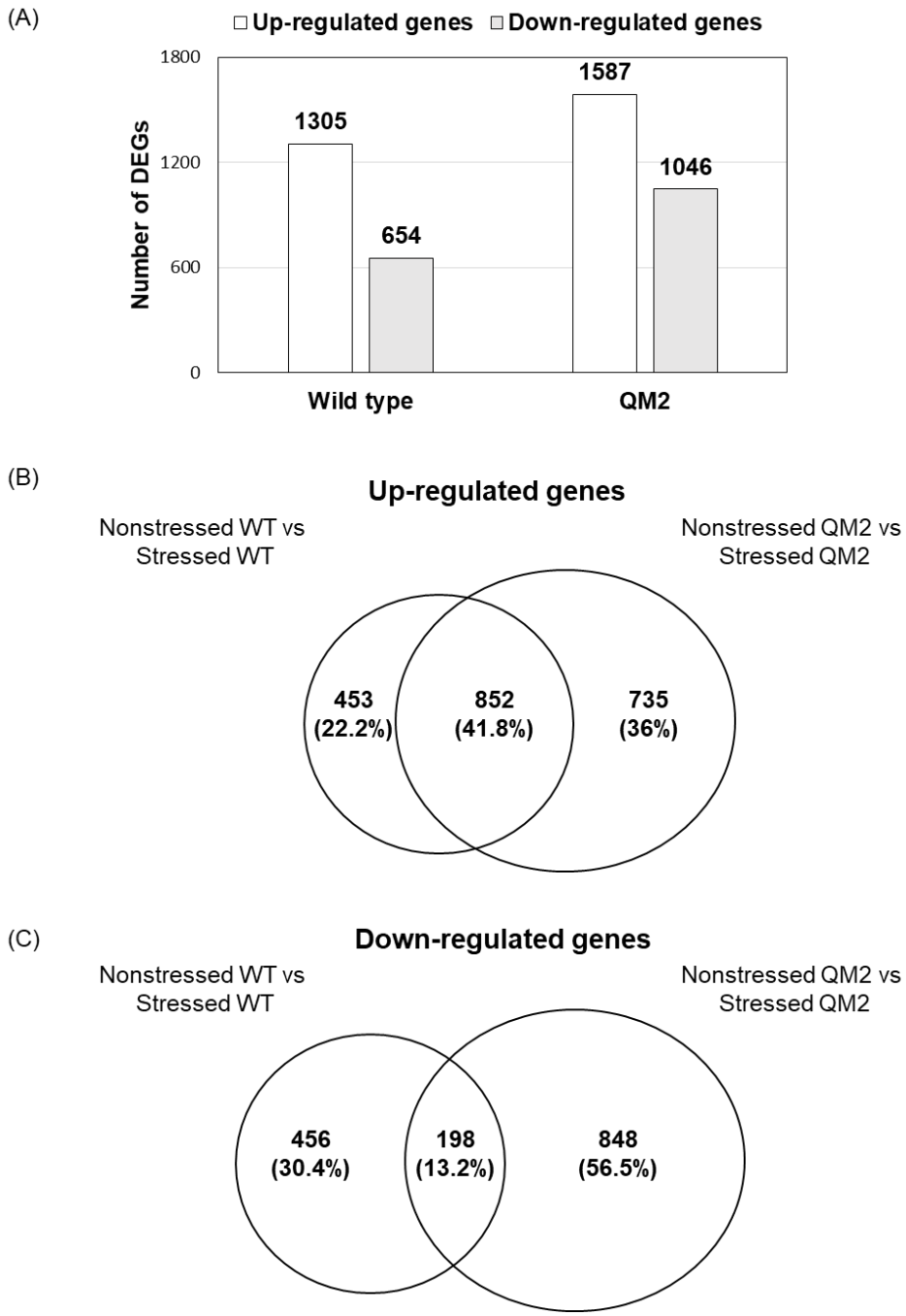

Figure 4.6. Genes upregulated and downregulated by the brushing treatment. (A) The numbers of differentially expressed genes (DEGs) detected in wild-type and QM2 plants. (B) Venn diagram for the upregulated genes. WT: wild type. (C) Venn diagram for the downregulated genes.

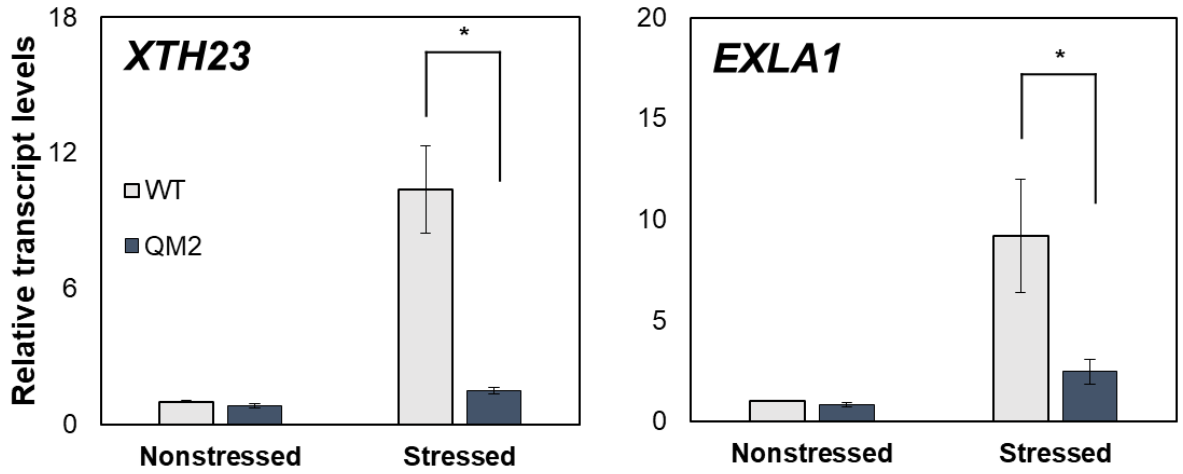

Figure 4.7. qRT-PCR to validate the RNA-Seq data. Relative expression levels of the putative VIP1 target genes *XTH23* and *EXLA1* were obtained by qRT-PCR with the comparative cycle threshold method. Data are means ± SD of three biological replicates. *, $P < 0.05$ according to the Student's t-test vs. the stressed wild-type samples.

Table 4.4. Motifs identified in promoters of genes that were either more weakly expressed in QM2 plants than in wild-type plants or up-regulated by the brushing treatment.

Motif[1]	Target genes (its number)[2]	% in targets	% in the background[3]	*P* value
AC[AC]GC[CT][AG]A TTT[AG]	Genes more weakly expressed in QM2 without brushing (86)	10.47	0.04	1.0E-12
TACAGCTG	Genes more weakly expressed in QM2 after brushing (217)	27.65	7.14	1.0E-16
ACGCGT[ACT][AGT]	Genes up-regulated by brushing in the wild type (1240)	27.82	8.8	1.0E-44
[ACT]A[ACGT]**ACGC GT**[AT]	Genes up-regulated by brushing in QM2 (1502)	48.2	18.92	1.0E-75

[1]The VIP1-binding sequence AGCTG[GT] is underlined and the CAMTA-binding sequence ACGCGT is in bold type.

[2]Only a representative gene model (or transcript) for each gene locus was used.

[3]Promoters of 2000 randomly chosen genes were used as the background.

4.3.3. QM1 and QM2 plants display prolonged ROS accumulation in response to the brushing treatment

ROS production is promoted by various stimuli such as wounding (L'Haridon et al., 2011), the microbe-associated molecular pattern flg22 (Asai et al., 2002), and high salinity (Kim et al., 2011). High levels of ROS were detected in leaves of all the genotypes studied (i.e., the wild type, VIP1-SRDXox, QM1 and QM2) one minute after they were brushed. In contrast, high levels of ROS were detected only in QM1 and QM2 plants and not in either wild-type or VIP1-SRDXox plants five and ten minutes after these plants were brushed (Figure 4.8). Excess ROS generated under stressed conditions and the failure to maintain ROS balance cause oxidative damages to cells, resulting in growth defects or the initiation of cell death (Torres and Dangl, 2005). The prolonged ROS accumulation in QM1 and QM2 plants after the brushing treatment may accelerate their cell death. No difference was observed in expression levels of ROS-scavenging genes in the RNA-Seq data between wild-type and QM2 plants. Further studies are necessary to identify the genes regulating the mechanical stress tolerance in leaves.

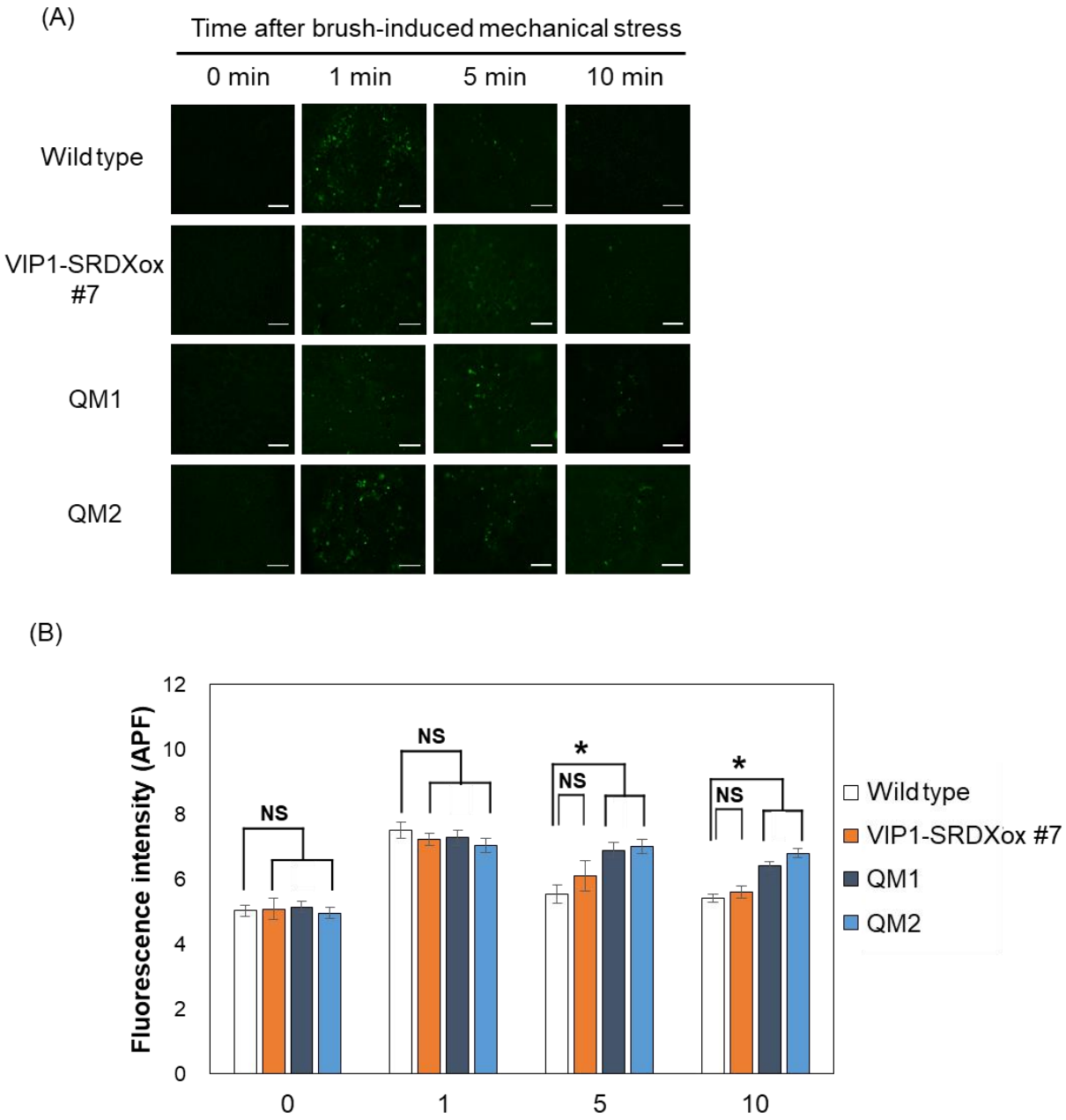

Figure 4.8. ROS production of brushed leaves of wild-type, VIP1-SRDXox #7, QM1, and QM2 plants. (A) Rosette leaves of four-week-old wild-type, VIP1-SRDXox #7, QM1, and QM2 plants were subjected to the brushing treatment for 10 seconds. Leaves were sampled 1 minute, 5 minutes, and 10 minutes after the brushing treatment, and incubated in a solution containing 5 μM APF, a fluorescent ROS probe. Resulting leaves were rinsed by distilled water. APF signals were detected by fluorescence microscopy. A representative image is presented for each sample. Scale bars = 50 μm. (B) Quantification of the APF signals. Data are means ± SD. *, $P < 0.05$ according to the Student's t-test vs. the wild type.

4.3.4. Leaves of QM1, QM2, and VIP1-SRDXox plants are rapidly damaged by the brushing treatment

DAPI can penetrate a denaturated cell membrane and bind DNA more efficiently than it can penetrate an intact cell membrane. DAPI can therefore selectively detect nuclei of damaged cells. Wild-type leaves exhibited stronger DAPI signals 1 minute, 5 minutes, 15 minutes, 60 minutes and one day after they were brushed than when they were not brushed (Figure 4.9, top panels). DAPI signals in leaves of VIP1-SRDXox, QM1, and QM2 plants were stronger than the DAPI signals in wild-type leaves at all the time points after the brushing treatment was imposed (Figure 4.9, middle panels). In contrast, VIP1-GFPox leaves exhibited as strong DAPI signals as the wild-type leaves at all the time points (Figure 4.9, bottom panels). These results suggest that the brushing treatment damages cells within 1 minute, and that VIP1-SRDXox, QM1, and QM2 plants are more severely damaged by the brushing treatment than the wild-type and VIP1-GFPox plants. In agreement, electrolyte leakage from leaves were more greatly enhanced by the brushing treatment in VIP1-SRDXox, QM1 and QM2 plants than in the wild-type and VIP1-GFPox plants (Figure 4.10).

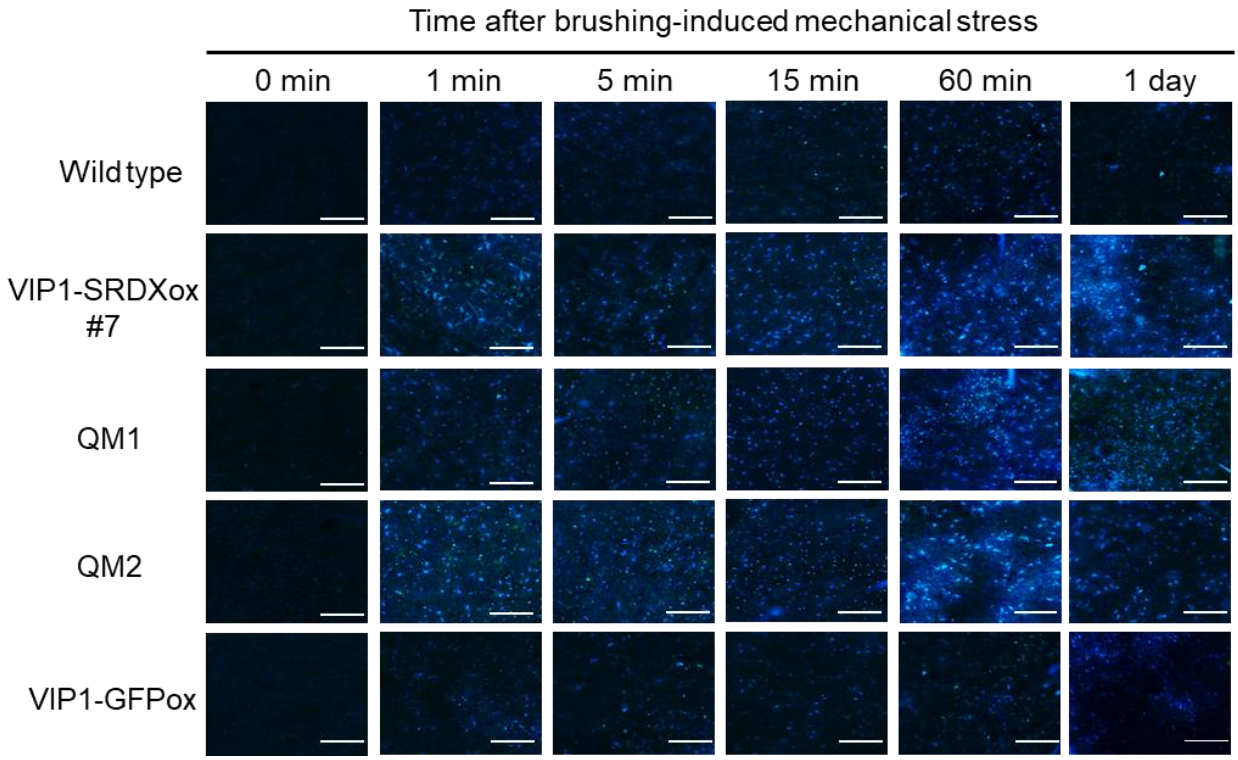

Figure 4.9. DAPI staining of brushed leaves of wild-type, VIP1-SRDXox #7, QM1, QM2, and VIP1-GFPox plants. Rosette leaves of four-week-old wild-type, VIP1-SRDXox #7, QM1, QM2, and VIP1-GFPox plants were subjected to the brushing treatment. Leaves were sampled at 1 min, 5 min, 15 min, 60 min, and 1 day after the treatment, and incubated in a DAPI staining solution. DAPI signals were detected by fluorescence microscopy. A representative image is presented for each sample. Scale bars = 200 μm.

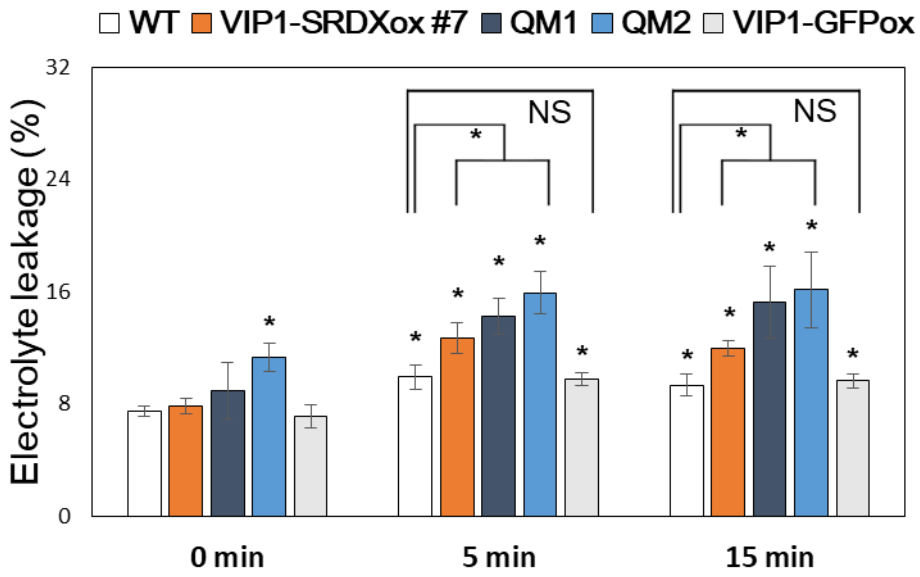

Figure 4.10. Electrolyte leakage from brushed leaves. Leaves of four week-old wild-type, VIP1-SRDXox #7, QM1, QM2, and VIP1-GFPox plants were sampled for the electrolyte leakage assay 0 minute, 5 minutes, and 15 minutes after they were brushed. Data are means ± SD (n = 6). *, $P < 0.05$ according to the Student's t-test vs. the wild-type samples.

4.3.5. Responses of QM1 and QM2 plants to other abiotic stresses and phytohormones.

Root VGIs of QM1 and QM2 plants were similar to the VGI of wild-type plants (Figure 4.11A, B). This may be because the close VIP1 homologs (such as bZIP52, bZIP18 and bZIP69) other than VIP1, PosF21, bZIP29, and bZIP30 can still suppress touch-induced root waving in QM1 and QM2 plants. Phenotypes of QM1 and QM2 plants were also similar to wild-type phenotypes under NaCl-stressed, mannitol-stressed, ACC-supplemented, 2,4-D-supplemented, and ABA-supplemented conditions (Figure 4.12). This may also be due to the functional redundancy between VIP1 and its close homologs, or because they are not involved in regulating plant growth under those conditions.

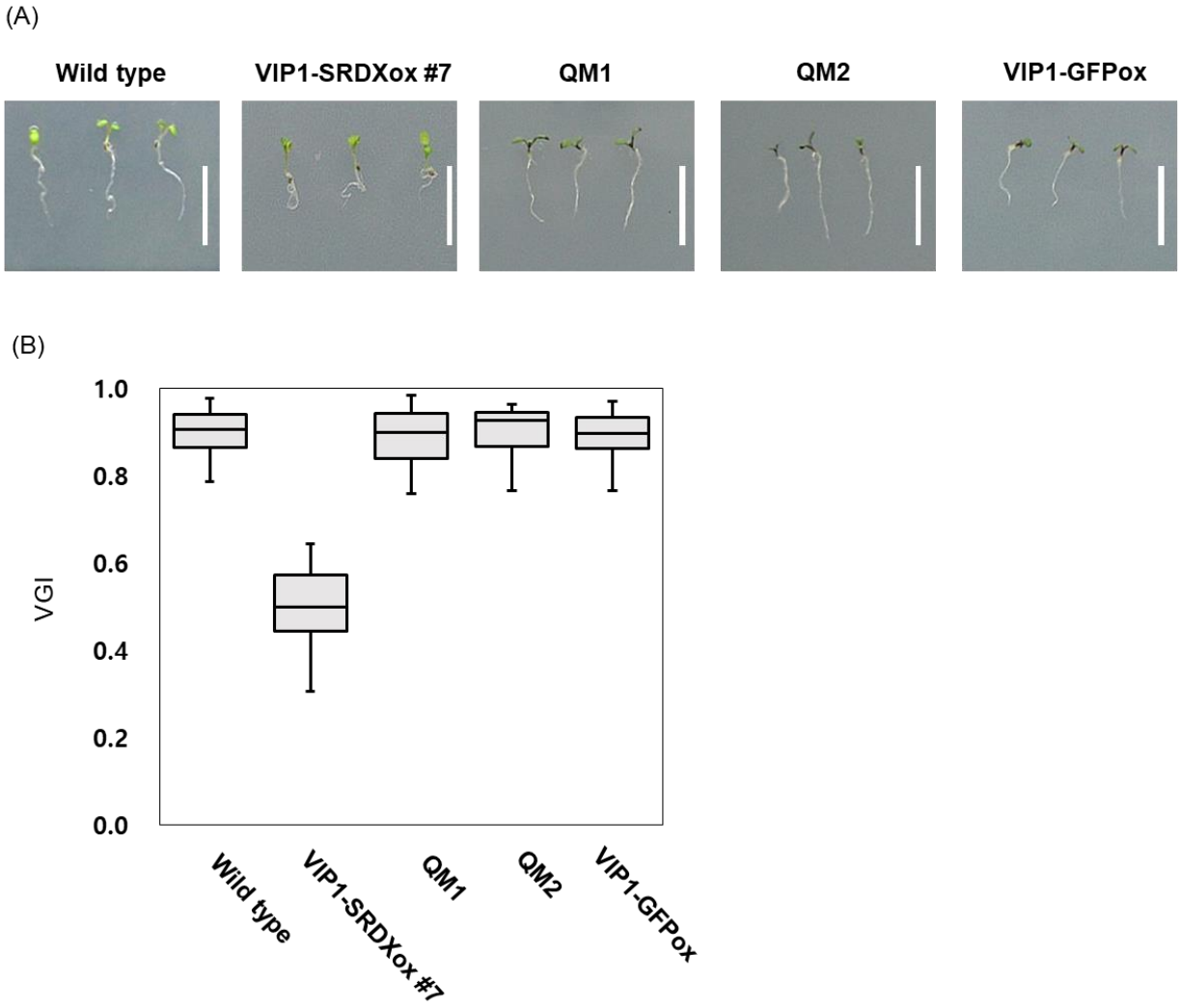

Figure 4.11. Root VGIs of QM1 and QM2 plants. (A) Phenotypes of wild-type, VIP1-SRDXox #7, QM1, QM2, and VIP1-GFPox seedlings. These plants were grown on an 1.6% agar 0.5x MS medium tilted at a 75° angle for 5 days. A representative image is presented for each genotype. Bars = 5 mm. (B) Root VGIs of wild-type, VIP1-SRDXox #7, QM1, QM2, and VIP1-GFPox seedlings. The top and bottom edges and the line in the middle of each box indicate quartiles, and the bar corresponds to the data range (n = 50/each line).

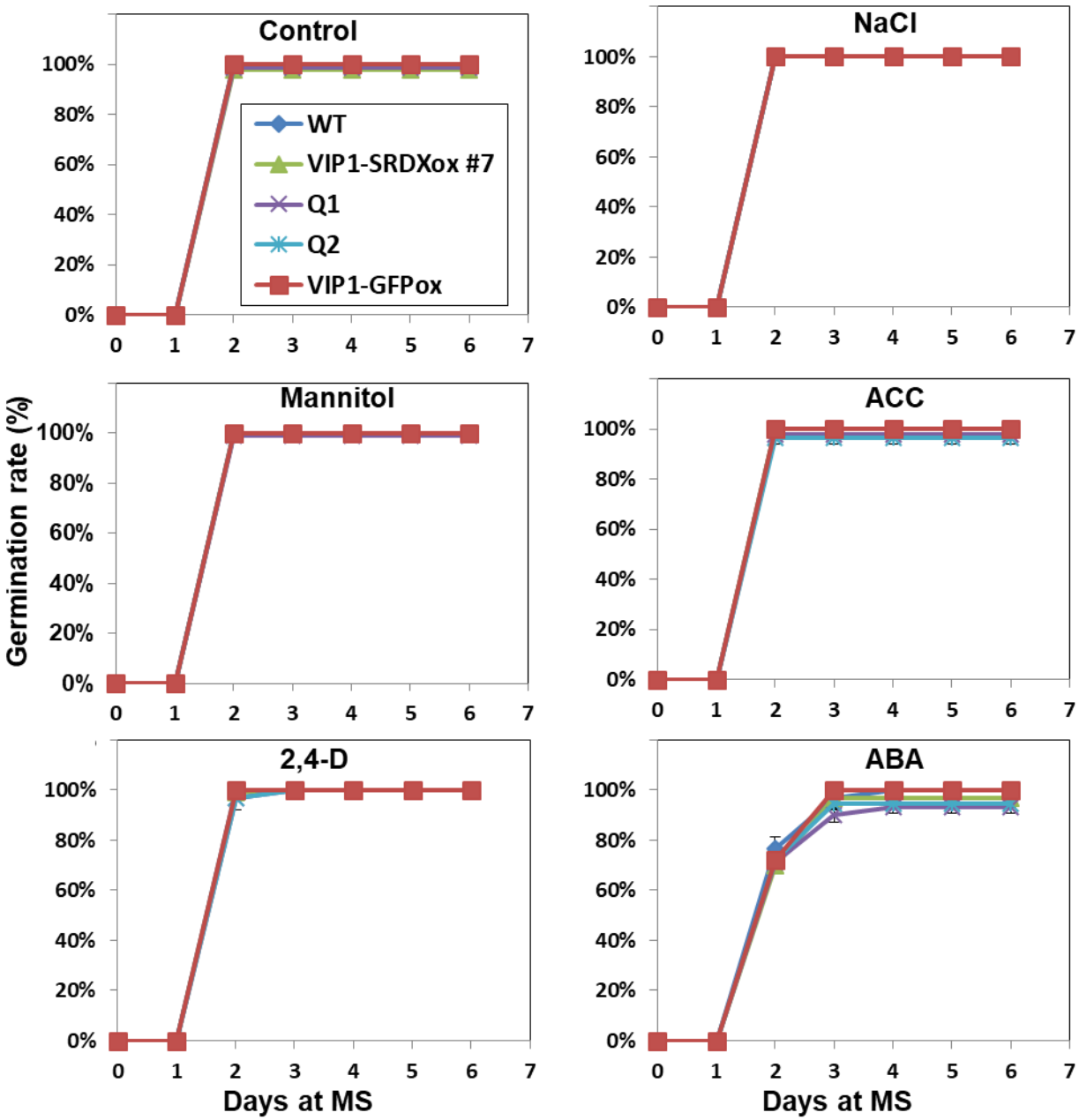

Figure 4.12. Germination rates of QM1 and QM2 plants under various conditions. Seeds of wild-type, VIP1-SRDXox #7, QM1, QM2, and VIP1-GFPox plants were sown on a medium containing 100 mM NaCl, 200 mM mannitol, 0.5 μM ACC, 0.2 μM 2,4-D, or 0.5 μM ABA, and incubated for 6 days to obtain their germination rates. Data are means ± SD of three replicates. Thirty plants were used for each genotype and each replicate.

4.4. Discussion

Leaves of QM1, QM2 and VIP1-SRDXox plants were shown to be severely damaged by the brushing treatment (Figure 4.3). These results provide the evidence that VIP1 and its close homologs confer the mechanical stress tolerance in Arabidopsis leaves. The cell wall is stiffened by mechanical stress to confer mechanical stress tolerance (Verhertbruggen et al., 2013). Some cell wall-modifying genes such as *XTH23* and *EXLA1* were up-regulated by the brushing treatment in the wild-type plants but not in QM2 plants (Table 4.3 and Figure 4.7). An *XTH23* homolog, *XTH9*, is also a putative target gene of VIP1 and bZIP29 (Van Leene et al., 2016). Such cell wall-modifying genes may be responsible for stiffening the cell wall and alleviating mechanical stress-induced damages downstream of VIP1 and its homologs. Further studies are necessary to elucidate roles for these genes in regulating the mechanical stress tolerance in leaves.

Neither *atb''αβγδ* nor *rcn1-6* plants were hypersensitive to the brushing treatment (Figure 4.3). Our RT-PCR (Figure 3.1) and RNA-Seq data indicate that *FASS* and *ATB''ε* as well as the other PP2A B'' subunit genes are strongly expressed in leaves. Thus, as discussed in the section 3.4, it is possible that *FASS* and *ATB''ε* cause the wild type-like responses of *atb''αβγδ* plants to the brushing treatment. The RNA-Seq data also indicate that all of the three PP2A A subunit genes, *RCN1, PP2A-A2* and *PP2A-A3*, are strongly expressed in leaves. Thus, it is also possible that *PP2A-A2* and *PP2A-A3* cause the wild type-like responses of *rcn1* plants to the brushing treatment.

Unlike VIP1-SRDXox plants, neither QM1 nor QM2 plants exhibited the enhanced wavy root phenotype (Figure 4.11). Our RNA-Seq data indicate that *bZIP52*, *bZIP69* and *bZIP18* are expressed in at least QM2 plants as strongly as in wild-type plants (Table 4.3). These genes may

repress touch-induced root waving in QM1 and QM2 plants. Alternatively, VIP1-SRDXox may alter expression of genes that are not targeted by native forms of VIP1 and its close homologs.

The CAMTA-binding sequence (ACGCGT) is enriched in promoters of the genes upregulated by the brushing treatment in both the wild-type and QM2 backgrounds (Table 4.4). CAMTAs can be activated by a Ca^{2+}-bound form of CaMs (Bouché et al., 2002). The brushing-induced activation of CAMTAs can be independent of the induction of the nuclear accumulation of VIP1 its close homologs. CAMTAs are involved in regulating the level of the defense-related phytohormone salicylic acid and in regulating expression of genes for plant immunity (Galon et al., 2008; Du et al., 2009). Gentle mechanical stress also induces expression of genes for plant defense, although jasmonic acid rather than salicylic acid is thought to mediate this process (Benikhlef et al., 2013). The pathways activated by mechanical stress are summarized in Figure 4.13. It should be interesting to further dissect the mechanical stress-responsive pathways in plants.

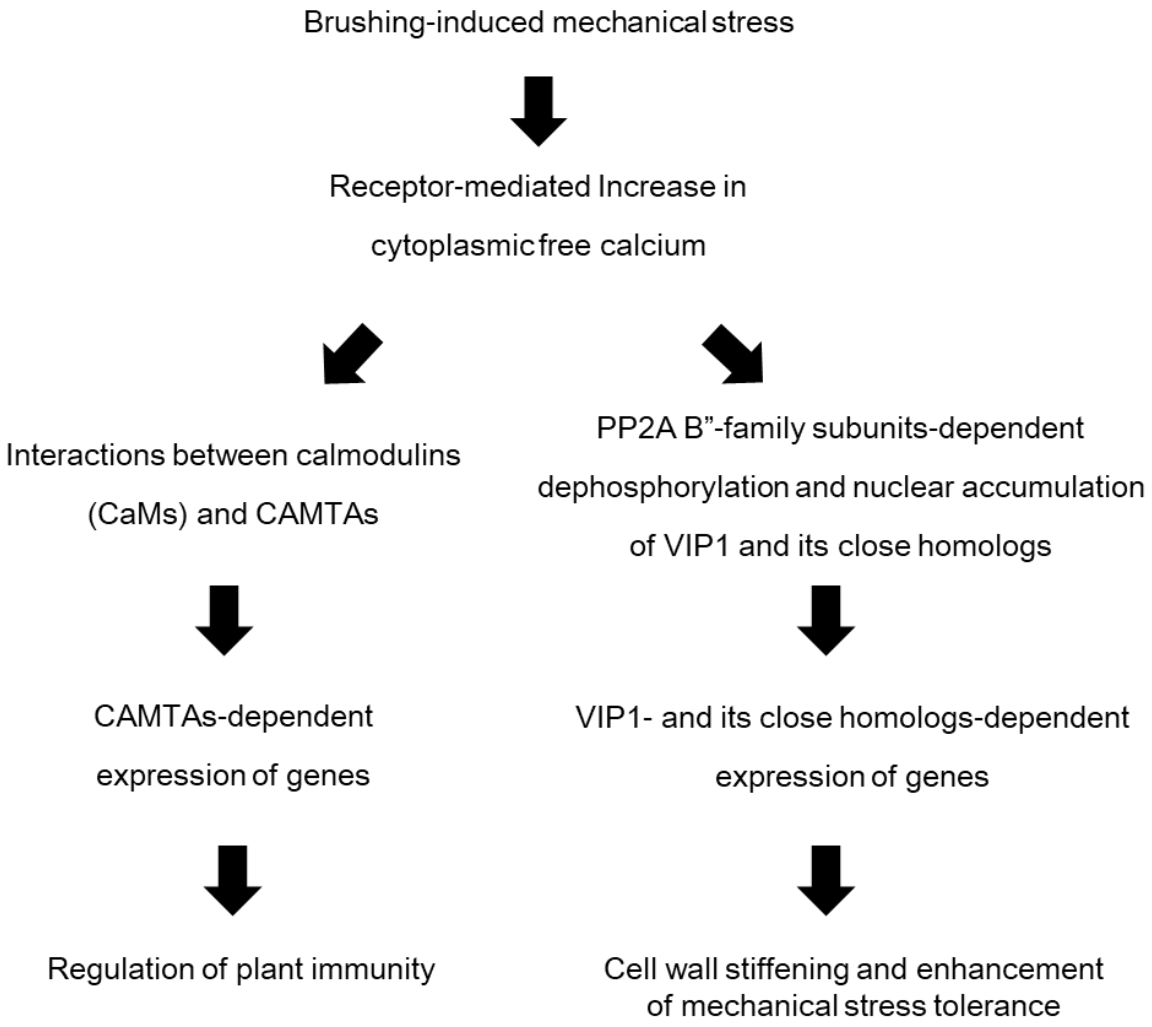

Figure 4.13. VIP1- or CAMTAs-mediated responses to mechanical stimuli.

Chapter 5

Conclusion

In conclusion, here we showed (1) that NDR/LATS protein kinases as well as CPK21 can phosphorylate VIP1 and are essential for embryogenesis, (2) that Arabidopsis PP2A B''-family subunits are indispensable for the *in-vitro* dephosphorylation of VIP1 and bZIP29, (3) that VIP1 and its close homologs are relevant to the mechanical stress-induced changes in gene expression and to the mechanical stress tolerance in leaves, and (4) that CAMTAs are also important for the mechanical stress-dependent induction of genes. Our data can help to further dissect plant mechanical stress responses in the future.

Abstract

Plants are exposed to mechanical stress caused by various factors such as rain, animals, pathogens, and plants themselves. Mechanical stress limits plant growth and productivity. Plants have adaptive responses to alleviate mechanical stress. For example, when roots touch an object, they bend to avoid the object. Moderate mechanical stress can enhance pathogen resistance if imposed on plant shoots. Characterizing mechanisms underlying plant mechanical stress responses is important because it can provide ways to improve crop development and yield under stressed conditions.

VIP1 is an *Arabidopsis thaliana* basic leucine zipper (bZIP) transcription factor that has a transcriptional activation potential and affinity to DNA with either AGCTGG or AGCTGT (AGCTG[GT]) and that is involved in regulating mechanical stress responses. VIP1 is phosphorylated by CALCIUM-DEPENDENT PROTEIN KINASE 21 (CPK21) and retained in the cytoplasm by 14-3-3 proteins under stable conditions but is dephosphorylated and localized to the nucleus when Arabidopsis cells are exposed to mechanical stress. The VIP1 dephosphorylation is likely mediated by protein phosphatase 2A (PP2A) because VIP1 interacts with PP2A B’’-family B subunits. Overexpression of a repression domain-fused form of VIP1 (VIP1-SRDX) causes enhanced touch-induced root bending, and this is suppressed by the expression of GFP-fused VIP1 (VIP1-GFP). Thus, VIP1 is thought to be a suppressor of the touch-induced root bending. Arabidopsis has 11 close VIP1 homologs, and at least six of them (bZIP29, bZIP30, PosF21, bZIP69, bZIP52, and bZIP18) share most of the above functions of VIP1. The aim of this study is to further characterize factors involved in the VIP1-mediated mechanical stress signaling and thereby to better understand plant mechanical stress responses.

1. NDR/LATS-family protein kinases phosphorylate VIP1

Serine residues at positions 35, 115, and 151 (S35, S115, and S151, respectively) of VIP1 are putative phosphorylation sites that interact with 14-3-3 proteins and that are responsible for cytoplasmic retention of VIP1. All of these three residues were found to be a part of the consensus sequence for NDR/LATS-family protein kinase phosphorylation. NDR/LATS-family protein kinases are conserved among eukaryotes and regulate the cell cycle in yeast and animals. However, the functions of these protein kinases in plants are unclear. This led us to determine that not only CPK21 but also NDR/LATS-family protein kinases phosphorylate VIP1, and to characterize physiological functions of these protein kinases in Arabidopsis. Arabidopsis has eight NDR/LATS-family protein kinase genes (*NDR1-8*). Reverse transcription-PCR detected the expression of all of these genes in seedlings, rosette leaves, roots, flower stalks and flowers. NDR2, NDR3, and NDR8 were expressed as recombinant (maltose-binding protein (MBP)-fused) proteins in *Escherichia coli*, and purified by affinity chromatography. All of these proteins phosphorylated GST-fused VIP1 (GST-VIP1) *in vitro* but did not phosphorylate a GST-fused VIP1 variant with S → A substitutions at S35 and S115. These results suggest that S35 and S115 of VIP1 are phosphorylated by Arabidopsis NDR/LATS-family protein kinases *in vitro*. Arabidopsis mutant lines lacking one, two, or three of *NDR4*, *NDR6*, *NDR7* and *NDR8* could be obtained, and their phenotypes were similar to the wild-type phenotype under a normal growth condition. However, a line lacking all of these four genes could never be obtained. Based on genetic analysis, this was shown to be because an *NDR4 NDR6 NDR7 NDR8* quadruple knockout causes embryonic (yet not gametophytic) lethality.

2. PP2A B”-family B subunits are indispensable for dephosphorylation of VIP1 and its close homologs *in vitro*

PP2A consists of the scaffolding A subunit, the regulatory B subunit, and the catalytic C subunit. PP2A B subunits bind substrates of PP2A, and are classified into B, B’, B”, and B’’’ families. PP2A B”-family B subunits have Ca^{2+}-binding EF-hand motifs. Arabidopsis has six genes encoding the PP2A B”-family subunits (ATB’’α-ε and FASS). Of these proteins, ATB’’δ and FASS bind VIP1 in the presence of Ca^{2+}. However, it is unclear whether PP2A B”-family subunits mediate the VIP1 dephosphorylation. We further characterized the interactions between these proteins and VIP1. By yeast two-hybrid and in-vitro pull-down assays, interactions between two Arabidopsis PP2A A subunits (RCN1 and PP2A-A2), two PP2A C subunits (PP2A-C3 and PP2A-C5) and all the six PP2A B’’-family subunits were confirmed. Pull-down assays also showed that His-tagged forms of ATB’’α-γ and ATB’’ε as well as ATB’’δ and FASS interact with GST-VIP1 in the presence of Ca^{2+} *in vitro*. GST-VIP1 and GST-fused bZIP29 were both dephosphorylated *in vitro* when mixed with protein solutions containing Myc-tagged ATB’’α, Myc-tagged ATB’’δ or Myc tagged FASS in addition to PP2A A and C subunits. This result suggests that the PP2A B’’-family subunits are indispensable for dephosphorylation of VIP1 and its close homologs *in vitro*. On the other hand, VIP1-GFP shuttled between the cytoplasm and the nucleus in mechanically stressed *ATB’’β ATB’’δ* double knockout plants as it did in wild-type plants. A mutant that lacks four (*ATB’’α-δ*) of the six PP2A B”-family subunit genes exhibited phenotypes similar to the phenotypes of the wild type under various growth conditions. These results support the idea that those PP2A B”-family subunits have functional redundancy. Further studies are necessary to elucidate the physiological functions of these proteins.

3. VIP1 and its close homologs confer the mechanical stress tolerance in Arabidopsis leaves

To further examine physiological functions of VIP1 and its close homologs, QM1 and QM2, two lines with mutations in *VIP1*, *PosF21*, *bZIP29* and *bZIP30*, were generated. In both QM1 and QM2 plants, *PosF21*, *bZIP29*, and *bZIP30* are knocked out by transfer DNA (T-DNA) insertions. QM1 plants have T-DNA in VIP1 as well but exhibits expression of *VIP1* 5' region that corresponds to the N-terminal 244 amino acids of the 341 amino acids of VIP1. QM2 plants have a two-base pair deletion in *VIP1* 5' region and should exhibit expression of N-terminal 140 amino acids of VIP1. Both QM1 and QM2 plants exhibited phenotypes similar to the phenotypes of the wild type under various growth conditions. However, although leaves of wild-type and VIP1-GFP-overexpressing plants survived mechanical stress induced by repeated brushing, leaves of QM1, QM2 and VIP1-SRDX-overexpressing plants did not. A high level of reactive oxygen species (ROS) was detected in wild-type leaves one minute after they were brushed, but not five minutes after. In contrast, a high level of ROS was detected in QM1 and QM2 leaves both one minute and five minutes after they were brushed. DAPI-stained areas and electrolyte leakage of VIP1-SRDXox #7, QM1, and QM2 plants after a brushing treatment were significantly higher than wild-type and VIP1-GFP-overexpressing plants. These results suggest that VIP1 and its close homologs confer the mechanical stress tolerance in Arabidopsis leaves. Transcriptomes of the brushed leaves of the wild-type and QM2 plants were analyzed by RNA sequencing. Expression (i.e., transcripts per million (TPM)) values obtained for *VIP1*, *PosF21*, *bZIP29* and *bZIP30* were all lower in the QM2 plants than in the wild-type plants. Expression values of previously identified putative VIP1 target genes, *XTH23* and *EXLA1*, were also lower in QM2 plants than in the wild-type plants. Consistent results were obtained in quantitative reverse transcription-PCR for *XTH23* and *EXLA1*. These results confirm the validity of our RNA

sequencing. Many genes that were either upregulated or downregulated by the leaf brushing were shared between the wild-type and QM2 plants. *De novo* motif scanning identified AGCTG[GT], which is bound by VIP1 and its close homologs (see above), as a part of a sequence motif enriched in the promoters of the genes that are more weakly expressed in the stressed QM2 leaves than in the stressed wild-type leaves. This suggests that AGCTG[GT], VIP1 and its close homologs are relevant to the mechanical stress-responsive gene expression. Such motif scanning also identified a CAMTA (calmodulin-binding transcription activator)-binding sequence as a part of a motif enriched in the promoters of the genes that are upregulated by brushing in either the QM2 or wild-type plants. This raises the possibility that CAMTAs are also important for the mechanical stress-dependent induction of genes in Arabidopsis.

References

Asai, T., Tena, G., Plotnikova, J., Willmann, M. R., Chiu, W. L., Gomez-Gomez, L., Boller, T., Ausubel, F.M., and Sheen, J. (2002) MAP kinase signalling cascade in Arabidopsis innate immunity. Nature. 415, 977-983.

Aylon, Y., Ofir-Rosenfeld, Y., Yabuta, N., Lapi, E., Nojima, H., Lu, X., and Oren, M. (2010) The Lats2 tumor suppressor augments p53-mediated apoptosis by promoting the nuclear proapoptotic function of ASPP1. Genes Dev. 24, 2420-2429.

Ballesteros, I., Domínguez, T., Sauer, M., Paredes, P., Duprat, A., Rojo, E., Sanmartín, M., and Sánchez-Serrano, J.J. (2013) Specialized functions of the PP2A subfamily II catalytic subunits PP2A-C3 and PP2A-C4 in the distribution of auxin fluxes and development in Arabidopsis. Plant J. 73, 862-872.

Benikhlef, L., L'Haridon, F., Abou-Mansour, E., Serrano, M., Binda, M., Costa, A., Lehmann, S., and Métraux, J.P. (2013) Perception of soft mechanical stress in Arabidopsis leaves activates disease resistance. BMC plant biology, 13, 1-12.

Benschop, J.J., Mohammed, S., O'Flaherty, M., Heck, A.J., Slijper, M., and Menke, F.L. (2007) Quantitative phosphoproteomics of early elicitor signaling in Arabidopsis. Mol. Cell. Proteomics. 6, 1198-1214.

Bichsel, S.J., Tamaskovic, R., Stegert, M.R., and Hemmings, B.A. (2004) Mechanism of activation of NDR (nuclear Dbf2-related) protein kinase by the hMOB1 protein. J. Biol. Chem. 279, 35228-35235.

Bögre, L., Okrész, L., Henriques, R., and Anthony, R.G. (2003) Growth signalling pathways in Arabidopsis and the AGC protein kinases. Trends Plant Sci. 8, 424-431.

Bouché, N., Scharlat, A., Snedden, W., Bouchez, D., and Fromm, H. (2002) A novel family of calmodulin-binding transcription activators in multicellular organisms. J Biol Chem. 277, 21851-21861.

Colman-Lerner, A., Chin, T.E., and Brent, R. (2001) Yeast Cbk1 and Mob2 activate daughter-specific genetic programs to induce asymmetric cell fates. Cell. 107, 739-750.

De la Fuente van Bentem, S., Anrather, D., Dohnal, I., Roitinger, E., Csaszar, E., Joore, J., Buijnink, J., Carreri, A., Forzani, C., Lorkovic, Z.J., Barta, A., Lecourieux, D., Verhounig, A., Jonak, C., and Hirt, H. (2008) Site-specific phosphorylation profiling of Arabidopsis proteins by mass spectrometry and peptide chip analysis. J. Proteome Res. 7, 2458-2470.

Du, L., Ali, G.S., Simons, K.A., Hou, J., Yang, T., Reddy, A.S., and Poovaiah, B.W. (2009) Ca^{2+}/calmodulin regulates salicylic-acid-mediated plant immunity. Nature. 457, 1154-1158.

Farkas, I., Dombrádi, V., Miskei, M., Szabados, L., and Koncz, C. (2007) *Arabidopsis* PPP family of serine/threonine phosphatases. Trends Plant Sci. 12, 169-176.

Galon, Y., Nave, R., Boyce, J.M., Nachmias, D., Knight, M.R., and Fromm, H. (2008) Calmodulin-binding transcription activator (CAMTA) 3 mediates biotic defense responses in Arabidopsis. FEBS Lett. 582, 943-948.

Grabov, A., Ashley, M.K., Rigas, S., Hatzopoulos, P., Dolan, L., and Vicente-Agullo, F. (2005) Morphometric analysis of root shape. New Phytol. 165, 641-651.

Haswell, E.S., Peyronnet, R., Barbier-Brygoo, H., Meyerowitz, E.M., and Frachisse, J.M. (2008) Two MscS homologs provide mechanosensitive channel activities in the Arabidopsis root. Curr Biol. 18, 730-734.

He, Y., Emoto, K., Fang, X., Ren, N., Tian, X., Jan, Y.N., and Adler, P.N. (2005) Drosophila Mob family proteins interact with the related tricornered (Trc) and warts (Wts) kinases. Mol Biol Cell. 16, 4139-4152.

Hein, A.L., Brandquist, N.D., Ouellette, C.Y., Seshacharyulu, P., Enke, C.A., Ouellette, M.M., Batra, S.K., and Yan, Y. (2019) PR55α regulatory subunit of PP2A inhibits the MOB1/LATS cascade and activates YAP in pancreatic cancer cells. Oncogenesis. 8, 63.

Heinz, S., Benner, C., Spann, N., Bertolino, E., Lin, Y.C., Laslo, P., Cheng, J.X., Murre, C., Singh, H., and Glass, C.K. (2010) Simple combinations of lineage-determining transcription factors prime cis-regulatory elements required for macrophage and B cell identities. Mol Cell. 38, 576-589.

Hu, R., Zhu, Y., Wei, J., Chen, J., Shi, H., Shen, G., and Zhang, H. (2017) Overexpression of PP2A-C5 that encodes the catalytic subunit 5 of protein phosphatase 2A in Arabidopsis confers better root and shoot development under salt conditions. Plant Cell Environ. 40, 150-164.

Jakoby, M., Weisshaar, B., Dröge-Laser, W., Vicente-Carbajosa, J., Tiedemann, J., Kroj, T., and Parcy, F. (2002) bZIP transcription factors in Arabidopsis. Trends in plant science, 7(3), 106-111.

Janssens, V. and Goris, J. (2001) Protein phosphatase 2A: a highly regulated family of serine/threonine phosphatases implicated in cell growth and signalling. Biochem J. 353, 417-439.

Jiang, L., Stanevich, V., Satyshur, K.A., Kong, M., Watkins, G.R., Wadzinski, B.E., Sengupta, R., and Xing, Y. (2013) Structural basis of protein phosphatase 2A stable latency. Nat Commun. 4, 1699.

Johnston, L.H., Eberly, S.L., Chapman, J.W., Araki, H., and Sugino, A. (1990) The product of the *Saccharomyces cerevisiae* cell cycle gene DBF2 has homology with protein kinases and is periodically expressed in the cell cycle. Mol. Cell. Biol. 10, 1358-1366.

Justice, R.W., Zilian, O., Woods, D.F., Noll, M., and Bryant P.J. (1995) The *Drosophila* tumor suppressor gene warts encodes a homolog of human myotonic dystrophy kinase and is required for the control of cell shape and proliferation. Genes Dev. 9, 534-546.

Kim, S.H., Woo, D.H., Kim, J.M., Lee, S.Y., Chung, W.S., and Moon, Y.H. (2011) Arabidopsis MKK4 mediates osmotic-stress response via its regulation of MPK3 activity. Biochemical and biophysical research communications, 412(1), 150-154.

Kumar, M., Gouw, M., Michael, S., Sámano-Sánchez, H., Pancsa, R., Glavina, J., Diakogianni, A., Valverde, J.A., Bukirova, D., Čalyševa, J., Palopoli, N., Davey, N.E., Chemes, L.B., and Gibson, T.J. (2020) ELM-the eukaryotic linear motif resource in 2020. Nucleic Acids Res. 48, D296-D306.

Kwak, J.M., Moon, J.H., Murata, Y., Kuchitsu, K., Leonhardt, N., DeLong, A., and Schroeder, J.I. (2002) Disruption of a guard cell-expressed protein phosphatase 2A regulatory subunit, RCN1, confers abscisic acid insensitivity in Arabidopsis. Plant Cell. 14, 2849-2861.

L'Haridon, F., Besson-Bard, A., Binda, M., Serrano, M., Abou-Mansour, E., Balet, F., Schoonbeek, H.J., Hess, S., Mir, R., Léon, J., Lamotte, O., and Métraux, J.P. (2011) A permeable cuticle is associated with the release of reactive oxygen species and induction of innate immunity. PLoS Pathog. 7, e1002148. 10.1371/journal.ppat.1002148.

Lai, Z.C., Wei, X., Shimizu, T., Ramos, E., Rohrbaugh, M., Nikolaidis, N., Ho, L.L., and Li, Y. (2005) Control of cell proliferation and apoptosis by mob as tumor suppressor, mats. Cell. 120, 675-685.

Lapham, R., Lee, L. Y., Tsugama, D., Lee, S., Mengiste, T., and Gelvin, S.B. (2018) *VIP1* and its homologs are not required for *Agrobacterium*-mediated transformation, but play a role in Botrytis and salt stress responses. Frontiers in plant science, 9, 749.

Lei, Q.Y., Zhang, H., Zhao, B., Zha, Z.Y., Bai, F., Pei, X.H., Zhao, S., Xiong, Y., and Guan, K.L. (2008) TAZ promotes cell proliferation and epithelial-mesenchymal transition and is inhibited by the hippo pathway. Mol. Cell. Biol. 28, 2426-2436.

Leivar, P., Antolín-Llovera, M., Ferrero, S., Closa, M., Arró, M., Ferrer, A., Boronat, A., and Campos, N. (2011) Multilevel control of Arabidopsis 3-hydroxy-3-methylglutaryl coenzyme A reductase by protein phosphatase 2A. Plant Cell. 23, 1494-1511.

Lemoine, F., Correia, D., Lefort, V., Doppelt-Azeroual, O., Mareuil, F., Cohen-Boulakia, S., and Gascuel, O. (2019) NGPhylogeny.fr: new generation phylogenetic services for non-specialists. Nucleic Acids Res. 47, W260-W265.

Li, J., Krichevsky, A., Vaidya, M., Tzfira, T., and Citovsky, V. (2005) Uncoupling of the functions of the Arabidopsis VIP1 protein in transient and stable plant genetic transformation by Agrobacterium. Proc Natl Acad Sci USA. 102, 5733-5738.

Lu, S., Yuejing, Z., Niu, Y., and Bingru, Z. (2008) Antioxidant responses of radiation-induced dwarf mutants of bermudagrass to drought stress. J Am Soc Hortic Sci 133:360-366.

Masclaux, F.G., Bruessow, F., Schweizer, F., Gouhier-Darimont, C., Keller, L., and Reymond, P. (2012) Transcriptome analysis of intraspecific competition in *Arabidopsis thaliana* reveals organ-specific signatures related to nutrient acquisition and general stress response pathways. BMC plant biology, 12, 227.

Mayer, U., Ruiz, R.A.T., Berleth, T., Miséra, S., and Jürgens, G. (1991) Mutations affecting body organization in the Arabidopsis embryo. Nature, 353, 402-407.

Mazanka, E., Alexander, J., Yeh, B.J., Charoenpong, P., Lowery, D.M., Yaffe, M., and Weiss, E.L. (2008) The NDR/LATS family kinase Cbk1 directly controls transcriptional asymmetry. PLoS Biol. 6, e203.

Millward, T.A., Heizmann, C.W., Schafer, B.W., and Hemmings, B.A. (1998) Calcium regulation of Ndr protein kinase mediated by S100 calcium-binding proteins. EMBO J. 17, 5913-5922.

Millward, T.A., Hess, D., and Hemmings, B.A. (1999) Ndr protein kinase is regulated by phosphorylation on two conserved sequence motifs. J Biol Chem. 274, 33847-33850.

Nagai, T., Ibata, K., Park, E.S., Kubota, M., Mikoshiba, K., and Miyawaki, A. (2002) A variant of yellow fluorescent protein with fast and efficient maturation for cell-biological applications. Nat. Biotechnol., 20, 87-90.

Nakagawa, Y., Katagiri, T., Shinozaki, K., Qi, Z., Tatsumi, H., Furuichi, T., Kishigami, A., Sokabe, M., Kojima, I., Sato, S., Kato, T., Tabata, S., Iida, K., Terashima, A., Nakano, M., Ikeda, M., Yamanaka, T., and Iida, H. (2007) Arabidopsis plasma membrane protein crucial for Ca^{2+} influx and touch sensing in roots. Proc Natl Acad Sci USA, 104, 3639–3644.

Nishiyama, Y., Hirota, T., Morisaki, T., Hara, T., Marumoto, T., Iida, S., Makino, K., Yamamoto, H., Hiraoka, T., Kitamura, N., and Saya, H. (1999) A human homolog of *Drosophila warts* tumor suppressor, h-warts, localized to mitotic apparatus and specifically phosphorylated during mitosis. FEBS Lett. 459, 159-165.

O'Malley, R.C., Huang, S.C., Song, L., Lewsey, M.G., Bartlett, A., Nery, J.R., Galli, M., Gallavotti, A., and Ecker, J.R. (2016) Cistrome and epicistrome features shape the regulatory DNA landscape. Cell. 165, 1280-1292.

Ohtani, Y. (1950) Studies on the stamping of wheat and barley. Bul Natl Agr Exp Stn Jpn. 67, 1-76.

País, S.M., Téllez-Iñón, M.T., and Capiati, D.A. (2009) Serine/threonine protein phosphatases type 2A and their roles in stress signaling. Plant Signal Behav. 4, 1013-1015.

Pinosa, F., Begheldo, M., Pasternak, T., Zermiani, M., Paponov, I.A., Dovzhenko, A., Barcaccia, G., Ruperti, B., and Palme, K. (2013) The *Arabidopsis thaliana Mob1A* gene is required for organ growth and correct tissue patterning of the root tip. Ann Bot. 112, 1803-1814.

Pitzschke, A., Djamei, A., Teige, M., and Hirt, H. (2009) VIP1 response elements mediate mitogen-activated protein kinase 3-induced stress gene expression. Proc Natl Acad Sci USA 106(43), 18414-18419.

Rashotte, A.M., DeLong, A., and Muday, G.K. (2001) Genetic and chemical reductions in protein phosphatase activity alter auxin transport, gravity response, and lateral root growth. Plant Cell. 13, 1683-1697.

Schneider, C.A., Rasband, W.S. and Eliceiri, K.W. (2012) NIH Image to ImageJ: 25 years of image analysis. Nat Methods. 9, 671-675.

Shakir, S.K., Irfan, S., Akhtar, B., ur Rehman, S., Daud, M. K., Taimur, N., and Azizullah, A. (2018) Pesticide-induced oxidative stress and antioxidant responses in tomato (*Solanum lycopersicum*) seedlings. Ecotoxicology, 27, 919-935.

Shih, H.W., Miller, N.D., Dai, C., Spalding, E.P., and Monshausen, G.B. (2014) The receptor-like kinase FERONIA is required for mechanical signal transduction in Arabidopsis seedlings. Curr Biol. 24, 1887-1892.

Shin, B., Feser, R., Nault, B., Hunter, S., Maiti, S., Ugwuagbo, K. C., and Majumder, M. (2019). miR526b and miR655 Induce Oxidative Stress in Breast Cancer. Int. J. Mol. Sci. 20, 4039.

Stanevich, V., Jiang, L., Satyshur, K.A., Li, Y., Jeffrey, P.D., Li, Z., Menden, P., Semmelhack, M.F., and Xing, Y. (2011) The structural basis for tight control of PP2A methylation and function by LCMT-1. Mol Cell. 41, 331-342.

Sun, L., Pehlivan, N., Esmaeili, N., Jiang, W., Yang, X., Jarrett, P., Mishra, N., Zhu, X., Cai, Y., Herath, M., Shen, G., and Zhang, H. (2018) Co-overexpression of AVP1 and PP2A-C5 in Arabidopsis makes plants tolerant to multiple abiotic stresses. Plant Sci. 274, 271-283.

Takeo, K. and Ito, T. (2017) Subcellular localization of VIP 1 is regulated by phosphorylation and 14-3-3 proteins. FEBS letters, 591, 1972-1981.

Tao, W., Zhang, S., Turenchalk, G.S., Stewart, R.A., St. John, M.A., Chen, W., and Xu, T. (1999) Human homologue of the *Drosophila melanogaster* lats tumour suppressor modulates CDC2 activity. Nat. Genet. 21,177-181.

Torres, M.A. and Dangl, J.L. (2005) Functions of the respiratory burst oxidase in biotic interactions, abiotic stress and development. Current opinion in plant biology, 8(4), 397-403.

Tsugama, D., Liu, S., and Takano, T. (2012a) A bZIP protein, VIP1, is a regulator of osmosensory signaling in Arabidopsis. Plant physiology, 159, 144-155.

Tsugama, D., Liu, H., Liu, S., and Takano, T. (2012b) Arabidopsis heterotrimeric G protein β subunit interacts with a plasma membrane 2C-type protein phosphatase, PP2C52. Biochimica et Biophysica Acta, 1823, 2254–2260.

Tsugama, D., Liu, S., and Takano, T. (2012c). Drought-induced activation and rehydration-induced inactivation of MPK6 in Arabidopsis. Biochemical and biophysical research communications, 426, 626-629.

Tsugama, D., Liu, S., and Takano, T. (2013) Metal-binding ability of VIP1: a bZIP protein in *Arabidopsis thaliana*. Protein J. 32, 526-532.

Tsugama, D., Liu, S., and Takano, T. (2014) Analysis of functions of VIP1 and its close homologs in osmosensory responses of *Arabidopsis thaliana*. PloS one, 9, e103930.

Tsugama, D., Liu, S., and Takano, T. (2016) The bZIP protein VIP1 is involved in touch responses in Arabidopsis roots. Plant Physiology, 171, 1355-1365.

Tsugama, D., Liu, S., Fujino, K., and Takano, T. (2018) Calcium signalling regulates the functions of the bZIP protein VIP1 in touch responses in *Arabidopsis thaliana*. Annals of botany, 122, 1219-1229.

Tsugama, D., Yoon, H. S., Fujino, K., Liu, S., and Takano, T. (2019) Protein phosphatase 2A regulates the nuclear accumulation of the Arabidopsis bZIP protein VIP1 under hypo-osmotic stress. Journal of experimental botany, 70, 6101-6112.

Tzfira, T., Vaidya, M., and Citovsky, V. (2001) VIP1, an Arabidopsis protein that interacts with Agrobacterium VirE2, is involved in VirE2 nuclear import and Agrobacterium infectivity. The EMBO Journal, 20, 3596-3607.

Van Leene, J., Blomme, J., Kulkarni, S.R., Cannoot, B., Winne, N.D., Eeckhout, D., Persiau, G., Slijke, E.V.D., Vercruysse, L., Bossche, R.V., Heyndrickx, K.S., Vanneste, S., Goossens, A., Gevaert, K., Vandepoele, K., Gonzalez, N., Inzé, D., and Jaeger, G.D. (2016) Functional characterization of the Arabidopsis transcription factor bZIP29 reveals its role in leaf and root development. J Exp Bot. 67, 5825-5840.

Verhertbruggen, Y., Marcus, S.E., Chen, J., and Knox, J.P. (2013). Cell wall pectic arabinans influence the mechanical properties of *Arabidopsis thaliana* inflorescence stems and their response to mechanical stress. Plant and cell physiology, 54, 1278-1288.

Vigneron, A.M., Ludwig, R.L., and Vousden, K.H. (2010) Cytoplasmic ASPP1 inhibits apoptosis through the control of YAP. Genes Dev. 24, 2430-2439.

Waadt, R., Manalansan, B., Rauniyar, N., Munemasa, S., Booker, M.A., Brandt, B., Waadt, C., Nusinow, D.A., Kay, S.A., Kunz, H., Schumacher, K., DeLong, A., Yates 3rd, J.R., and Schroeder, J.I. (2015) Identification of open stomata1-interacting proteins reveals interactions with sucrose non-fermenting1-related protein kinases2 and with type 2A protein phosphatases that function in abscisic acid responses. Plant Physiol. 169, 760-779.

Weiss, E.L., Kurischko, C., Zhang, C., Shokat, K., Drubin, D.G. and Luca, F.C. (2002) The *Saccharomyces cerevisiae* Mob2p-Cbk1p kinase complex promotes polarized growth and acts

with the mitotic exit network to facilitate daughter cell-specific localization of Ace2p transcription factor. J. Cell Biol. 158, 885-900.

Wlodarchak, N., Guo, F., Satyshur, K.A., Jiang, L., Jeffrey, P.D., Sun, T., Stanevich, V., Mumby, M.C., and Xing, Y. (2013) Structure of the Ca^{2+}-dependent PP2A heterotrimer and insights into Cdc6 dephosphorylation. Cell Res. 23, 931-946.

Wu, F.H., Shen, S.C., Lee, L.Y., Lee, S.H., Chan, M.T., and Lin, C.S. (2009) Tape-Arabidopsis Sandwich-a simpler Arabidopsis protoplast isolation method. Plant Methods. 5, 16.

Wu, Y., Zhao, Q., Gao, L., Yu, X.M., Fang, P., Oliver, D.J., and Xiang, C.B. (2010) Isolation and characterization of low-sulphur-tolerant mutants of Arabidopsis. Journal of experimental botany, 61(12), 3407-3422.

Xi, W., Gong, X., Yang, Q., Yu, H., and Liou, Y.C. (2016) Pin1At regulates PIN1 polar localization and root gravitropism. Nat Commun. 7, 1-10.

Xu, T., Wang, W., Zhang, S., Stewart, R.A., and Yu, W. (1995) Identifying tumor suppressors in genetic mosaics: the *Drosophila lats* gene encodes a putative protein kinase. Development. 121, 1053-1063.

Yamanaka, T., Nakagawa, Y., Mori, K., Nakano, M., Imamura, T., Kataoka, H., Terashima, A., Iida, K., Kojima, I., Katagiri, T., Shinozaki, K., and Iida, H. (2010) MCA1 and MCA2 that mediate Ca^{2+} uptake have distinct and overlapping roles in Arabidopsis. Plant Physiol. 152, 1284-1296.

Yoo, S.D., Cho, Y.H., and Sheen, J. (2007) Arabidopsis mesophyll protoplasts: a versatile cell system for transient gene expression analysis, Nat. Protoc. 2, 1565-1572.

Yoon, H.S., Fujino, K., Liu, S., Takano, T., and Tsugama, D. (2020) VIP1, a bZIP protein, interacts with the catalytic subunit of protein phosphatase 2A in *Arabidopsis thaliana*. Plant Signal Behav. 15, 1706026.

Yoon, H.S., Fujino, K., Liu, S., Takano, T., and Tsugama, D. (2021) The B″-family subunits of protein phosphatase 2A are necessary for *in-vitro* dephosphorylation of the Arabidopsis mechanosensory transcription factor VIP1. Biochemical and Biophysical Research Communications. 534, 353-358.

Yu, J.S. (1998) Activation of protein phosphatase 2A by the Fe^{2+}/ascorbate system. J Biochem. 124, 225-230.

Zhang, Z., Zhang, X., Wang, S., Xin, W., Tang, J., and Wang, Q. (2013) Effect of mechanical stress on cotton growth and development. PloS one, 8, e82256.

Zhao, B., Wei, X., Li, W., Udan, R.S., Yang, Q., Kim, J., Xie, J., Ikenoue, T., Yu, J., Li, L., Zheng, P., Ye, K., Chinnaiyan, A., Halder, G., Lai, Z.C., and Guan, K.L. (2007) Inactivation of YAP oncoprotein by the Hippo pathway is involved in cell contact inhibition and tissue growth control. Genes Dev. 21, 2747-2761.

Zhou, H.W., Nussbaumer, C., Chao, Y., and DeLong, A. (2004) Disparate roles for the regulatory A subunit isoforms in Arabidopsis protein phosphatase 2A. The Plant Cell, 16, 709-722.

Zhou, P.M., Liang, Y., Mei, J., Liao, H.Z., Wang, P., Hu, K., Chen, L.Q., Zhang, X.Q., and Ye, D. (2021) The Arabidopsis AGC kinases NDR2/4/5 interact with MOB1A/1B and play important roles in pollen development and germination. Plant J. 105, 1035-1052.

Acknowledgments

I greatly thank Drs. Daisuke Tsugama Tetsuo Takano, Asian Natural Environmental Science Center (currently Asian Research Center for Bioresource and Environmental Sciences), Graduate School of Agricultural and Life Sciences, The University of Tokyo, for providing valuable guidance and discussion about my study. I am also grateful to Dr. Kaien Fujino and Dr. Hanako Shimura, Laboratory of Crop Physiology, Hokkaido University, who helped and advised me with their valuable ideas and suggestions. I also thank Dr. Shenkui Liu, State Key Laboratory of Subtropical Silviculture, Zhejiang A & F University for supporting my work. I would like to extend my gratitude to Prof. Ho-min Kang, Department of Horticulture Science, Kangwon National University, South Korea, who gave me a lot of advice for my future. I am also grateful to Prof. Jae-Yun Heo, Department of Plant Science, Gangneung-Wonju National University, South Korea, who helped me with valuable ideas about future plans. I am also grateful to Dr. Stanton Gelvin and ABRC for useful and valuable research materials.

I am also grateful for precious time to all members of Laboratory of Crop Physiology and Laboratory of Environmental Stress tolerance Mechanisms. They are Dr. Hangil Kim, Dr. Dong Geun Lee, Dr. Cheolwoo Park, Mr. Kyeongmin Lee, Mr. Michihiro Yamazaki, Mr. Naoya Kazuta, and Mr. Toshinori Tsutsumi. I also greatly appreciate scholarship programs from Hokkaido International Exchange and Cooperation Center (HIECC), Graduate school of agricultural and life sciences (The University of Tokyo), Yamamoto International Academic Exchange Foundation, and The Korean Scholarship Foundation. I was able to focus on my research because of financial support from these programs.

Lastly, I thank my family for support and encouragement throughout my entire life.